National Library of Canada

Acquisitions and Bibliographic Services Branch

395 Wellington Street
Ottawa, Ontario
K1A 0N4

Bibliothèque nationale du Canada

Direction des acquisitions et des services bibliographiques

395, rue Wellington
Ottawa (Ontario)
K1A 0N4

Your file Votre référence

Our file Notre référence

NOTICE

The quality of this microform is heavily dependent upon the quality of the original thesis submitted for microfilming. Every effort has been made to ensure the highest quality of reproduction possible.

If pages are missing, contact the university which granted the degree.

Some pages may have indistinct print especially if the original pages were typed with a poor typewriter ribbon or if the university sent us an inferior photocopy.

Reproduction in full or in part of this microform is governed by the Canadian Copyright Act, R.S.C. 1970, c. C-30, and subsequent amendments.

AVIS

La qualité de cette microforme dépend grandement de la qualité de la thèse soumise au microfilmage. Nous avons tout fait pour assurer une qualité supérieure de reproduction.

S'il manque des pages, veuillez communiquer avec l'université qui a conféré le grade.

La qualité d'impression de certaines pages peut laisser à désirer, surtout si les pages originales ont été dactylographiées à l'aide d'un ruban usé ou si l'université nous a fait parvenir une photocopie de qualité inférieure.

La reproduction, même partielle, de cette microforme est soumise à la Loi canadienne sur le droit d'auteur, SRC 1970, c. C-30, et ses amendements subséquents.

Canada

THE ELECTRON PROBE X-RAY MICROANALYSIS OF THE ADULT MAMMALIAN CARDIAC MUSCLE

by
Jean Langlois

Thesis presented
to the School of Graduate Studies and Research
in partial fulfillment of the requirements for the degree of M.Sc.

Department of Anatomy and Neurobiology
Faculty of Medicine
University of Ottawa
Ottawa, Ont., Canada

ISBN 0-612-00611-5

UNIVERSITÉ D'OTTAWA
UNIVERSITY OF OTTAWA

ACKNOWLEDGEMENTS

I would like to thank my thesis supervisor, Dr. J.A. Hinke, for sharing his research expertise of more than 35 years and his daily presence throughout the course of this project.

I would also like to thank all the staff of the Faculty of Medicine which has been of assistance during this project.

I would finally like to thank the Department of Anatomy and Neurobiology for the opportunity to complete Graduate Studies.

ABSTRACT

THE ELECTRON PROBE X-RAY MICROANALYSIS OF THE ADULT MAMMALIAN CARDIAC MUSCLE.

Langlois, J. and J.A. Hinke.
Department of Anatomy and Neurobiology, Faculty of Medicine, University of Ottawa, Ottawa, Ontario, Canada.

The main objective of this project was to master the electron probe x-ray microanalysis technique to permit one to obtain physiologically meaningful quantitative elemental profiles (Na, Cl, K, P, Mg, Ca & S) for the components of a given cell.

The techniques which had to be mastered were: preparation of mammalian (rat) cardiac muscle; 'rapid' cryofixation using a Reichert-Jung MM80E 'impact freezer'; cryosectioning using a Reichert-Jung FC4 cryoultramicrotome; transfer and freeze-drying; electron probe x-rays collection using the EDAX 9100 Series Energy Dispersive X-ray Analysis Systems attached to a Philips TEM 420; quantitative analysis using the Hall equation and thin membrane aminoplastic standards.

Different methods of transfer and freeze-drying were compared. **Method I-a:** cryotransfer to the electron microscope using a modified Philips Cryotransfer system, freeze-drying in the column of the electron microscope, x-rays collection at low temperature; **Method I-b:** cryotransfer to the electron microscope using a modified Philips Cryotransfer system, freeze-drying in the column of the electron microscope, x-rays collection at ambient temperature; **Method II:** cryotransfer to a vacuum chamber (Edward-Coating System E306 A) using a precooled metal carrier, freeze-drying in a vacuum chamber while warming at ambient temperature, transfer and x-rays collection at ambient temperature. Only the elemental content of Si & S were statistically ($p < 0.05$) different. The higher Si in Method II is probably related to dust contamination. The lower S found with Methods I-b & II seems to be related to a change in temperature but the exact nature of the change cannot be explained. A morphological 'melting' of the filamentous ultrastructure was consistently observed with Method II. It may indicate incomplete extraction of tightly bound water to macromolecules, perhaps because of insufficient vacuum. The easier Method II is recommended for the quantitative analysis of Na, Cl, K, P, Mg & Ca. Recooling of the sections after freeze-drying was not found essential to x-rays collection. However, if S is important, Method II cannot be recommended and Method I-a is the method of choice.

Quantitative (mmole/Kg water) physiological elemental profiles were established for the A-band, the mitochondrion and the nucleus of the myocyte in

the fast frozen quickly excised cardiac muscle. The profiles were compared favorably with comparable data in the literature. Heterogeneity was observed between intracellular and extracellular spaces and also between cellular components.

Elemental profiles for the myocyte components were also obtained from Langendorff perfused hearts. Compared to the data obtained from the quickly excised unperfused hearts, the elemental profiles in all cellular components were radically altered. The components had higher Na & Cl and lower K & Mg. The Ca was sequestrated in the mitochondria. The P was lower in A-bands, but not in mitochondria. Simple stoichiometric arguments revealed significant changes in the apparent osmolarity and in the apparent fixed charge of cellular components. These changes indicate that serious deteriorations of structural macromolecules might also have occurred. The authors advise caution when a Langendorff perfused mammalian heart preparation is being contemplated as a model of 'normal' physiology.

TABLE OF CONTENTS

LIST OF FIGURES

LIST OF TABLES

1. INTRODUCTION

1.1. THE MAINTENANCE OF THE CELLULAR ELEMENTAL AND WATER CONTENT

The elemental and water content of a living cell is different from its extracellular milieu and the maintenance of the typical normal cellular elemental and water profiles requires an intact membrane (Guyton 1991).

In the typical living intact membrane, ions move across it through low resistance pathways confined to the non-lipid hydrophilic membrane inclusions which are manufactured and maintained by the living cell as selective transmembrane diffusion channels or carriers. If a net transmembrane movement of a given ion in a given direction is incompatible with the ion electrochemical potential gradient across the membrane, the ion is said to be actively transported. Active transport requires an expenditure of energy, transduced by the living cell from chemical reactions (e.g. Krebs cycle) to maintain an incompatible thermodynamic equilibrium (e.g. transmembrane ionic gradients). When the structure of a plasma membrane is rendered non-intact by physical or chemical disruption, the cell ions change to a profile similar to the external milieu. (Guyton 1991)

The membrane also regulates cell volume (cell water) by actively transporting ions (e.g. active electrogenic Na efflux; Guyton 1991) and by permitting intracellular macromolecules and water to order themselves into unique metastable quaternary structures which straddle the solid and liquid states (liquid-crystal; Elliott and Rome 1969; Aldoroty et al. 1987). These quasicrystalline macromolecules exert very little osmotic force. Swelling is an early sign of a malfunctioning or dying cell (Majno et al. 1960; Cotran et al. 1989). The swelling is due to an influx of water occurring because of a change in the internal osmotic needs of the cell interior (Leaf 1959; Leaf 1970). The

osmotic changes relate to the absence of energy required for the active membrane transport of ions and to the production of new osmotic effectors by metabolic conversion of osmotically less active larger molecules (e.g. glycogen, DNA, RNA, etc.) which leads to an increasing number of osmotically active solutes (e.g. lactate, inorganic phosphate and purines nucleosides; Tranum-Jensen et al. 1981; Reimer and Ideker 1987; Cotran et al. 1989). The progressive disruption of the liquid-crystal order (disruption of proteins quaternary structures, depolymerisation and increased solubility) may also contribute to the increased osmolarity.

The elemental and water contents of various cellular membranous components are also different because each component membrane regulates differently the ions, the water content and the quaternary structure of its internal molecules. Furthermore, the elemental and water content within a non-membranous or membranous cellular components may also be different from one point to the other because of differing macromolecular structures. For example, differences were found between the potassium contents in myofibril and mitochondrion and the potassium contents in the A-band and the I-band within a myofibril (von Zglinicki and Bimmler 1987).

The equilibria within a living cell implies an interdependency of ions, water and macromolecules located in membranous and non-membranous cellular components.The corollary to this statement is that a disequilibrium in one location of the cell has the potential to produce disequilibria throughout the cell although the rate of change may be different from one location to the other.

1.2. QUANTITATIVE MEASUREMENT OF THE CELLULAR ELEMENTAL CONTENT

All the facts mentioned in section 1.1 are a challenge to the cell biologist interested in the quantitative measurement of the distribution of

elements and water within a cell and its components under normal and pathological conditions.

Cellular elemental contents have been measured most frequently with techniques such as flame spectroscopy, radioactive isotopes, ions-selective microelectrodes and dye techniques but these techniques are limited to the measurement of total cellular content or the mean ionic content of the cytoplasm, including all cellular components.

In the last 15-20 years, an increasing number of investigators have applied the electron-probe x-ray microanalysis technique to ultrathin freeze-dried cellular sections in order to detect differences in elemental content at the cellular level. Although this technique cannot differentiate between the bound and the free state, it can give an accurate total composition profiles for components as small as the lateral cistern of the sarcoplasmic reticulum.

1.3. MAIN OBJECTIVE OF THESIS

The main objective of this thesis was to develop the electron-probe x-ray microanalysis technique which would permit one to obtain physiologically meaningful elemental profiles (especially the soluble ions) for the components of a given cell which could be compared subsequently to a pathological state.

1.4. ELECTRON PROBE X-RAY MICROANALYSIS TECHNIQUE

The electron probe x-ray microanalysis technique involves many steps of various levels of difficulty:

PREPARATION OF THE BIOLOGICAL SAMPLE

(1) Choice of the sample

(2) Cryofixation of the sample

(3) Cryosections of the sample

(4) Transfer to the electron microscope and freeze-drying

CORRELATION OF MORPHOLOGY WITH QUANTITATIVE MEASUREMENT OF ELEMENTAL PROFILES

(5) Morphological characterization

(6) Electron-probe x-ray microanalysis

(7) Quantitative analysis

Obtaining morphology (5) and performing an electron-probe x-ray microanalysis (6) are the easiest. The interpretation of the data obtained and the translation into quantitative data (7) is more difficult. Even more difficult are the steps involved in the preparation of the specimen where artefacts in the elemental profile may be easily introduced at every step (1, 2, 3 & 4) if not properly executed.

The following pages outline the rationale, the literature review and the author's approach for every step involved in the electron probe x-ray microanalysis technique as tabulated above.

1.4.1. PREPARATION OF THE BIOLOGICAL SAMPLE

1.4.1.1. CHOICE OF THE SAMPLE

1.4.1.1.1. Rationale

The biological specimen should be representative of the 'normal' in vivo state. All handling of the specimen should be such as to preserve the 'normal' state.

1.4.1.1.2. Literature review

The in vivo preparation is accepted as the standard to which other preparations should be compared. It is well known that the elements in many in vitro preparations differ from the in vivo standard: a) tissues processed after different periods of time after the sacrifice (von Zglinicki et al. 1986); b) dissected tissues (Warley 1989; Zierold 1989); c) isolated cells (Kendall et al. 1985; Warley 1989; Zierold 1989). The changes found in the isolated cells can be reversed when the cells are cultured (Warley 1987; Zierold 1989). Increased time between the sacrifice and further processing of the specimen, and techniques of dissection of tissues or cell segregation, are recognized as factors which contribute to 'cell damage', i.e. deviation from the standard.

1.4.1.1.3. Author's approach

The heart muscle was chosen as our test tissue since there seemed to be a need for 'normal' elemental profiles in myocytes to better understand the changes occurring in pathological states. For example, the understanding of the reversible and irreversible changes following hypoxia would be improved if the

subcellular profile changes could be documented during the development of hypoxia. Changes in the diffusible (e.g. Na, Cl & K) and less diffusible (e.g. Mg & Ca) ions can provide information on the fixed charges of the macromolecules in a given cellular component and on the progression of the denaturation process. Changes in the organically-bonded elements (e.g. P, S, Mg & Ca) can provide information on the integrity and composition of the organic matrix within a cellular component while it denatures, depolymerizes and dissolves. Improvement in the understanding of the mechanisms involved in subcellular myocyte damage and the possible reversal of such damage would be of value in the management of coronary artery disease and heart transplantation.

The first year of this project was used to prepare successfully isolated myocytes, since this preparation offers a better control on the extracellular milieu when compared to the tissue preparation for physiological experiments (Dow et al. 1981; Dow et al. 1981; Powell 1985). This preparation involves typically a retrograde aortic perfusion (Langendorff 1895) of the heart with physiological solution containing respectively normal calcium concentration, micromolar calcium concentration, and normal calcium concentration with lytic enzymes such as collagenase. After perfusion, the heart is finally cut into pieces that are further processed with lytic enzymes.

In order to simplify the steps involved in the development of the electron probe x-ray microanalysis technique during the second year of this project, it was decided to use tissue from a heart perfused (Langendorff) only with a physiological solution containing normal concentration of calcium. After establishment of the technique, the isolated myocytes preparation would finally be used.

Early microanalyses of sections from Langendorff perfused hearts used in the second year indicated unphysiological elemental profiles. Since elemental redistribution occurred during the Langendorff heart perfusion, an <u>in vitro</u> unperfused heart tissue was finally used in the third year of this project to obtain

a physiological profile. The results related to Langendorff perfused heart tissue are presented to demonstrate the magnitude of the intracellular changes. Although the isolated myocytes preparation offers advantages for physiological experiments, it was not used in this thesis because it became clear that a step in its preparation induced pathological damages in myocytes.

1.4.1.2. FIXATION OF TISSUE

1.4.1.2.1. Rationale

The main goal in adopting a technique of fixation is to maintain the elemental profiles of the living state. A technique should not permit a redistribution of elements, whether soluble or bound.

1.4.1.2.2. Literature review

1.4.1.2.2.1. Principles of fixation

The elements in biological specimens are redistributed and washed out by conventional methods of fixation (i.e. aldehydes and/or osmium tetraoxide; Morgan et al. 1978; Chandler 1985; Zierold and Schafer 1988). Freezing (cryofixation) of the biological specimen (Altmann technic; Altmann 1890; Gersh 1932) offers the best alternative to chemical fixation. Unfortunately, ice crystals can occur. These can disrupt structure (e.g. heart muscle; Dalen et al. 1983; Dalen and Scheie 1991) and redistribute elements (Zierold 1984).

Crystal formation can be inhibited by chemical cryoprotectants (Meryman 1971; Farrant et al. 1977; Franks 1977; Skaer 1982). They have been divided traditionnally as penetrating (e.g. glycerol and dimethyl sulphoxide) and non-penetrating (e.g. sucrose) the cell (Meryman 1971). Barnard (1980) has

challenged this classification by reporting a cellular penetration by endocytosis of so-called non-penetrating cryoprotectants (Dextran and polyvinyl pyrrolidone). Nonetheless, cryoprotectants by their very nature may initiate cellular elemental redistribution. For example, glycerol and dimethyl sulphoxide (DMSO) increase the permeability of the cell membranes (Skaer 1982), and sucrose changes the osmotic equilibrium of the cytoplasm (Skaer 1982). Not enough work has been done with others such as Dextran, polyvinyl pyrrolidone (PVP) and hydroethyl starch (HEV) to know how effective they might be in maintaining the cellular elemental distribution (Franks 1977; Barnard 1980; Skaer 1982).

Damage from crystal formation over distances from 5-30 μm can be prevented by increasing the speed of cooling at greater than 10,000°C/second to permit only the growth of small crystals ('rapid' freezing; Plattner and Bachmann 1982; Robards and Sleytr 1985; Gilkey and Staehelin 1986; Sitte et al. 1987). This method uses the principle that the crystal size is inversely related to the speed of cooling. A number of 'rapid' freezing methods are described (Stephenson 1956; Riehle 1968; Van Venrooij et al. 1975; Kopstad and Elgsaeter 1982; Jones 1984; Bald 1986).

A speed of cooling of more than 1,000,000°K/second ('ultrarapid' freezing) was estimated necessary for the formation of a thickness of non-crystalline (vitrified) ice (Luyet 1937; Bald 1986). Vitrification at lower speeds of cooling was expected for biological specimens since cytoplasm contains natural cryoprotectants (Dubochet 1987). Reproducible methods of vitrification of water confirmed by x-ray diffraction were reported for pure and aqueous water (Bruggeller and Mayer 1980; Dubochet and McDowall 1981; Dubochet et al. 1982), for biological suspensions (Lepault et al. 1983; Adrian et al. 1984), and tissues (depth of vitrification of 10 μm) such as liver (McDowall et al. 1983; Livesey et al. 1991) and kidney (Dubochet et al. 1987). Despite the success obtained with liver and kidney tissues without chemical cryoprotectant, Dubochet et al. (1987) advocate their use to assure vitrification beyond 1 μm in tissues with

relatively large interstitial spaces (e.g. muscle tissue).

1.4.1.2.2.2. Methods of cryofixation

The most convenient 'rapid' freezing method for the cryofixation of a block of tissue with a diameter larger than 0.5 mm is the 'impact freezing' method (Plattner and Bachmann 1982; Sitte 1987).

The 'impact freezing' method makes use of the principle that cooling and freezing occur more rapidly between tissue and a precooled metal than between tissue and a liquid cryogen (Simpson 1942; Eranko 1954; Kulenkampff 1955; Wollenberger et al. 1960; Christensen 1971; Demsey and Bullivant 1976; Hagler and Buja 1984; Ingram and Ingram 1984; Bearer and Orci 1986). In 1964, Van Harreveld and Crowell designed an apparatus which permitted one to drive a small piece of tissue onto the surface of a silver block cooled by liquid nitrogen ('impact freezing'; 'slam freezing'). They reported absence of crystal damages over depths of 10-15 μm (Van Harreveld and Crowell 1964; Van Harreveld et al. 1974), although not consistently (Sitte 1987). In one study, Sitte (1979) confirmed that better in depth freezing was obtained with the Van Harreveld method provided the guide was at a near perfect right angle to the surface of metal.

Initially, a flow of liquid helium over the cold metal surface was used to prevent condensation which function as an insulator (Van Harreveld and Crowell 1964; Van Harreveld et al. 1974). It soon became apparent, however, that air could be kept away from the cold metal surface simply by placing the metal surface in the gaseous phase of the cryogen (Dempsey and Bullivant 1976; Phillips and Boyne 1984). Evaporation of the liquid cryogen could be initiated and controlled by means of a heating coil (Sitte 1977; Sitte et al. 1985). Silver was replaced by copper (Heuser et al. 1979; Boyne 1979; Philips and Boyne 1984) to increase the thermal conductivity at the liquid nitrogen temperature

(Bald 1983). The liquid helium replaced liquid nitrogen to increase the speed of cooling by 50% (Kopstad and Elgsaeter 1982) and the depth of morphological preservation to 15-20 μm (Heuser et al. 1979; Escaig 1982). The bouncing of the specimen after impact was reduced with the introduction of a magnetic catch (Heuser et al. 1979), an hydraulic-pneumatic damping device (Boyne 1979; Philips and Boyne 1984), a secondary pressure at the point of impact and a reverse motion stop lock (Sitte 1987). The tissue damage secondary to the speed of descent of the specimen (Pinto da Silva and Kachar 1980) was reduced by the introduction of damping devices: a piece of liver (Heuser et al. 1979); a piece of dry foam (Boyne 1979; Philips and Boyne 1984); a soft foam rubber (Escaig 1982) and compressed air (Sitte 1987). With these improvements, depths of morphological preservation of 10-15 μm are consistently obtained (Boyne 1979; Philips and Boyne 1984; Heuser et al. 1979; Escaig 1982) using either liquid nitrogen or helium. Sitte (1987) argues that deeper preservation may be impossible since thermal conductivity decreases as the depth of freezing increases. Many home-made 'impact freezers' have been described (Verna 1983; Heath 1984; Allison et al. 1987), some of which are commercially available (e.g. Rash 1983; Robards and Sleytr 1985).

Morphological preservation as deep as 600 μm have been reported with the 'high pressure (2100 bar) freezing' method (Riehle 1968; Riehle and Hoechli 1973; Moor et al. 1980; Moor 1987). This method was compared favorably to the 'impact freezing' method (Zierold et al. 1991). Its theoretical rationale is that large crystal formation should be inhibited under high pressure conditions.

1.4.1.2.3. Author's approach

The 'impact freezing' technique was adopted because of its general recognition as an acceptable method to obtain subcellular elemental profiles identical to those in the cell prior to fixation. The relatively inexpensive Reichert-

Jung (MM80E) unit was used in all experiments. This unit permits: a) the placement of a small tissue sample on the surface of an alumimium pin; b) the controlled impaction of the sample onto a highly polished copper surface precooled in liquid nitrogen; c) four mechanisms designed to minimize rebound (an hydraulic damping device; a reverse motion stop lock; the creation of a secondary pressure at impact to maintain contact between tissue and the cold copper surface; foam cushion); d) control of evaporation of $N_{2(l)}$ and flow of $N_{2(g)}$ around the copper surface to keep ambient air away from it.

Cryoprotectants were never used. Also, at no time was the tissue treated with chemical fixatives. It is well documented that these treatments may significantly alter both the content and the distribution of both the mobile and bound elements in the cell (Morgan et al. 1978; Skaer 1982; Chandler 1985; Zierold and Schaffer 1988).

The 'ultrarapid' freezing was considered impractical at this time for heart muscle tissue because of an insufficient reported depth of vitrification (1 μm) without cryoprotectant.

Financial constraints prevented the use of liquid helium and the adoption of the 'high pressure freezing' technique.

1.4.1.3. CRYOSECTIONS OF TISSUE

1.4.1.3.1. Rationale

An ultrathin section is required both for the identification of the subcellular components in the electron microscope and for the collection of x-rays from them. Of course, the embedding medium used for ultramicrotomy should respect the original elemental distribution.

1.4.1.3.2. Literature review

A number of workers have developed low temperature freeze-substitution and/or freeze-drying methods leading to plastic embedding without warming, hence presumably without redistributing elements. Using these techniques, a number (Van Zyl et al. 1976; Marshall 1980; Harvey 1980, 1982; Ingram and Ingram 1980, 1984; Wroblewski and Wroblewski 1984; Wroblewski et al.1990; Edelman 1986, 1991) have insisted that the original elemental profiles were not altered, whereas others (Roos and Barnard 1985, 1986; Zierold 1992) have demonstrated that the profiles were indeed altered.

This controversy can be avoided if the frozen hydrated section can be obtained with cryoultramicrotomy (Fernandez-Moran 1951; Bernhard and Nancy 1964; Bernhard and Leduc 1967; Iglesias et al. 1971; Christensen 1971; Appleton; Sevéus and Kindel 1974; Hagler 1986; Zierold 1987) of the 'fast-frozen' specimen without plastination. The pioneers were convinced of this, hence laboured intensively, and eventually a technique emerged which although difficult proved to be the preferred one for those wishing to obtain elemental profiles in cellular components closest to those expected in the living physiological state (Gupta et al. 1976; Somlyo et al. 1977; Roomans and Sevéus 1976; Sevéus 1978; Barnard and Sevéus 1978; Dorge et al. 1978; Wendt-Gallitelli and Wolburg 1981; Zierold 1982; Buja et al. 1983; Sasaki et al. 1983; Wheeler-Clark and Tormey 1987; von Zglinicki and Bimmler 1987; Tvedt et al. 1987; LeFurgey 1987).

1.4.1.3.3. Author's approach

From the literature, it is clear that freeze-substitution or freeze-drying followed by plastic embedding and ultramicrotomy is the easier technique. However, the more difficult technique of cryoultramicrotomy was selected

primarily because of its acceptance in the literature as the best technique available to date for the preservation of the original elemental distribution.

1.4.1.4. TRANSFER TO THE ELECTRON MICROSCOPE AND FREEZE-DRYING

1.4.1.4.1. Rationale

Once ultrathin cryofixed sections are mounted on a grid, they should be transferred to the electron microscope and be stable under the electron beam without elemental redistribution.

1.4.1.4.2. Literature review

The transfer at low temperature of non-vitreous frozen hydrated sections to the electron microscope was demonstrated years ago (Gupta and Hall 1981; Saubermann et al. 1981) but 'etching' of the section by the electron beam proved to be a limiting factor to general use (Zierold 1988). The 'etching' was found to be secondary to the production of free radicals (OH^- and H^+) by radiolysis (Talmon et al. 1979; Talmon 1982). It could be controlled by lowering the temperature (Heide and Grund 1974; Heide 1984; Glaeser and Taylor 1978). Vitreous frozen-hydrated biological sections prove to be more stable under the electron beam (Dubochet 1987) since vitrified ice is ten times more resistant to etching than crystalline ice (Talmon 1982; Talmon 1987).

Since non-vitreous cryofixed frozen-hydrated sections are unstable under the electron beam, workers (Zierold 1982; Hagler 1984; Walsh and Tormey 1988; von Zglinicki and Uhrik 1988) obtained stable cryosections by sublimating the ice in the sections in the electron microscope vacuum column (freeze-drying) at about -85°C.

Stable freeze-dried cryosections were also obtained by transferring the cryosections in a precooled metal carrier to a vacuum chamber (at less than 10^{-3} torr) and permitting the temperature to rise 'slowly' to ambient temperature (Dorge et al. 1978; Somlyo et al. 1977; Wendt-Gallitelli and Wolburg 1981; Sasaki et al. 1983; Hagler 1986; Tvedt et al. 1987; von Zglinicki and Bimmler 1987; Jorgensen et al. 1988; Bond et al. 1989; Moravec and Bond 1991; Warley 1991; Ziegler et al. 1992). Some of the freeze-dried sections were transferred at ambient temperature from the vacuum chamber to the electron microscope using a conventional specimen holder (Dorge et al. 1978; Tvedt et al. 1987; Warley 1991). Some freeze-dried sections were recooled (Somlyo et al. 1977; Jorgensen et al. 1988; Bond et al. 1989; Moravec and Bond 1991; Ziegler et al. 1992) in a cryospecimen holder before transfer to the electron microscope. This recooling was found protective against lipid melting (Hagler and Buja 1986) but probably unnecessary to protect against beam damage and subsequent elemental redistribution (von Zglinicki and Uhrik 1988).

It is generally accepted that the rate of warming must be 'slow' in order to prevent crystal formation. Although one can now find sophisticated protocols which control temperature (-130 to -80°C) over precise preselected time periods and under differing vacuum levels (Linner et al. 1984; Linner et al. 1986; Livesey et al. 1991), simple 'slow' warming of a precooled metal carrier in a vacuum chamber is believed to be sufficient to preserve both morphology and the elemental profiles (von Zglinicki and Uhrik 1988).

1.4.1.4.3. Author's approach

Since 'impact freezing' of muscle tissue rarely if ever achieves a vitreous state for most of its intracellular water, one could not expect a frozen hydrated section of heart tissue to be stable under the electron beam. Hence, it became necessary to achieve stability through freeze-drying.

Since it could not be decided from the literature whether freeze-drying in the electron microscope was more effective at preserving morphology and elemental distribution than freeze-drying in a conventional vacuum chamber, both were tried and compared. The literature does indicate that the latter method is more commonly used, probably because it is more 'user-friendly'.

1.4.2. CORRELATION OF MORPHOLOGY WITH QUANTITATIVE MEASUREMENT OF ELEMENTAL PROFILES

The primary purpose of producing an ultrathin freeze-dried section is to be able finally to focus an electron beam on a specimen and to collect the x-rays from all the elements in the focused region with the security that the elemental content calculated will be a true measure of the elemental content of that region in vivo.

1.4.2.1. MORPHOLOGICAL CHARACTERIZATION

1.4.2.1.1. Literature review

X-ray detectors (see section 1.5.2.2.) can be attached to scanning electron microscopes (SEM; Gupta et al. 1976; Saubermann et al. 1981), transmission electron microscopes (TEM; Chiesi et al. 1981; Sasaki et al. 1983; Wendt-Gallitelli and Isenberg 1985; Walsh and Tormey 1988; von Zglinicki and Bimmler 1987; Jorgensen et al. 1988; Bond et al. 1989; Moravec and Bond 1992) and scanning transmission electron microscopes (STEM; Wendt-Gallitelli and Wolburg 1981; Buja et al. 1983; Wheeler-Clark and Tormey 1987; Warley 1991) with or without real time imaging (Somlyo 1984; Saubermann 1988; LeFurgey et al. 1992). Real time imaging is applied to the STEM in order to achieve the lowest detection limit. In theory, a minute moving beam (STEM)

rastered over the area of a cellular component is preferred to a fixed beam (TEM) because heat concentration and mass loss are minimized.

Generally, freeze-drying produces enough contrast so that staining can be avoided (Zierold 1985). The contrast can be improved by treating the freeze-dried section with osmium vapour, but one runs the risk of altering the elemental content (Morgan et al. 1978). Cryosectioning is associated with artefacts (e.g. crystals, surface defects, fractures, crevasses, chattering, knife marks, shrinking) which must be recognized as such (Frederik 1982; Frederik et al. 1984; Zierold 1984; Dubochet and McDowall 1984).

1.4.2.1.3. Author's approach

Our x-ray detector and analysis system (EDAX) was attached to a TEM (Philips 420). After complete freeze-drying, the optical contrast was such that osmium staining was not required. The STEM was not used for a number of technical reasons.

1.4.2.2. ELECTRON PROBE X-RAY MICROANALYSIS

1.4.2.2.1. Literature review (from review articles: Chandler 1977; Morgan 1985; Hall 1986; Roomans 1988; Hall 1989; Gupta 1991)

1.4.2.2.1.1. Principle

When a beam of energized (i.e. fast moving) electrons strikes a thin specimen, an energized electron may do one of several things (Figure 1) : a) it may be reflected or backscattered, either with or without a loss of energy (i.e. secondary or primary); b) it may be absorbed in the specimen to have its energy converted to heat or light; c) it may pass through the specimen, either with or

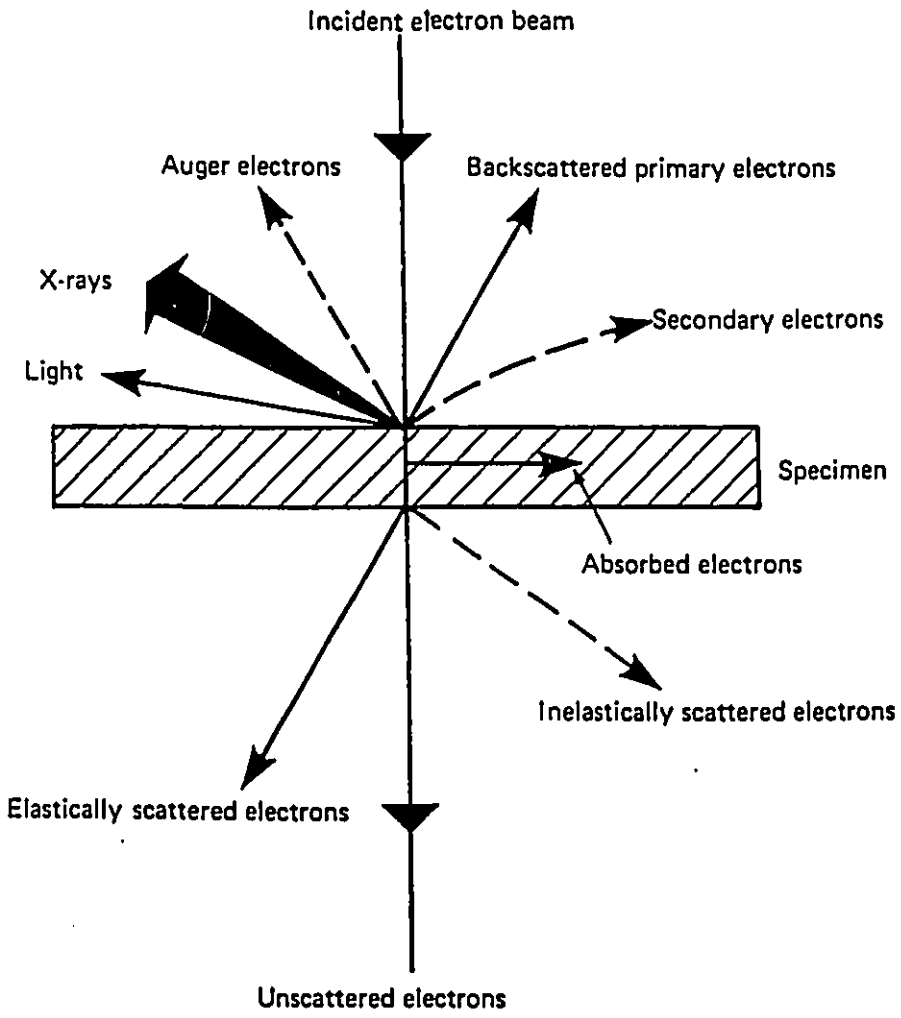

FIGURE 1 : Electron-specimen interactions (Chandler 1977)

without diffracting; d) it may enter the domain of an atom in the specimen, decelerate, then continue on as a transmitted diffracted electron with energy loss (white radiation); e) it may enter an atom in the specimen, strike and displace an electron from one shell, to be replaced by an electron from an outer shell, which must of necessity give up energy in the form of an x-ray (Figure 2).

Each x-ray photon emitted from an atom has its own unique wavelength and energy content. Table 1 lists the elements which make up nearly 100% of all the atoms in an untreated biological specimen. They are listed to illustrate the important fact that the energy content of an emitted x-ray photon is proportional to the atomic number of the atom which emitted it. If one can collect and measure all the quanta of energies emitted from the sample under the electron beam, then one has a measure of the kinds and quantities of atoms in the sample under the beam. This is the principle behind the electron probe x-ray microanalysis system.

1.4.2.2.1.2. Specimen considerations

When a fast moving electron leaves the vacuum to enter the more dense specimen, it bends as it decelerates. Furthermore, it will change its course a number of times as it is deflected by orbital electrons. The diffractions and the deflections continue to produce a lateral diffusion vector to the electron travel pathway in the specimen. This lateral diffusion vector is directly proportional to the thickness of the specimen but inversely proportional to the accelerating voltage (HT).

Spatial resolution is maximized when the interactive volume (where x-rays are being produced) is confined to that volume of the specimen immediately under the electron beam. This is achieved when lateral diffusion of penetrating electrons is at a minimum. It is generally understood that the interactive diameter does not exceed the beam diameter by more than 10% if the specimen is < 200nm and the HT is > 50 KV.

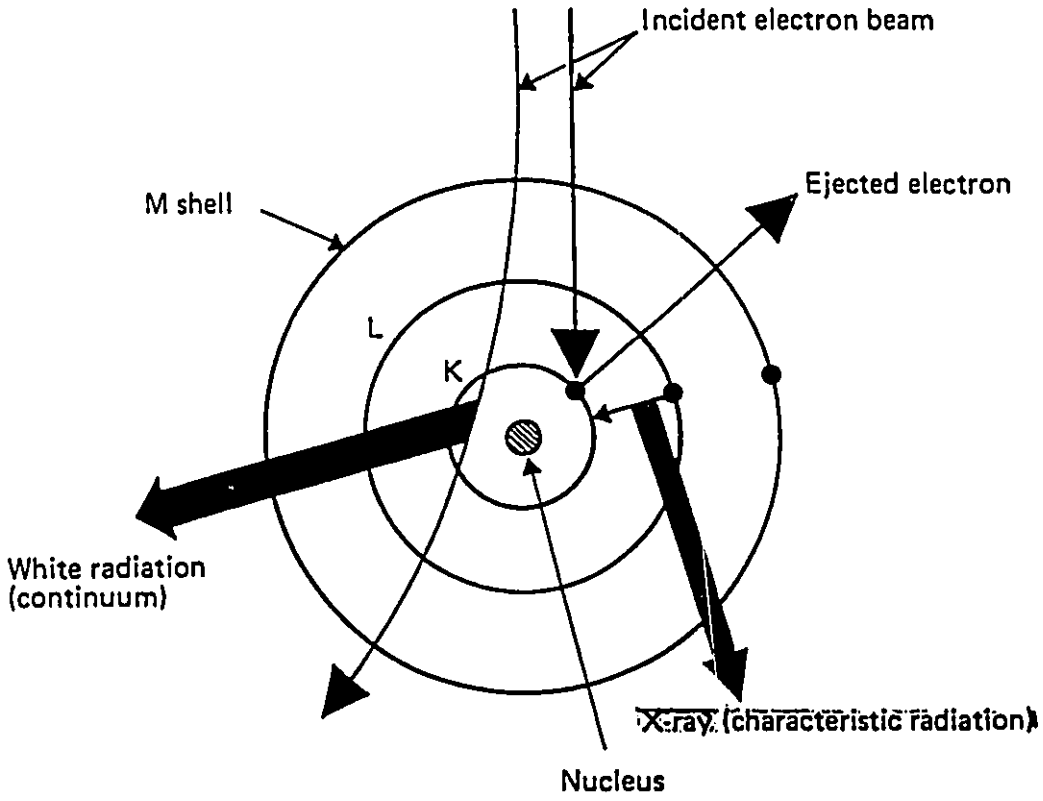

FIGURE 2 : Production of x-ray from an atom by an incident electron beam (Chandler 1977)

TABLE 1 : X-ray (Kα1)[1] energies from some elements* listed by atomic number*

element	atomic number	energy (eV)
C	6	280
N	7	392
O	8	523
Na	11	1040
Mg	12	1252
P	15	2013
S	16	2307
Cl	17	2623
K	19	3316
Ca	20	3693
Fe	26	6402

Legend

1 Only energies of the Kα 1 type (i.e. when the α 1 electron of the L shell drops into the K shell) are listed.

* These elements plus H (not listed) account for over 99.9% of the atoms in an untreated biological specimen.

Data taken from EDAX EPIC TABLES-Energy and Wavelength Tables for Elemental X-Ray Emission and Absorption, EDAX Laboratories, P.O. Box 135, Prairie View, Illinois, U.S.A..

Spatial resolution is important when one wishes to detect differences in the elemental spectra obtained from adjacent cellular components. It also becomes important when one wishes to translate an elemental peak into an elemental concentration (say mmole/Kg dry weight) in the interactive volume.

As one decreases the interactive volume (by decreasing the specimen thickness, or by decreasing beam diameter) one will eventually reach a volume in which not enough atoms of a given element will be available for the creation of a significant peak (above background). Consider, for example the Ca content in the A-band of a sarcomere in a resting muscle fiber. Detectability can be improved if one is able to measure the loss of electron energy (e.g. Somlyo and Shuman 1982; Somlyo 1985; LeFurgey and Ingram 1990) or if the STEM mode (rather than TEM) is used.

1.4.2.2.1.3. Detection of x-rays

The first x-ray measuring spectrometers were designed to measure the wavelength of an x-ray. These instruments were highly sensitive but they could only measure one wavelength (therefore one element) at a time in real time. Later, wavelength spectrometers were designed to measure several elements at a time, but at the expense of resolution.

The x-ray spectrometers most frequently used today are of the type designed to measure the energy content of an x-ray rather than its wavelength. These are referred to most frequently as energy dispersive x-ray spectrometers. The detector-preamplifier assembly of an energy dispersive x-ray spectrometers must be attached to an electron microscope. Only the end of the probe containing the detector need to be inserted through a port into the vacuum column above the specimen, between the condenser and objective lenses. The actual detection part of the assembly consists of a single crystal of Si carefully and homogeneously doped with Li so that it can function as a semi-conductor when a bias voltage is

applied across it. When an x-ray enters the crystal, Si atoms ionize in the amount of one electron per 3.8 eV of x-ray energy. In less than a microsecond, these released electrons are drawn to the FET (field effect transistor) where they are discharged as a pulse of a given height (i.e. proportional to the numbers of electrons). These pulses are instantaneously amplified then sent on to a multichannel analyzer, designed to group (according to height), count and store in memory channels. The contents of these channels can be displayed (in real or delayed time) as an energy spectrum.

To minimize electronic noise, both the Si (Li) wafer and the FET have to be kept at liquid nitrogen temperatures. Newer detectors (> 1989) can be operated at ambient temperature.

A thin beryllium window pane is required to isolate the environment of the detector from the vacuum in the electron microscope column. Unfortunately, this thin window (i.e. 8 μm) is capable of stopping photons having energies smaller than 750 eV. Thus, it can be seen from Table 1 that this detector (with a 8 μm Be window) is unable to detect the H, C, N and O atoms in the specimen by their photon energies. These four elements account for about 95% of the atoms in a dried biological specimen. Newer windowless detector are now available to measure these four elements but they do not appear to be used by biologists.

1.4.2.1.2. Author's approach

The electron beam of a transmission electron microscope was used as a source of accelerated electrons to probe ultrathin sections of specimen. Furthermore, this instrument was designed to produce a small beam of electrons (as small as 40 nm) and to focus them on a target (i.e. specimen).

Most x-rays collections were made on 50 nm thick freeze-dried specimens using a beam diameter of 200 nm and a HT of 80 KV so that our interactive volume was 1.6 (10^{-15}) cm^3 and the spatial resolution was less than 20

nm. In the case of a typical mitochondrion in a mammalian myocyte with smallest dimension of about 500 nm, the thickness of an hydrated section of 200 nm was filled with a high percentage of mitochondrion and the positioning of a 200 nm electron beam over a single mitochondrion was simple. The same rationale was also true for the nucleus and the A-band of a myofibril. But accurate profiles from regions such as the sarcoplasmic reticulum and t-tubules were more problematic. Real time imaging with elemental mapping or the electron energy loss analysis technique were not available to obtain meaningful spectra from the sarcoplasmic reticulum and t-tubules.

The detection of elements was limited to those having an atomic number greater than 10 for reasons already given.

1.4.2.3. QUANTITATIVE ANALYSIS

1.4.2.3.1. Literature review

A conversion of the energy spectrum displayed on the monitor of the energy dispersive x-ray spectrometers to an elemental concentration (say mmole/Kg dry weight) can be done using the Hall equation (Hall et al. 1973; see Materials and Methods). The Hall equation has been validated for biological specimen (Shuman et al. 1976).

The preparation of standards to which unknown specimens are compared is an essential part of the Hall equation. The following appropriateness of a standard rests on the following considerations: a known composition of all elements similar to the unknown specimen; homogeneity of the elements in the medium; a behavior similar to the specimen under the electron beam. Many types of standards have been used with varying suitability: cryosectioned standards; the protein thin films; the embedding resins; the aminoplastic with inorganic salts (Roomans 1979; Russ 1980; Warley 1990).

The Hall equation is based on two unproven assumptions. First, it assumes that mass loss is similar in the standard and in the specimen, provided their compositions and geometries are comparable and provided the beam characteristics are identical (Hall 1989). Second, the Hall equation assumes that the state of dehydration is complete, both in the standard and in the unknown specimen. Realizing that the state of total dehydration may not always be achieved in freeze-drying protocols, a number of investigators have attempted to measure water content (e.g. Dorge et al. 1978; Zierold 1986; Warner 1986; von Zglinicki et al. 1987; Roomans 1990; von Zglinicki 1991; Hall 1991). Unfortunately, many of these methods introduce new assumptions which can be questioned.

1.4.2.3.2. Author's approach

The energy spectra were analysed in this thesis with an EDAX computer system. The Hall equation was used in all quantitative analyses. Homogeneous aminoplastic of known composition and doped with a salt were used as standards because accurate compositions similar to the specimen could be obtained. Mass loss was assumed to be similar in the standard and in the specimen provided their compositions and geometries were comparable and provided the beam characteristics were identical. Standards and specimens were assumed to be fully dehydrated.

1.5. SPECIFIC OBJECTIVES OF THESIS

The specific objectives of this thesis are here summarized:

(1) To compare two methods of freeze-drying of cryosections;

(2) To compare collections of x-rays done at low and ambient temperatures;

(3) To establish a quantitative baseline of elemental profiles for the

cellular components of a cardiac myocyte in its physiological state and to compare the obtained baseline with comparable data in the literature;

(4) To establish the heterogeneity of elemental profiles between the intracellular and extracellular spaces and between components of a cardiac myocyte;

(5) To compare the elemental profiles of unperfused and Langendorff perfused heart muscle preparations.

2. MATERIALS AND METHODS

2.1. PREPARATION OF THE SPECIMEN

2.1.1. PREPARATION OF SAMPLES OF HEART TISSUE

This thesis reports on the data collected from seven hearts. Five of them were cryofixed within three minutes after euthanasia without perfusion (unperfused hearts); two were cryofixed within fifteen minutes after euthanasia after being perfused in vitro for 10 minutes (Langendorff perfused hearts). Many trial and error, pilot, and incomplete experiments were done prior to these seven complete experiments.

2.1.1.1. UNPERFUSED HEARTS

2.1.1.1.1. Preparation of the physiological solution

The physiological solution was a modified Krebs-Henseleit balanced salts solution (Krebs and Henseleit 1932). The composition was as follows (mM): NaCl, 118.5; KCl, 3.8; KH_2PO_4, 1.2; $MgSO_4$-$7H_2O$, 1.2; $NaHCO_3$, 24.9; $CaCl_2$-$2H_2O$; 2.6; sucrose 10. The solution was prepared before hand from dessicated solid chemical products and distilled water prepared from demineralized water. Addition of sucrose and aeration with O_2 95%-CO_2 5% for 30 minutes was done the day the stored solution was to be used because of increased bacterial proliferation in stored solutions containing sucrose and decrease of the pO_2 and pCO_2 in aerated stored solutions. The pH and the osmolarity of the solution were measured with a Fisher Accumet pH Meter

Model 620 and a Fisher Osmette A-Automatic Osmometer at 7.4 +/- 0.10 and 295 +/- 5 mOsm.

2.1.1.1.2. Dissection of the hearts

Male Wistar rats (400-500 g; Charles River) were decapitated and the hearts were excised through a left anterior thoracotomy. The excised hearts were immediately submerged in the physiological solution (ambient temperature). The right ventricular wall was cut away from the heart, exposing its endocardium. A piece measuring 2 mm by 2 mm by 2 mm was cut away using a razor blade and a tissue slicer. The sample was positioned on an aluminium pin with the endocardial surface faced outward as shown in Figure 3.

2.1.1.2. LANGENDORFF PERFUSED HEARTS

The Langendorff perfused hearts were prepared as described above except for three points: rats were injected with Heparin (1000 U.S.P. I.P.) at least one hour before euthanasia; the aorta (ascending aorta and aortic arch) was excised along with the whole hearts and the hearts were perfused in vitro as described below.

2.1.1.2.1. Preparation of the perfusing apparatus

The perfusing apparatus is schematized in Figure 4. The temperature of the solution was maintained at 37°C with a Heating Bath and Circulator FE2 (Haake) and a W13 Haake Bath circulating heated distilled water through water-jacketed reservoirs, condenser and container. A constant flow rate of perfusion of 8 ml/min was obtained with a LKB 2132 Microperpex Peristaltic Pump modified to receive two cartridges rather than one. The time to empty the 'dead

FIGURE 3 : Schema of the contruction of the pin-specimen assembly

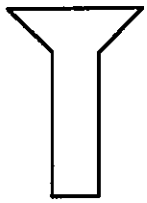

Stage A : cross section of the aluminium pin

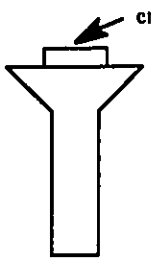

Stage B : cross section of the pin-specimen assembly before cryofixation

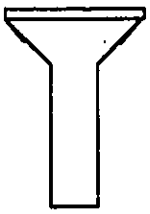

Stage C : cross-section of the pin-specimen assembly after cryofixation

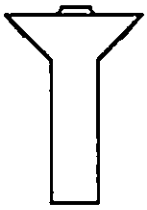

Stage D : pin-specimen assembly after trimming

FIGURE 4 : Schema of the perfusing apparatus

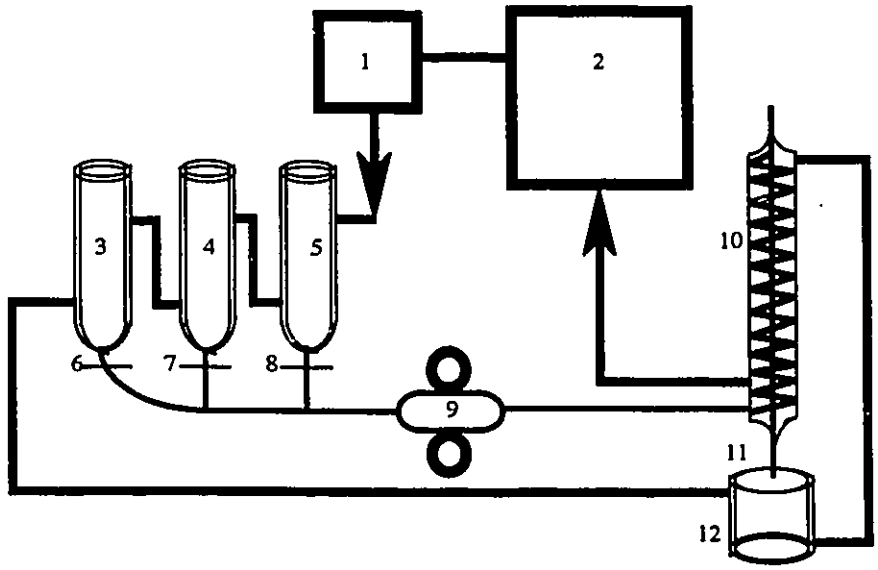

Legend

▬ tube containing water at 37 degrees Celsius
— tube containing the physiological solution

1 Heating Bath and Circulator FE2 (Haake)
2 Haake W13 Bath
3 reservoir A for physiological solution (double-wall)
4 reservoir B (double wall)
5 reservoir C (double wall)
6 valve A
7 valve B
8 valve C
9 modified LKB 2132 Microperpex Peristaltic Pump
10 counter current heat exchange condenser
11 end point of the condenser perfusing the heart
12 container (double wall)

space' between the reservoir A and the end of the condenser was measured with a dye (methylene blue) and was used to fill the 'dead space' with solution before the start of the perfusion. Before the perfusion, the air was flushed from the system with distilled water, the pump was installed and calibrated manually, the reservoir A was filled with the physiological solution, the distilled water in the 'dead space' was replaced by the physiological solution and the aeration system delivering O_2 95%-CO_2 5% was installed in the reservoir A.

2.1.1.2.2. Langendorff perfusion of the hearts

The hearts were perfused using the retrograde aortic perfusion principle of Langendorff (Langendorff 1895). A cannula (16G 1/2" needle cut at 3/8") was inserted into the aorta in the reverse direction of the blood flow from the aortic arch to the proximal ascending aorta to irrigate the coronary arteries after closure of the aortic valves upon retrograde perfusion. The aorta was fixed on the cannula with 2 separate tied loops of silk O to prevent detachment of the aorta from the cannula during perfusion. The loops were placed proximal to the brachiocephalic trunk to prevent leakage of perfusate at that level. After the cannula was connected to the end of the condenser, the physiological solution was perfused for 10 minutes. The vascular bed of the hearts was cleaned from blood by the solution and the color of the hearts changed from red brown to pale brown. Ventricular contractions were observed during the perfusion.

2.1.2. CRYOFIXATION OF THE HEART TISSUE

A Reichert-Jung MM80E (Reichert-Jung Optische Werke AG Austria) device was used to obtain a cryofixation by driving the heart tissue onto a copper disk cooled in a chamber filled with liquid nitrogen. Operational instructions can be obtained from the MM80E Instructions (Reichert-Jung Optische Werke AG

Austria).

2.1.2.1. Preparation of the copper disk

After the chamber of the device was filled with liquid nitrogen, the copper disk was allowed to cool to the liquid nitrogen (< - 190 °C) temperature on a metal plate in the chamber before transfer to the metal mirror support. Maximal thermal conductivity of the disk was achieved by caring for the copper disk surface as follows: polish with Wenol metal polish; keep surface clear of liquid nitrogen; cryofix only one specimen per copper disk.

2.1.2.2. Preparation of the pin carrier

The pin carrier was assembled as shown in Figure 5. Its main function is to hold a pin (with a specimen attached) upside down and perpendicular to the surface of the copper disk (to maximize surface contact of the specimen upon impact with the copper disk). By doing so, one is more likely to minimize crystal damage in the first 10-12 μm and to maximize the area of the sections (Sitte 1979; Figure 6). The followings must be routinely checked to ensure perpendicularity: dents and bends in the metal component are removed; old glue (Krazy Glue) between metal and plastic components is removed before applying new glue; the hole in the styrofoam cushion is centered; the pin is fit snugly in the styrofoam cushion; the entire assembly is centered on the magnet.

FIGURE 5 : Schema of the pin-carrier assembly

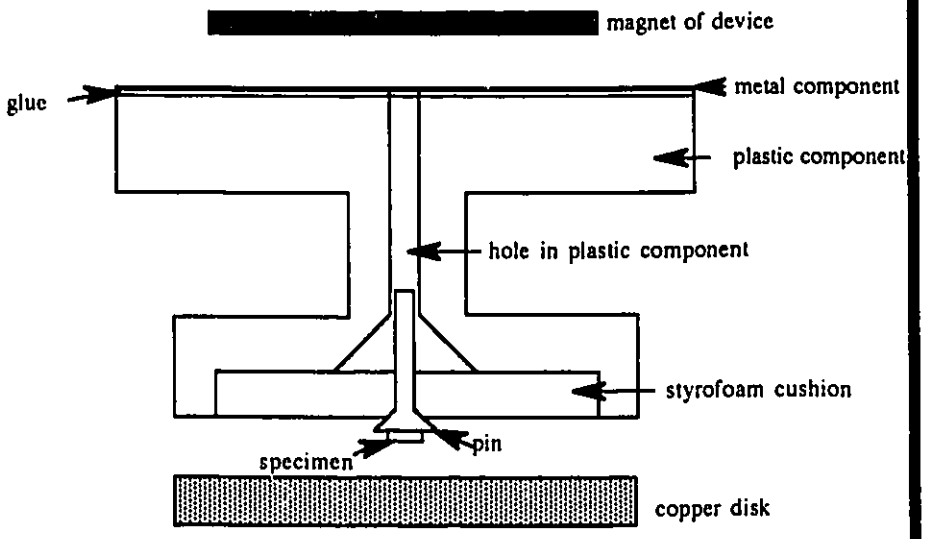

FIGURE 6 : Schema of the effect of angle between the axis of the pin and copper disk on area of sections

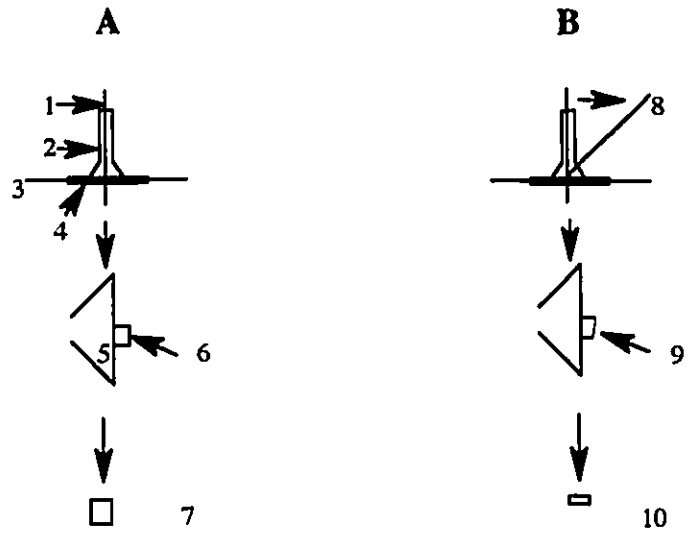

Legend

1 axis of aluminium pin
2 aluminium pin
3 axis of copper disk
4 copper disk
5 head of aluminium pin
A if axis of pin is at right angle from the axis of disk ⟶ face of specimen (6) is parallel to surface of head of pin ⟶ optimal area sectioned (7)
B if axis of pin is moved away from the right angle axis of disk (8) ⟶ face of specimen (9) is not parallel to surface of head of pin ⟶ smaller area sectioned (10)

2.1.2.3. Settings of the cryofixation apparatus

The Reichert-Jung apparatus permits one to adjust the compression of the spring which, when released, produces the velocity of impact. The apparatus also prevents bouncing of the specimen on the copper disk after the first impact. It does this with a reverse motion stop lock, an hydraulic-pneumatic damping device, a secondary pressure invoked at a certain height to hold the specimen against the copper disk during cooling, and a foam cushion.

The settings of the velocity at impact (Force and Speed) were fixed at 6. Higher velocities produced more elastic deformation of the specimen and lower velocities led to poor fixation of the specimen to the aluminium pin (Figure 3-Stage C).

It was necessary to shorten the central pedestal (for the copper disk) by 4 mm to obtain optimal secondary pressure upon impact. With this modification, optimal cryofixation was achieved with a Thickness setting of 12.

In Figure 5, it can be seen that the vertical hole in the plastic assembly must be larger than the pin diameter, otherwise jamming occurs after impact. This was found to be the case for many of the plastic carriers. Hence, they all had to be re-drilled to an appropriate diameter. This adjustment also ensured that the pin compressed the styrofoam cushion upon impact.

Finally, it was essential to ensure that the hole through the styrofoam cushion was smaller than the pin diameter to support the head of the pin and to hold the specimen in contact with the copper disk after impact.

2.1.2.4. Preparation of the specimen for cryofixation

The prepared heart tissue sample was placed on a 'flat' pin head (Figure 3), then inserted into a pin carrier (Figure 5). The endocardial side of the tissue was dried with filter paper, then the carrier was attached as shown in Figure 5 to

the magnetic end of the plunger rod. After impact, the specimen was permitted to remain against the copper disk for two minutes.

The pin-specimen assembly (Figure 3-stage C) was removed from the carrier, placed in a plastic container filled with liquid nitrogen, then transferred to a storage Dewar tank (XC 43/28-Minnesota Valley Engineering Inc.) filled with liquid nitrogen. At no time, was the pin-specimen assembly exposed to the atmosphere or to ambient temperature.

2.1.3. CRYOSECTIONS

A Reichert-Jung FC4 cryoultramicrotome was used. Operational instructions can be obtained from the FC4 Reichert-Jung Operating Instructions (Reichert Optische Werke AG Austria).

The temperatures of the knife, the specimen and the chamber were set at -115, -120 and -120°C respectively.

The trimming of the specimen was done with the cylindrical metal knife provided. Different shapes (i.e. square, rectangle or trapezium) were used but the final cutting surface dimensions (for cryosectioning) of the frozen block were around 0.5 mm.

The traditional glass knife (Latta and Hartmann 1950) was prepared from a glass strip of 6 mm by 25 mm (LKB) using the LKB Knife Maker type 7801A. The concepts of 'free break' (Cameron 1956) and 'balanced break' (Tokuyasu and Okumura 1959) were applied (Sevéus and Tarras-Wahlberg 1984). The 'wet method' (Michalske and Bunker 1987; Slabe et al. 1990) was used. The breaking angle was varied to produce deviations from the 45° from 0.1 to 1 mm. The knives with the smaller deviations from 45° were the best (Griffith 1984). A nickel grid (100 mesh), covered by a pioloform membrane (0.25% in chloroform) and carbon coated (Edward Coating System E306A) was placed on

the knife using electrician's tape as shown in Figure 7 (Robards and Sleytr 1985). The knife was installed on the knife carrier with an angle of +6 degrees. The knife edge was placed parallel to the lower edge of the specimen using the adjustment and swivelling device controls for the knife carrier.

Illumination was improved by directing a fiberoptic beam (Introlux 500-H Volpi AG Urdorf-Zurich; Wild Leitz Canada) on the work area. The static was diminished by grounding of the cryochamber, by using a grounded mat on the floor, by removing shoes, and by using a Zerostat (3) antistatic gun (Discwasher, Shiller Park, Il., U.S.A.). The cutting speed was set at 0.8 mm/s. Sections of approximate thickness of 200 nm in the first 10-12 μm of the block were transferred on the grid using a glasstool (2 mm diameter capillary pulled to infinity using a Vertical Pipette Puller-Model 700C manufactured by David Kopf Instruments). The grid was then transferred to the 'grid deposit plate' of the cryochamber.

2.1.4. TRANSFER TO THE ELECTRON MICROSCOPE AND FREEZE-DRYING

2.1.4.1. METHOD I (a & b)

2.1.4.1.1. Cryotransfer

The transfer of the grid from the cryochamber of the ultramicrotome to the electron microscope was done with a modified Cryo-Specimen Holder PW6599/00 (Philips), a modified Cryo-Transfer Unit PW 6361 (Philips) and an Automatic Temperature Control Unit PW6362/00 (Philips). Operational instructions can be obtained from the Cryo-Specimen Holder 9432 06599001 Handbook (Philips First edition). The purpose of these specialized devices was to permit the transfer of cryosections at a constant low temperature and without

FIGURE 7 : Schema of the position of the grid on the knife

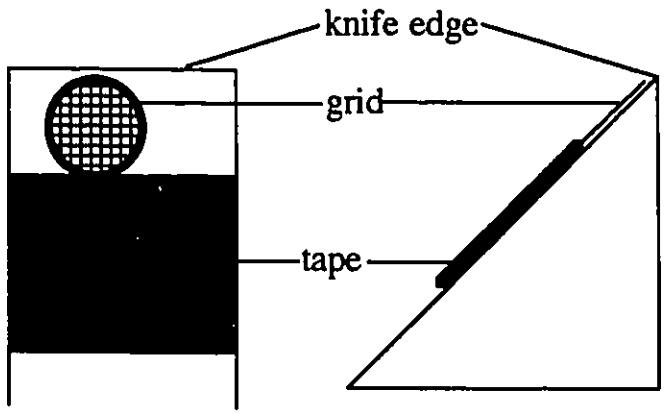

a) frontal view of the knife

b) lateral cross section of knife

exposure to ambient air.

The temperature of the section in the Cryo-Specimen Holder could be selected and maintained from ambient to liquid nitrogen temperature (< -190°C) by mixing $N_{2(l)}$ with ultra high purity $N_{2(g)}$ (at ambient temperature). The usual transfer temperature was set at -140°C.

Using the tool provided, the depth of the injection of the C ring in the Cryo-Specimen Holder from the Cryo-Transfer Unit varied greatly and could not be corrected. The stiffness of the injector mechanism often resulted in displacement of the spacer rods and sphere at the tip of the Cryo-Specimen Holder. For these reasons, the specimen injector and the loading block of the Cryo-Transfer Unit were removed and a new injection method was designed. A copper table and a cap were constructed (Figure 8), then placed in the transfer vessel. A grid in the cryochamber of the ultramicrotome was transferred to the table and covered. After transfer of the vessel from the ultramicrotome to the Cryo-Transfer Unit, the copper table was removed from the vessel and then placed on the metal table of the Cryo-Transfer Unit. After removal of the cap, the grid was manually transferred to the Cryo-Specimen Holder using precooled jeweller self-closing forceps. The beryllium ring (from the old assembly) was also placed on the Cryo-Specimen Holder with a precooled jeweller self-closing forceps. The injection of the C-clip was done with a precooled manual injector. To equilibrate the force applied at the tip of the holder with the injector and to prevent displacement of the rods and sphere, a special support was designed as shown in Figure 9 and was placed on the metal table of the Cryo-Transfer Unit under the tip of the holder. The precooled tools and the manual injector were placed inside an open copper box (5 cm long x 3 cm wide x 1 cm high) which was installed on the metal plate of the Cryo-Transfer Unit to prevent a fall in the liquid nitrogen of the Unit through the holes of the metal table.

FIGURE 8 : Schema of copper table and cap

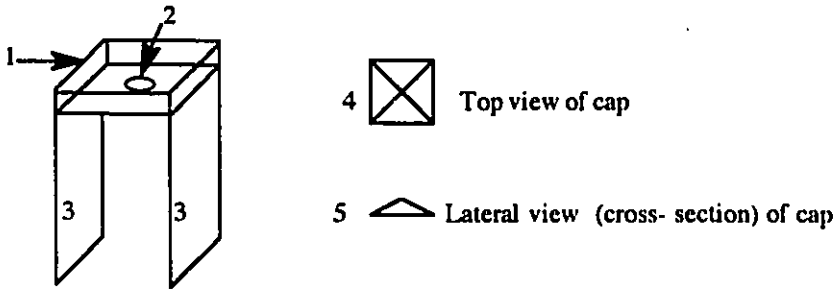

Legend

All structures were built from a sheet of copper
The cap has an open base pyramid shape

1 open box (1.5 cm x 1.5 cm x 0.3 cm)
2 indentation in open box to receive grid (diameter 0.4 cm)
3 legs (1.5 cm x 2 cm x thickness of sheet of material)
4 base of cap = 1 cm x 1 cm
5 height of cap = 0.4 cm

FIGURE 9 : Schema of Cryo-Specimen Holder support

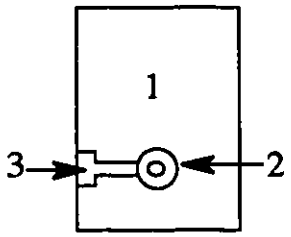

a) Top view

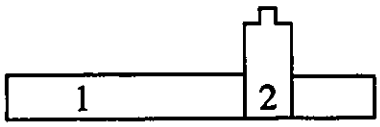

b) Lateral view (cross section)

Legend

1 piece of plexiglass of 6.2 cm x 4.2 cm x 1.2 cm
2 cylindrical supporting element (detached from the Philips Cryo-Specimen Holder support and passed through a full thickness hole in plexiglass piece
3 hole receiving a screw to press fit the cylindrical supporting element to the plexiglass (permits fixation of height of supporting element)

The stiffness of the conduit portion of the Cryo-Specimen Holder Unit often produced misalignment after insertion into the goniometer, leading to air bleeding and reduction in vacuum in the electron microscope column. Furthermore, the length of the conduit made manipulation of the Cryo-Specimen Holder into the goniometer difficult. To overcome these difficulties, the conduit was replaced by a teflon tube (O.D. 2 mm; I.D. 1 mm) passed through a polyvinylchloride tube (O.D. 25 mm; I.D. 18 mm; length = 90 cm) containing high density polyethylene spacers and insulating talc powder (calcium carbonate). The cold gas nitrogen was passed through the teflon tube.

When the old support platform for Dewar of the Cryo-Transfer Unit was used, the insertion of the Cryo-Specimen Holder into the goniometer was difficult. Therefore, it was replaced with a custom-made platform of wood (9" x 24" x 0.75") supported by two legs on the right hand side and by a platform attached at the level of the pointer of the electron microscope on the left hand side.

The sleeve of the Cryo-Specimen Holder often opened before transfer to the electron microscope was complete. This was remedied by applying a layer of Fomblin grease under the sleeve before cooling (applying too much often leads to jamming at low temperatures).

2.1.4.1.2. Freeze-drying in the electron microscope

Once the Cryo-Specimen Holder was in place and full vacuum restored, the temperature of the cryosections was adjusted to -85°C and freeze-drying was permitted to proceed for two hours. During this period, no beam was applied because it was learned that the partially hydrated section is unstable to additional instabilities caused by asymmetric heat distribution. After two hours, the dehydrated sections were usually found to withstand an 80 KV electron beam, even when finely focused. The use of a sandwich grid (i.e. the cryosections placed

between two grids) was tried and found to be unnecessary.

After freeze-drying of the cryosections, visualization and x-rays collections were done in the electron microscope at -120°C (Method I-a) and at ambient temperature (Method I-b; warming overnight to ambient temperature in the electron microscope column).

2.1.4.2. METHOD II

In order to cryotransfer the cryosections to a more conventional vacuum chamber (other than the electron microscope column) and to permit 'slow' warming (from -190°C to ambient temperature) during a prolonged freeze-drying period (e.g. 12 hours), a special brass transfer unit (Figure 10) was constructed. The carrier unit consisted of a grid block, a grid plate and a lid for the block. These were pre-cooled and stored in the cryochamber of the cryoultramicrotome. The large brass transporting blocks were precooled in a styrofoam container filled with liquid nitrogen.

Once the carrier unit was assembled in the chamber of the cryoultramicrotome and transferred on top of precooled transporting blocks, the transfer unit was placed inside the vacuum chamber of an Edwards Coating System E306A. Freeze-drying was carried out for at least 12 hours at $< 10^{-5}$ torr. When the grid was removed, the brass unit was still cold but not to a degree that it could not be handled. The freeze-dried cryosections were transferred to a conventional specimen holder for visualization and x-rays collection in the electron microscope at ambient temperature.

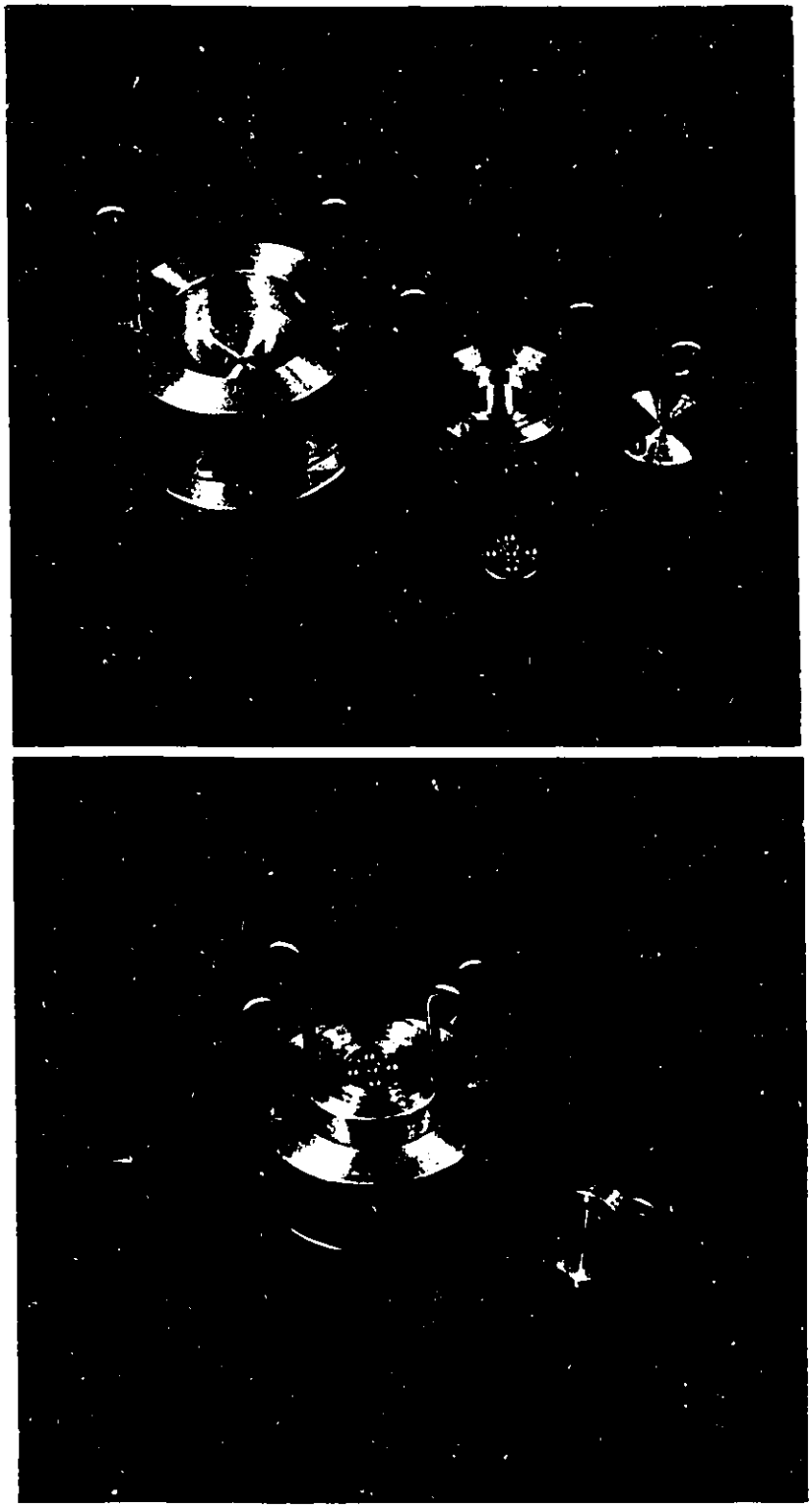

FIGURE 10 (10-1 & 10-2). Brass transfer unit. Figure 10-1 shows the individual components of the unit. 1 = lower brass transporting block (cylinder); 2 = upper brass transporting block; 3 = grid block (curved arrow shows one of the four holes between the interior of the grid block and the vacuum chamber; 4 = grid plate (notice five locations to deposit grids, and four holes to permit communication between the interior of the grid block and the grids); 5 = lid for the grid block. Figure 10-2 shows the assembled unit (the lid is not assembled on the grid block to show the position of the grid plate). Bar = 1.5 cm.

2.2. CORRELATION OF MORPHOLOGY WITH QUANTITATIVE MEASUREMENT OF ELEMENTAL PROFILES

2.2.1. MORPHOLOGY

The Philips TEM 420 was used throughout. A Philips filament 9432 061 00021, an 200 μm condenser aperture and an 50 μm objective aperture were used.

Optical alignment was routinely checked. Specimen height in the goniometer was adjusted to achieve best focusing on the specimen. Focusing at all magnification was aided by the Wobble technique. Finally, series of through-focus pictures were taken for later selection for the best micrographs. All these precautions were necessary because the freeze-dried sections were devoid of fixative, stain and cryoprotectant.

After exposure of Kodak Electron Microscope Film 4489 (ESTAR thick base), the processing was done at 68°F. The emulsions were developed with the Kodak Developer D-19 for 105 seconds, fixed with the Kodak Fixer for 10 minutes and bathed in the Kodak Clearing Agent for 5 minutes. Rinsing with tap water was done 2 minutes after the development, 2 minutes after the fixation and 30 minutes after the treatment with the clearing agent.

Pictures were printed from the developed emulsions on photographic paper (Ilford #1 and #2) in the dark room using a Durst Laborator S45 Special (Durst s.p.a. Bolzano, Bozen, Italy) and an Electronic Interval Timer Model TM-560 (Lektra Laboratories Inc., College Point, N.Y., U.S.A.). After printing, the processing was done at 68°F. The paper was developed with Ilford Ilfospeed developer for 90 seconds and fixed in water acidified with drops of acetic acid glacial (Fisher Scientific) for 30 seconds and with the Ilford Ilfospeed Fixer for 3 minutes. The paper was finally rinsed for 30 minutes with tap water and dried at ambient temperature. After trimming of the pictures with a guillotine, the

letters and signs were applied on the pictures.

2.2.2. ELECTRON PROBE X-RAY MICROANALYSIS

The x-rays were detected with the EDAX 9100 Series Energy Dispersive X-Ray Analysis System (Edax International Inc., Prairie View, Illinois, U.S.A.).

Figure 11 indicates the geometric relationships between the thin specimen in the goniometer and the Si (Li) detector. The fixed parameters are: E = 20; D = 4.5. The equation relating the Take Off Angle (T) to the Specimen Tilt Angle (M), when E = 20 and y = S is as follows:

$$T = M + \tan^{-1}\left[\frac{(W-D) + y\mathrm{Sin}(20)}{y\mathrm{Cos}(20)}\right]$$

If the height of the specimen (in the goniometer) is always adjusted so that W = D = 4.5 mm, then the equation reduces to T = M + 20. It is essential that the geometry be identical for the standard and the specimen (see section 2.2.3.).

Pilot experiments revealed that maximal counts from homogeneous standards (see section 2.2.3.3.) for the elements of interest were obtained when M in the goniometer was set at 15 degrees (to the right). This Tilt Angle (and the associated Take Off Angle) was used routinely for all x-rays collections, both from standards and from specimens.

The zero reference point of the abscissa of our EDAX spectrum display changed by about ± 10 eV per 24 hours. Therefore, a calibration of the spectrum abscissa (from 1 to 8 KeV) was routinely carried out before a collection of x-rays from a specimen. An automatic calibration protocol could be initiated using a calibration program in the software for the EDAX computer. It was only necessary to direct an electron beam onto an Al and a Cu grid (superimposed) in a way which generated x-rays both from an Al and a Cu bar at approximately the

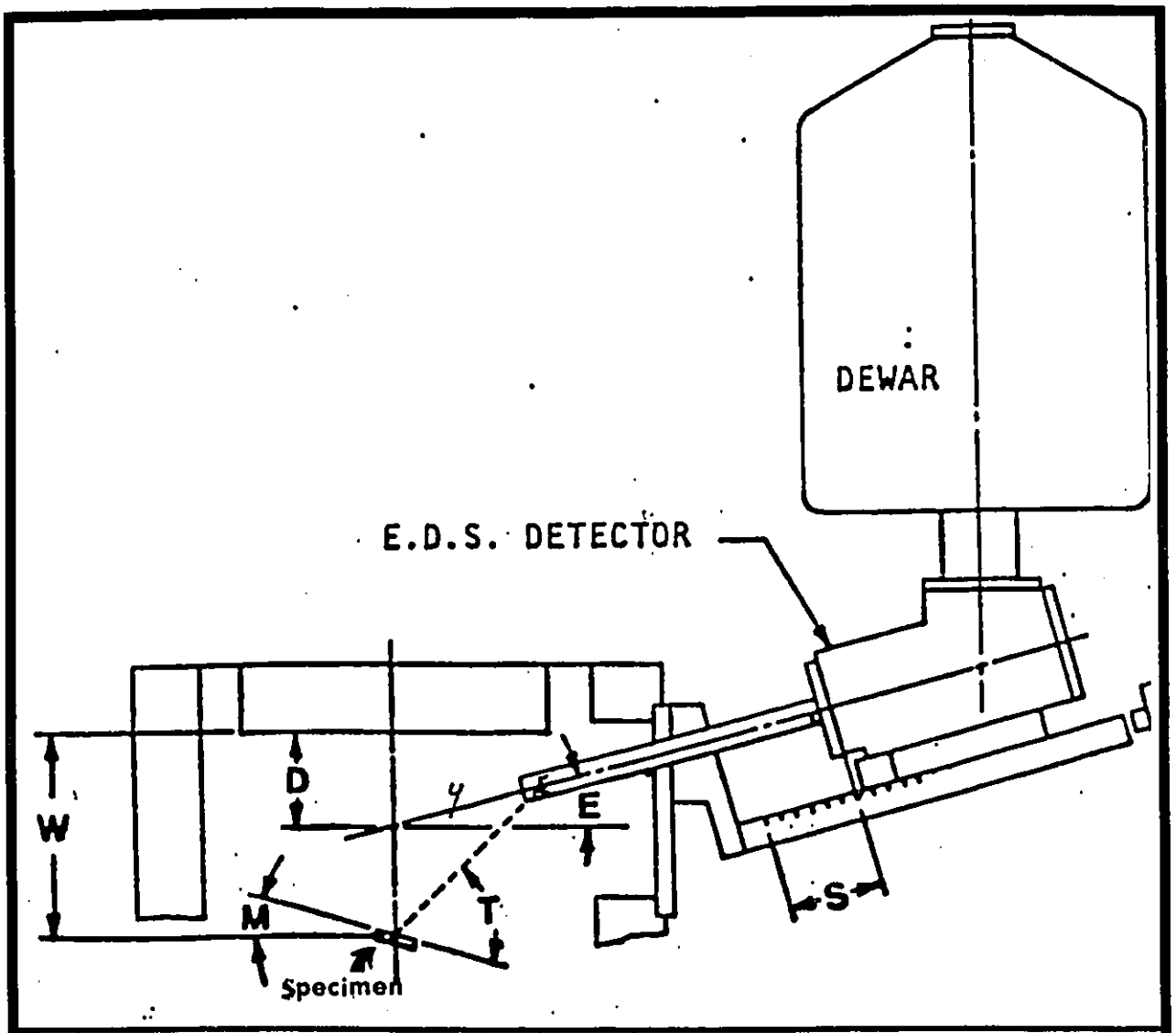

FIGURE 11 : Geometric relationships between the detector and the specimen (from Edax Laboratories, Prairie View, Illinois, U.S.A.). E.D.S. = Energy Dispersive Spectrometer.

same rate. Figure 12 shows the spectrum from superimposed Al-Cu grids after a successful automatic calibration. The Kα1 peak for Al is at 1.485 KeV and for Cu is at 8.040 KeV.

The gain of our detector was routinely set to read 10 ± 10 cps in the absence of a specimen and an electron beam.

Figure 13 is a raw (i.e. no computer-assisted smoothing) x-ray spectrum from a thin aminoplastic film on a 200 mesh Cu grid. The composition of the aminoplastic was such that its H, C, N and O content was closely similar to the content of a freeze-dried thin tissue section (see section 2.2.3.3.). The only additional elements added were K & Cl in the form of KCl salt (to a final concentration of 90 mmole/Kg dry weight). The spectrum clearly reveals the following peaks from left to right: Cu-Lα, Cl-Kα, K–Kα, Cu-Kα, Zn-Kα and Cu-Kβ. X-rays can arise from a grid bar or to a lesser degree from the grid holder. Usually, the stimulating electron is either an elastically scattered electron or a backscattered primary electron since neither of these has lost energy. Obviously, the grid related to the spectrum in Figure 13 was a Cu one and the surrounding grid holder was composed of Cu & Zn. X-rays from grid bars can be minimized by selecting a 100 mesh grid (rather than a 200 or 300 type) and by collecting x-rays from specimen regions located in the middle of a grid square.

Table 2 indicates that the Lα peak of Cu is only 108 eV from the Na peak. Since the Cu-Lα and the Na-Kα peaks need 130 eV between them to stand alone, one can expect some overlap. Although the SQ software permits subtraction of such overlap, the problem was avoided by using 100 mesh Ni grid instead of Cu grid. Since the Ni-Lα and the Na-Kα peaks are 187 eV apart, there should be no overlap. Hence, the **P/b** ratio (see section 2.2.3.) for the Na-Kα peak should be a true reflection of Na content.

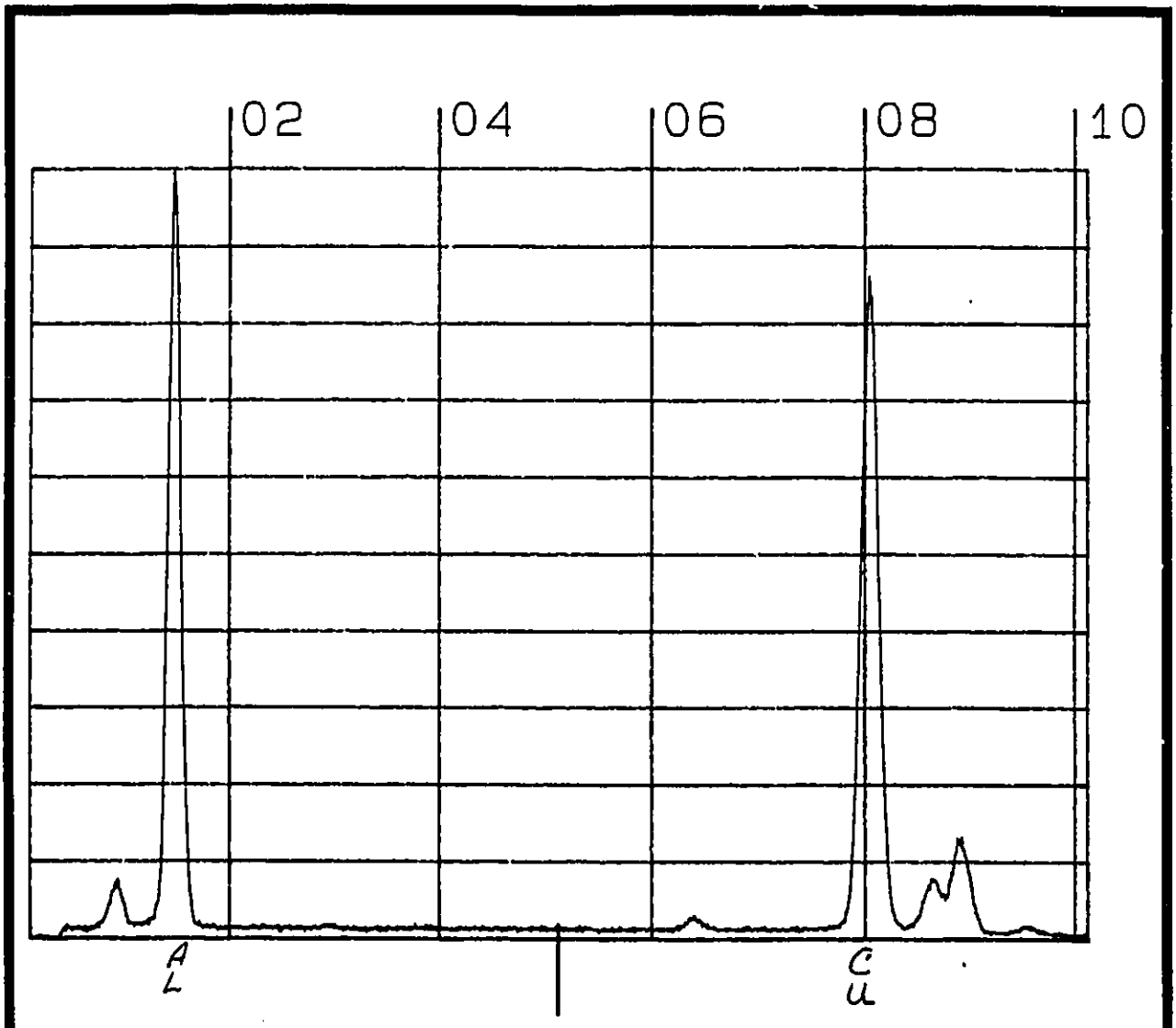

FIGURE 12 : Energy spectrum obtained after calibration with Al and Cu grids

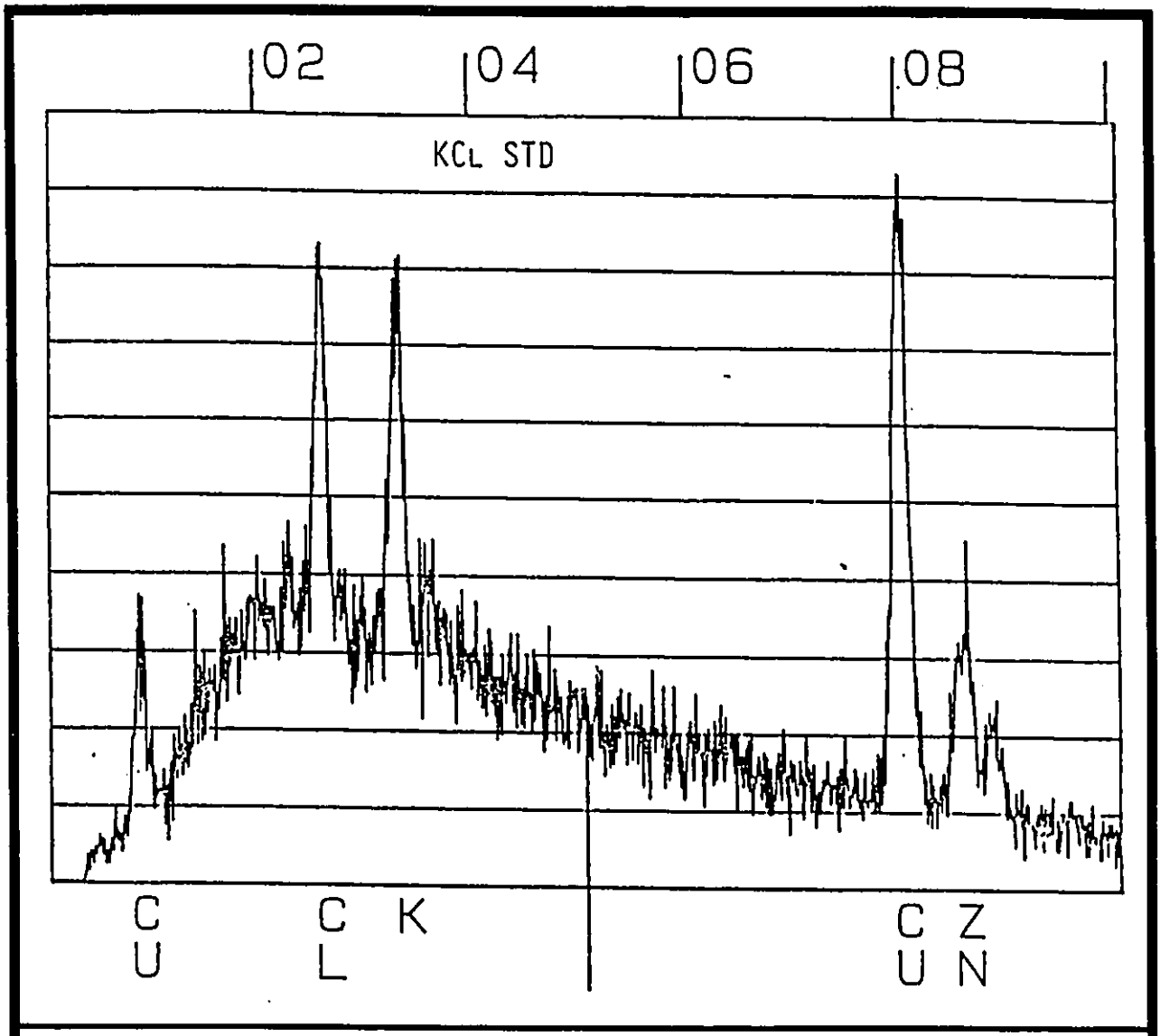

FIGURE 13 : Energy spectrum obtained for KCl (90 mmole/Kg dry weight) in aminoplastic standard

TABLE 2 : Some x-ray energies (eV) from elements of biological interest*

element	shell[1]	eV	element	shell	eV
Cu	Lα	932	U	Mα	3174
Zn	Lα	1014#	K	Kα	3316
Na	Kα	1040	U	Mβ	3340
Mg	Kα	1252	Ca	Kα	3693
Al	Kα	1485	I	Lα	3939
Si	Kα	1739	Ba	Lα	4469
Os	Mα	1913	Ti	Kα	4511
Os	Mβ	1987	La	Lα	4654
P	Kα	2013	Cr	Kα	5414
Pt	Mα	2053	Mn	Kα	5897
Au	Mα	2125	Fe	Kα	6402
Hg	Mα	2199	Ni	Kα	7475
S	Kα	2307	Cu	Kα	8044
Pb	Mα	2349	Zn	Kα	8636
Cl	Kα	2623	Os	Lα	8910
Ag	Lα	2982	Hg	Lα	9988

Legend

* The real biological elements are listed in Table 1.
Some listed here appear as artefacts (e.g. Al & Si).
Some are from the housing, holder or grid (e.g. Cu, Zn, Ag, Ti & Ni).
Some may be included as a stain (e.g. Os, Pb & U), an additive (e.g. Au & Pt) in certain techniques or as a substitute (e.g. I, Ba, La, Cr & Mn).

1 This refers to the electron shells (K, L & M, as in Figure 2) in the atom.

\# For a peak to be visually distinct (resolved), it must be at least 130 eV from its closest neighbour peak. Notice, if the specimen were exposed to Os, the P peak would merge with two Os peaks.

Data taken from EDAX EPIC TABLES-Energy and Wavelength Tables for Elemental X-Ray Emission and Absorption, EDAX Laboratories, Prairie View, Illinois, U.S.A..

The operator is allowed to vary parameters such as the accelerating voltage of the electron beam (High Tension; HT) (KiloVolt; KV), the size of the electron probe (spot), the time of detection (Live sec) and the intensity of the electron beam (count per second; cps). It was learned from preliminary experiments that variations in these parameters can change the energy spectrum quantitatively. It is therefore important to fix these parameters for all readings to permit quantitative analysis using standards (see section 2.2.3.). All electron probe x-ray microanalyses on frozen-dried ultrathin sections (circa 50 nm) were done with the following parameters: HT 80 KV, spot 4 (200 nm of diameter), 200 Live sec and cps between 250 and 800. Myocyte components, such as A-band of sarcomeres, mitochondria and nucleus, and extracellular space of myocardium were probed routinely on each section if seen. Figures 11-14 show typical energy spectra displayed after electron-probe x-ray microanalysis of fast-frozen freeze-dried heart muscle for different myocyte components and the extracellular space of myocardium.

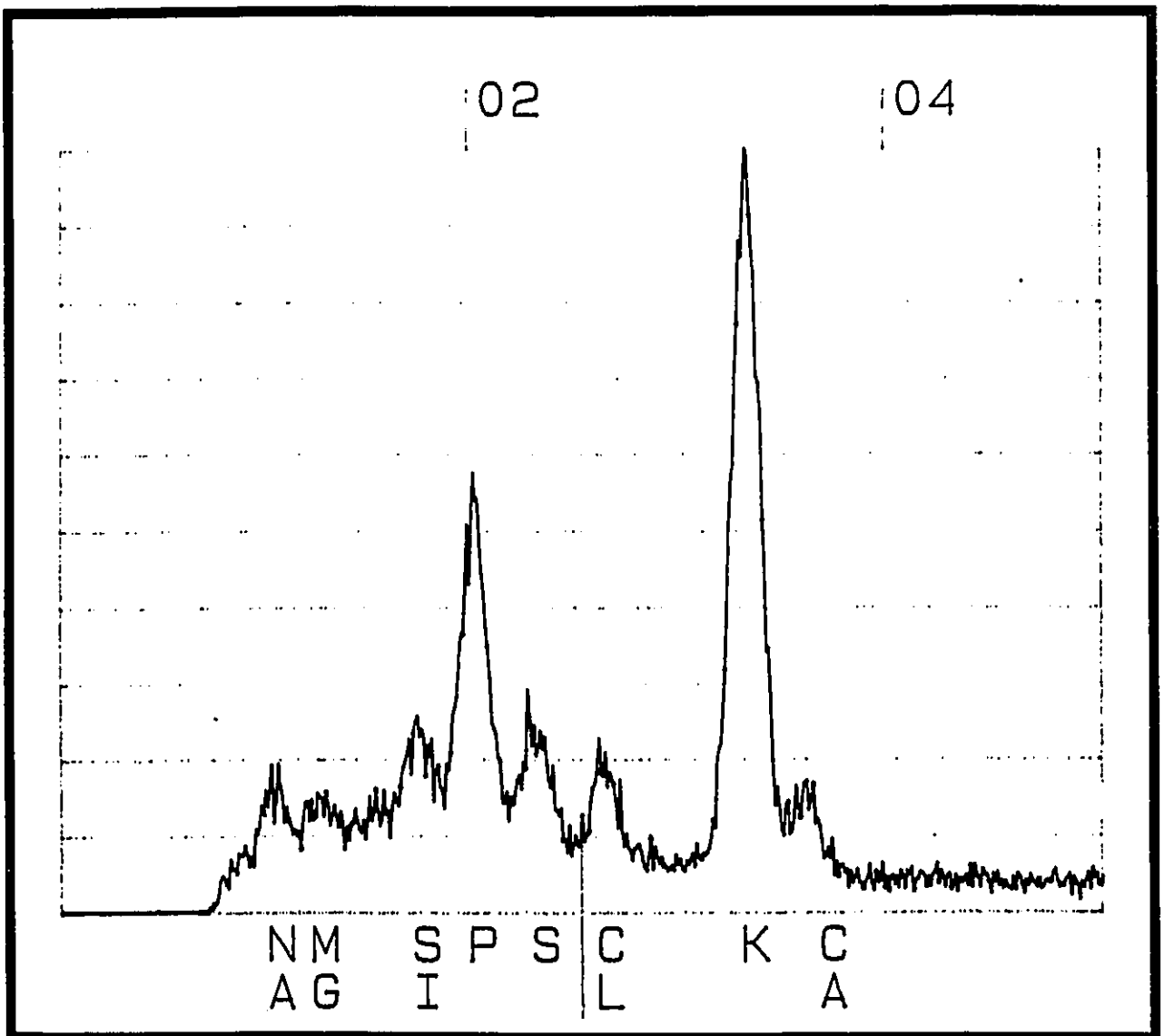

FIGURE 14 : Energy spectrum obtained for an A-band in a myocyte

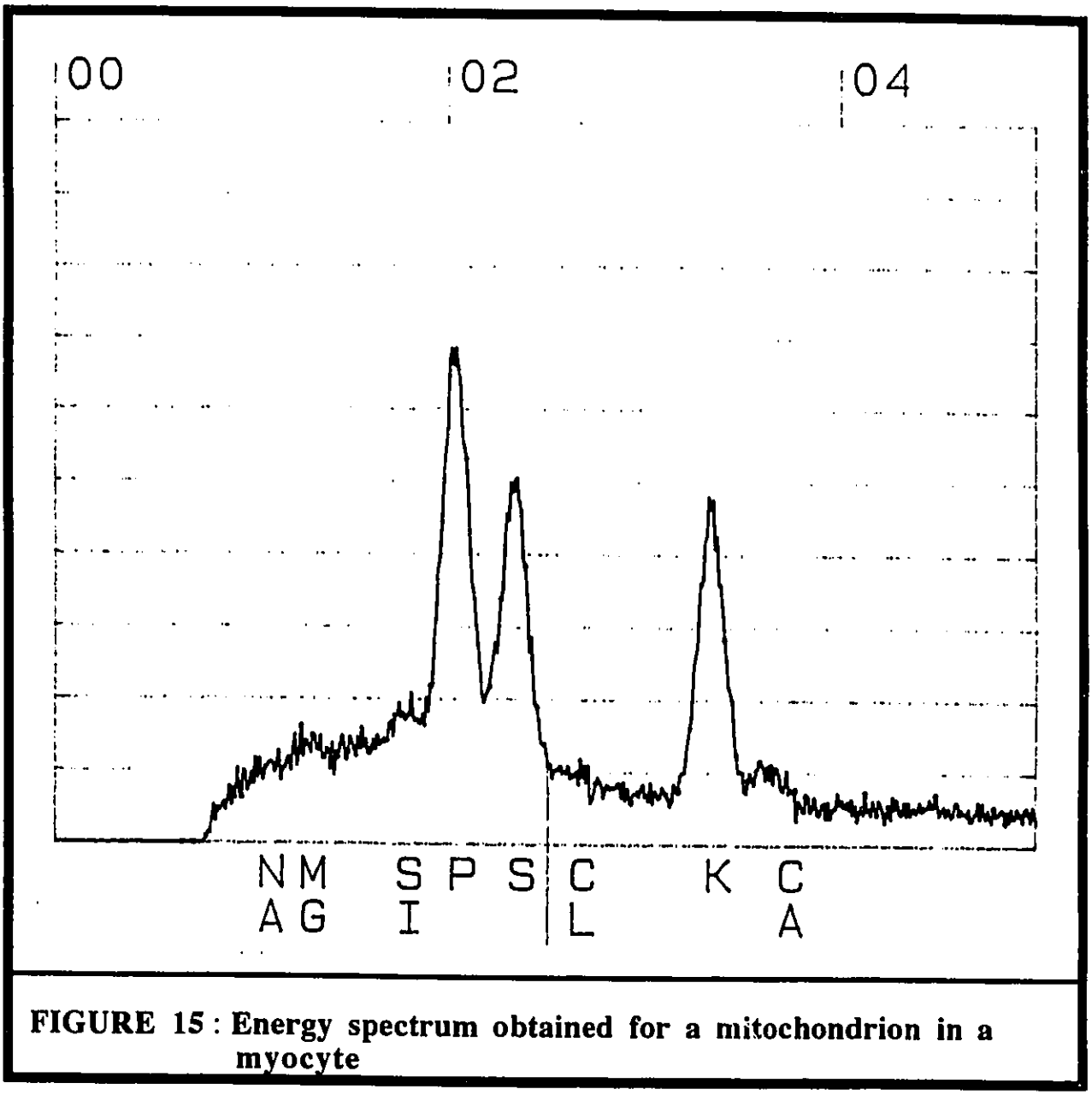

FIGURE 15 : Energy spectrum obtained for a mitochondrion in a myocyte

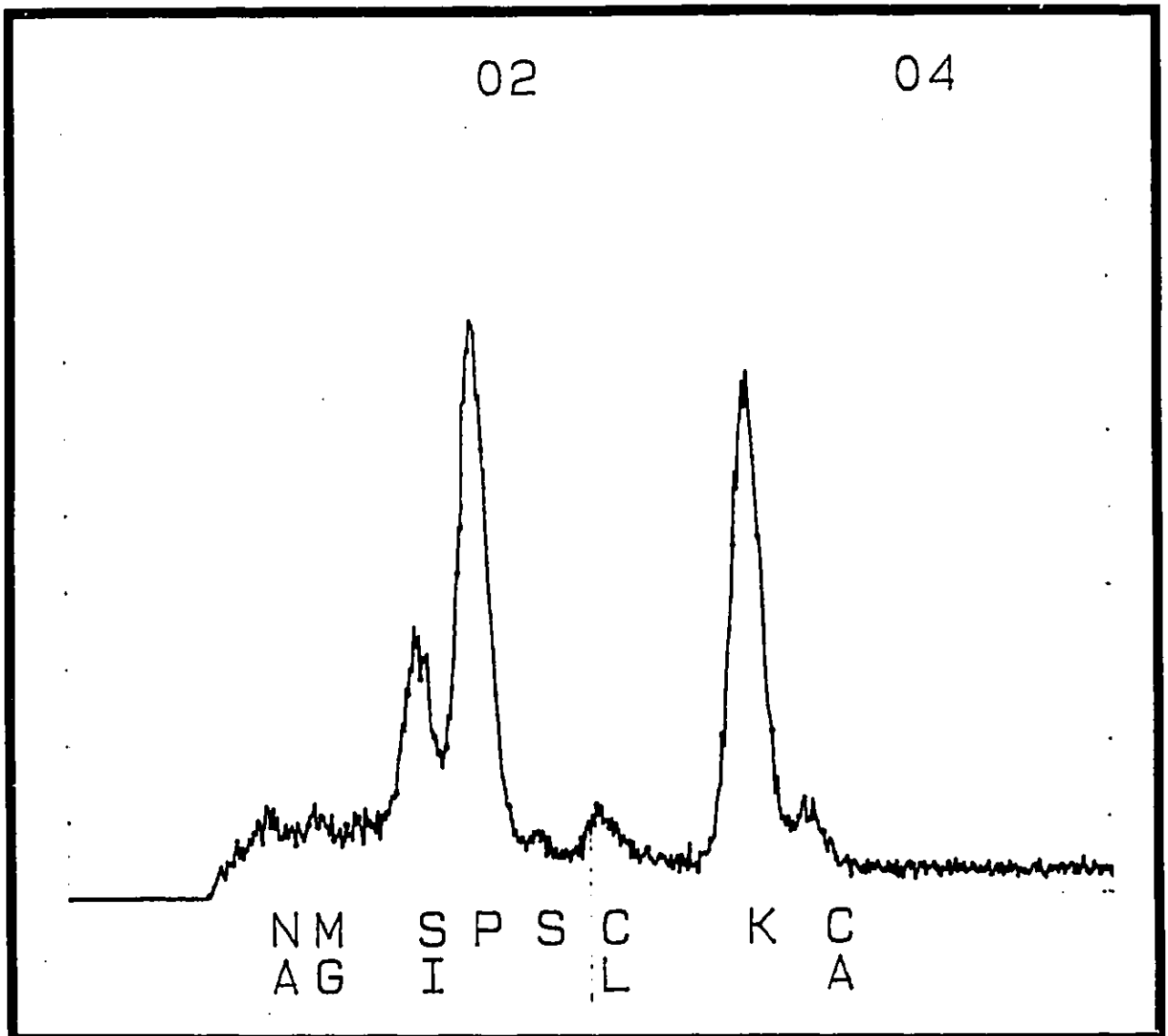

FIGURE 16 : Energy spectrum obtained for a nucleus in a myocyte

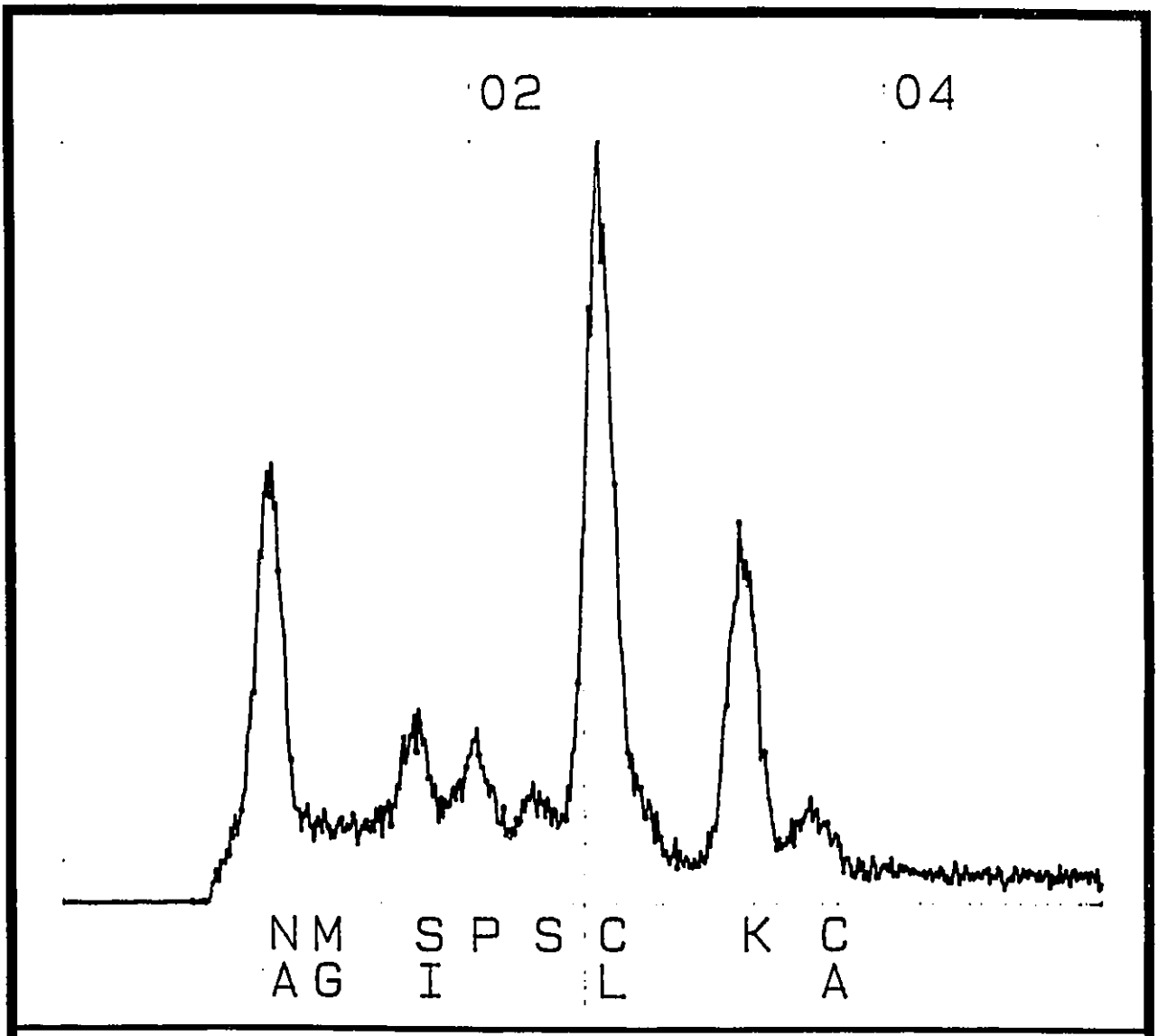

FIGURE 17 : Energy spectrum obtained for an extracellular space in myocardium

2.2.3. QUANTITATIVE ANALYSIS

2.2.3.1. ANALYSIS OF SPECTRAL PEAKS

The energy spectrum is automatically displayed on a monitor while the energies are being collected and counted by the energy dispersive x-ray spectrometers.

If one finds that the elemental peak for phosphorus is twice as high as the calcium elemental peak, one may not conclude that the molar concentration of phosphorus is double that of calcium because the detection efficiency is different for each element. The detector is nearly 100% efficient for energies between about 4.0 KeV and 18.0 KeV. Below 4.0 KeV, the efficiency varies between 50 and 100%. Since mc elements of biological interest generate energies < 4.0 KeV, the detector must alibrated for each element in a biological specimen. A formal quantitative ana. should be done with reference standards as shown in the next sections before concluding on molar ratios of elements within a given specimen.

The x-axis can be scrolled and expanded to permit the centering of an enlarged portion of any segment of the spectrum. For example, the Al peak in Figure 18 is the same Al peak shown in Figure 12. Except now, the x-axis is expanded and the Al peak has been moved into the centre of the screen. From such an expansion, one can readily see that an elemental energy peak (Al in this case) is a Gaussian distribution of a family of energies within precise limits. The base of the ideal Gaussian peak is about 1.8 times the width of the peak at half its height above background. In Figure 18, the width of the peak at half maximal height is shown by the horizontal line labelled FWHM, and the calculated lower and upper limits of the base (1.485 ± 0.9 x FWHM) are 1.370 and 1.610 KeV respectively. The area of the Gaussian curve between such limits is proportional to the content of that element in the specimen.

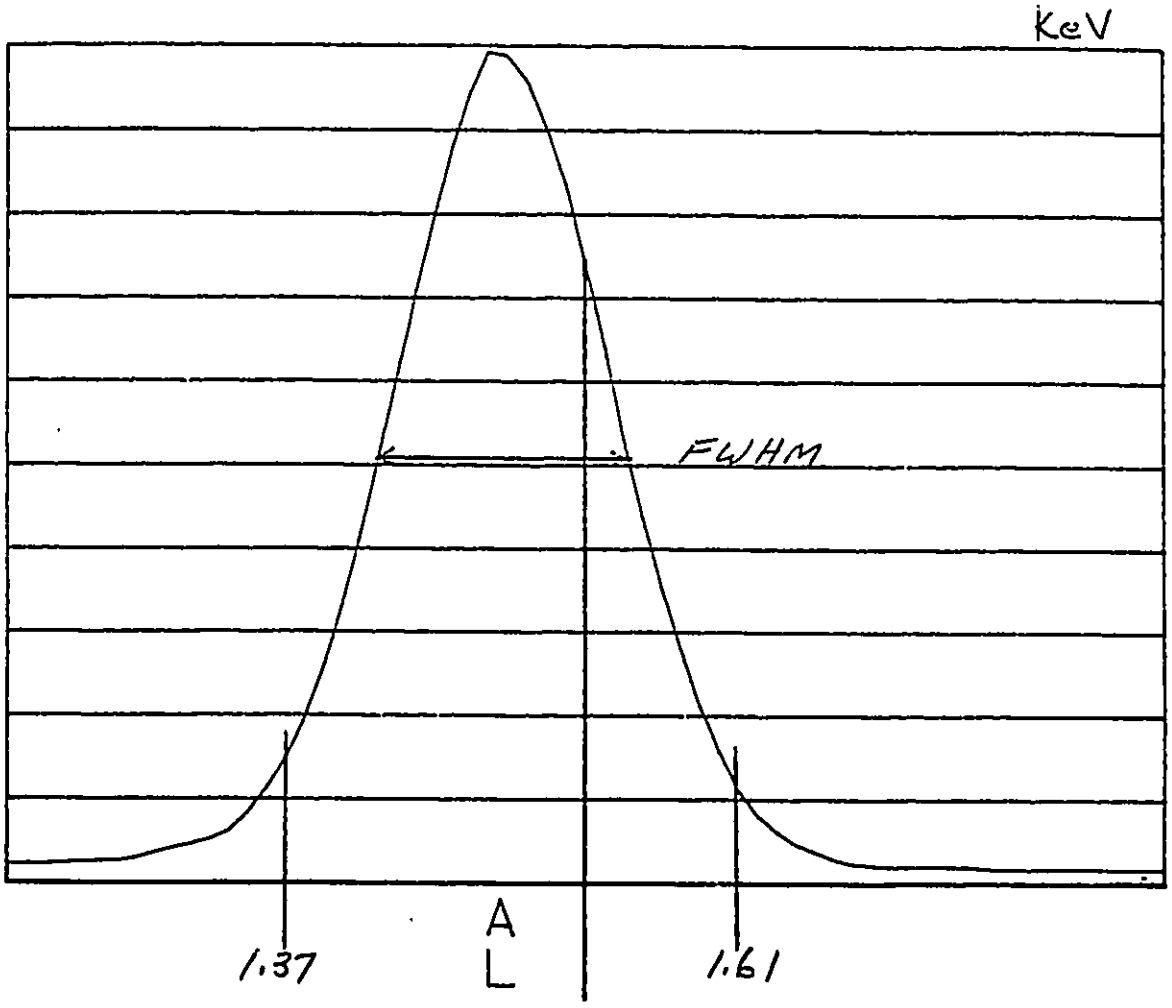

FIGURE 18 : Energy spectra obtained after amplification of peak for Al in Figure 12

The diagram in Figure 19 helps to illustrate the essential areas of a spectrum required for quantitation. Let **P** be the area of a Gaussian peak (as in Figure 18) for a given element having an atomic number > 10, and let **b** be that area of P which belongs to the background (or the continuum). It can be shown that the ratio **P/b** is a measure of the atomic fraction of the element in that portion of the organic specimen which was energized by the primary electron beam (see section 2.2.3.2.).

The SQ program of the EDAX software assists one to obtain **P/b** ratios for any peak (of a spectrum on display) which has been previously identified. Most of the statistical analyses presented in this thesis were done with the **P/b** ratios. Only some of the final **mean P/b**'s were compared to the **P/b**'s of standards, then converted to concentrations using the Hall equation (see next sections).

FIGURE 19 : Diagram of the typical "whale back" shape of the continuum for an organic specimen with a single spectral peak (P) rising out of the continuum

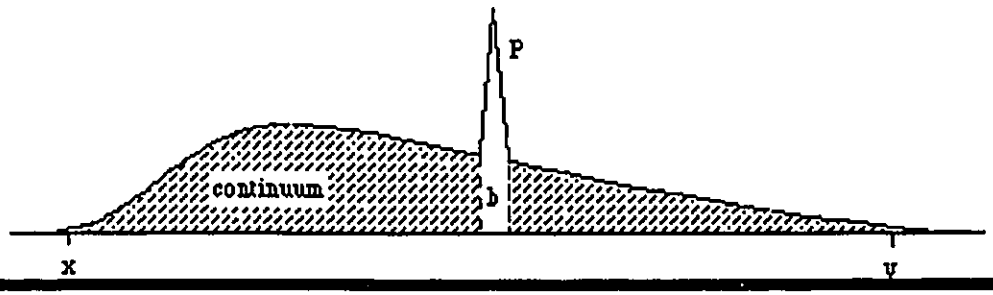

2.2.3.2. HALL EQUATION

Based on the facts that the detected x-ray intensity for an element is proportional to the number of atoms of a given element in a given volume and that the intensity of the white radiation is also proportional to the total number of atoms in this given volume, Hall (Hall et al. 1973) derived an equation to obtain the concentration (C_x) for element x (in mmole/Kg dry weight) from an energy spectrum (as in Figure 19):

$$(C_x)_{sp} = \frac{(I_x/W)_{sp}}{(I_x/W)_{st}} \times \frac{(N_x)_{st}}{(\sum Nz^2)_{st}} \times (A_x)_{sp} \times \overline{(z^2/A)}_{sp} \qquad \text{(equation 1)}$$

Essentially, it relates the ratio **Ix/W** of the specimen (**sp**) to the **Ix/W** ratio of a standard (**st**) which has **similar composition and geometry** as the specimen. The **W** in the ratio refers to the White Radiation or the continuum as illustrated in Figure 19; the I_x refers to the area of the energies making up a peak for a single element. If the **W**'s of the specimen and the standard are similar and if both are ultrathin sections, then it can be shown that the **P/b** ratio defined in section 2.2.3.1. can be substituted for the **Ix/W** ratios in the Hall equation. For the sake of completeness, the remaining terms in the Hall equation are defined as follows: N_x equals the number of x atoms present; $\sum Nz^2$ equals the total number of atoms, weighted by the square of the atomic number z of each atom; A_x is the atomic weight of element x; $\overline{(z^2/A)}_{sp}$ is called the **mean atomic composition**.

Table 3 indicates how one calculates $\overline{(z^2/A)}_{sp}$ for a dried biological specimen from its known (mean) elemental percent composition (excluding Na, Mg, Cl, K & Ca). The calculated value of **3.28** has been routinely used when applying the Hall equation to spectra from ultrathin freeze-dried specimens.

TABLE 3 : $\overline{(z^2/A)}$ for a dried biological specimen

element	z	z^2	A	(z^2/A)	%	$\overline{(z^2/A)}$
H	1	1	1	1	7	0.07
C	6	36	12	3	50	1.50
O	8	64	16	4	25	1.00
N	7	49	14	3.5	16	0.56
S/P*	15.5	240	31.5	7.6	2	0.15
					100	**3.28**

Legend

* For simplicity, Hall (Hall et al. 1973) combined S & P because their z's were similar (15 & 16) and their total content was relatively small.

2.2.3.3. STANDARDS

All the data subscripted with "st" in the Hall equation must come from a standard having a $(\overline{z^2/A})_{st}$ value similar in magnitude to $(\overline{z^2/A})_{sp}$ and with comparable H, C, O and N content. To achieve this, we elected to use the method of Roos and Barnard (1984). Basically, the making of a standard consists of dissolving a salt in a mixture of urea, gluteraldehyde and water. As the water component is permitted to evaporate, spontaneous polymerization between the urea and the gluteraldehyde occurs. The end result is a plastic with $(\overline{z^2/A})_{st}$ having a value of 3.242 (excluding the salt) and with a H, C, O and N content comparable to that listed in Table 3.

Rather than cut sections from plastic blocks, we elected an easier method described by Lupton and Saubermann (1986) that makes thin membranes. We dipped clean 100 mesh grids into the still liquid gluteraldehyde-urea-water-salt solution, drained off the excess by touching filter paper, then stored the grids in a dessicator at ambient temperature for two days to a constant weight. Many of the grid squares of a given grid were covered with a transparent film. The thickness of the film in the squares of a given grid was usually uniform, but the thickness varied from 100 to 400 nm from grid to grid. X-rays collections at different locations on a given film revealed that the salt distribution was as uniform (+/- 5%) as reported by Roos and Barnard (1984) on thin sections.

Table 4 indicates the four salts which were selected and the final molar concentrations for each aminoplastic standard (four per salt). Also listed is the mean P/b value (+/- s.e. & n) for each element (Na, Mg, P, S, Cl, K & Ca) and the $(\overline{z^2/A})_{st}$ value for each standard. The latter data show that $(\overline{z^2/A})_{st}$ increases with increasing concentration of the added salt but not to the extent that it renders itself ineligible as a Hall standard for the freeze-dried biological specimen.

TABLE 4 : Mean P/b values of elements in the aminoplastic standards

$(C_x)_{st}$= $NaH_2PO_4.H_2O$ (mmole/Kg dry weight)

	Na		P			
n	P/b	s.e.	P/b	s.e.	$(C_x)_{st}$	$\overline{(z^2/A)}_{st}$
25	1.31	±0.03	2.51	±0.07	420	3.3635
18	0.58	±0.03	1.37	±0.03	208	3.3180
20	0.33	±0.08	0.77	±0.02	108	3.2960
16	0.18	±0.01	0.50	±0.01	57	3.2754

$(C_x)_{st}$= $MgSO_4.7H_2O$ (mmole/Kg dry weight)

	Mg		S			
n	P/b	s.e.	P/b	s.e.	$(C_x)_{st}$	$\overline{(z^2/A)}_{st}$
20	1.82	±0.07	2.65	±0.12	261	3.3543
9	0.73	±0.03	1.54	±0.03	138	3.3156
10	0.58	±0.04	0.94	±0.07	72	3.2925
15	0.25	±0.01	0.50	±0.02	35	3.2841

$(C_x)_{st}$= KCl (mmole/Kg dry weight)

	K		Cl			
n	P/b	s.e.	P/b	s.e.	$(C_x)_{st}$	$\overline{(z^2/A)}_{st}$
13	6.40	±0.30	4.35	±0.20	676	3.5437
7	3.86	±0.24	2.65	±0.16	338	3.4089
13	2.79	±0.20	1.54	±0.09	179	3.3435
11	1.68	±0.16	1.24	±0.09	90	3.3076

$(C_x)_{st}$= $Ca(NO_3)_2.4H_2O$ (mmole/Kg dry weight)

	Ca			
n	P/b	s.e.	$(C_x)_{st}$	$\overline{(z^2/A)}_{st}$
9	6.81	±0.17	288	3.379
12	3.62	±0.33	146	3.327
9	1.73	±0.09	73	3.300
10	0.94	±0.05	36	3.285

2.3.3.4. CONVERSION TO CONCENTRATION (mmole/Kg dry weight and mmole/Kg water)

Ideally, each unknown P/b value for a specimen should be matched to a known similar P/b value of a standard of similar composition and geometry obtained under the same conditions. If a specimen and a standard have the same composition and geometry, and the same P/b value under the same conditions, then the known concentration of the standard should be the value of the unknown concentration for a specimen. If the P/b's are different, then the standard having P/b value closest to the unknown should be retained and the concentration for the unknown is obtained with the Hall equation. Unfortunately, a breakdown of the EDAX system near the end of this project did not permit us to apply this preferred analytical approach.

The use of a calibration line constructed from several standards is the next best tool for quantitative analysis. If a straight line with a R^2 value > 0.95 is obtained with standards, then, one has the confidence that the line can be applied to the unknown provided that the standards and the unknown have similar compositions and geometries and their P/b's are collected under the same conditions. Table 5 lists the slopes (b) and y-intercepts (a) for each calibration line obtained after applying linear regression analyses to the P/b and (Cx)st data shown in Table 4. The R^2 value for each regression is close to 1.0, indicating high confidence in the assumption that a linear relation exists between P/b and (Cx)st, at least over the range covered by the four standards for each element. However, a prediction of a concentration for K or Cl below 50 mmole/Kg dry weight must be viewed with caution and scepticism because the y-intercepts for both of these linear regressions (i.e. 1.18 for K; 0.7 for Cl) deviate significantly from zero. With reference to normal heart tissue, one should not expect to obtain a reliable quantitative estimation of either extracellular K or intracellular Cl (since both are close to zero).

TABLE 5 : Calibration lines for the aminoplastic standards listed in Table 4

$$(P/b)_{st} = b(C_x)_{st} + a \quad \text{(equation 2)}$$

Element	a	b	R^2
Na	-0.01742	0.00311	0.995
Mg	-0.00386	0.006714	0.962
P	0.1860	0.00556	0.999
S	0.2234	0.00937	0.998
Cl	0.6965	0.00544	0.995
K	1.1834	0.00779	0.993
Ca	0.0990	0.02340	0.999

Legend

(Cx)st is in mmole/Kg dry weight.
If an unknown **(P/b)sp** for a given element falls within the limit of the **P/b**'s (Table 4) used to create the calibration line for that element, then the calibration line may be used to obtain **(Cx)sp** (instead of the Hall equation).

Tables 4 and 5 summarize the mean data from spectra collected when an HT of 20 KV was used to energize the aminoplastic standards. X-rays collected at 20 KV (rather than at 80 KV) are considered more reliable for quantitative analysis because the calibration curves tend to be more linear over a larger range of concentrations and less mass loss can be expected. Unfortunately, to identify cellular components on freeze-dried, unfixed and unstained sections, an electron beam energized with 40 to 60 KV acceleration voltage is required.

An initial protocol involved the identification, focusing and centering of the cellular components at HT 80 KV followed by a 'step down' procedure designed to achieve HT 20 KV without altering the relation between beam and cellular components. This 'step down' procedure depended on an almost perfect optical alignment of the electron microscope Philips 420. It proved to be time consuming just to make routine checks of the optical alignment. However, this protocol was abandoned because the x-ray count at HT 20 for 200 nm beams on ultrathin sections were often below 200 counts per second (i.e. < ten times background) even when the filament emission was maximum. All the P/b's from heart muscle sections in this thesis were therefore obtained from spectra when HT was 80 KV.

Fortunately, our (computer stored) library of spectra from aminoplastic standards contained three series of spectra (for the NaCl, KCl & $Ca(NO_3)_2$ salts) collected at increasing HT's from 20 to 120 KV (data collected by J.A. Hinke). Furthermore, pilot experiments produced readings on five myocardial sites (A-band, mitochondrion and nucleus of myocyte; extracellular space and nucleus of endothelial cell of capillary of myocardium) of freeze-dried ultrathin sections of heart muscle with variation of HT from 20 to 100 KV. Analyses of these data produced the following relations between the P/b's at HT 20 and 80 KV:

$$(P/b)_x^{20} = (P/b)_x^{80} - 60b'_x \qquad \text{(equation 3)}$$

$$b'_x = s_x(P/b)^{80}_x + y_x \qquad \text{(equation 4)}$$

When these equations are inserted into the calibration equation 2 (from Table 5 re-arranged),

$$b(C_x) = (P/b)^{20}_x - a \qquad \text{(equation 5)}$$

the desired relation (equation 6) between (C_X) and $(P/b)_X$ at HT 80 KV is achieved.

$$bC_x = (1 - 60s_x)(P/b)^{80}_x - (60y_x + a) \qquad \text{(equation 6)}$$

The new constants, s_X and y_X for each element x, are listed in Table 6.

Since these constants (s_X and y_X) are regression coefficients (as are b & a), one can calculate the accompanying R^2 values as a measure of reliability of the original data and of the linear fit. Notice that the R^2 values are > 0.90 for the elements in Group 1 (where the data came from 'so-called' homogeneous aminoplastic membrane standards) but less than 0.90 for Group 2 (where the data came from freeze-dried sections of heart muscle). The lower R^2 values in Group 2 might be a reflexion of the heterogeneity in distribution of each element in the different sites probed.

Notice that equation 6 can be written like equation 2 as follows :

$$b''(C_x) = (P/b)^{80}_x - a'' \qquad \text{(equation 7)}$$

where $b'' = [b/(1 - 60s_x)]$ and $a'' = [(60y_x + a)/(1 - 60s_x)]$. This exercise illustrates the consistency of our assumptions in deriving the conversion equations 3 and 4. Equation 6 confirms that we assumed a linear relation between P/b and C_X at 80 KV as we did at 20 KV (equation 2) over the same concentration range.

TABLE 6 : Constants required in the equations which relate the P/b's at HT's 20 and 80 KV

$$(P/b)_x^{20} = (P/b)_x^{80} - 60b'_x \quad \text{(equation 3)}$$

$$b'_x = s_x(P/b)_x^{80} + y_x \quad \text{(equation 4)}$$

	(x)	s_x	y_x	R^2
Group 1				
1	Na	0.0053	0.0031	0.93
2	Cl	0.0060	-0.0053	0.99
3	K	0.0110	-0.0117	0.93
4	Ca	-0.0027	0.0041	0.90
Group 2				
5	Mg	-0.0170	0.0100	0.53
6	P	0.0050	0.0110	0.56
7	S	0.0030	0.0013	0.77

Legend

In Group 1, the linear regressions were done with data from spectra from aminoplastic membrane standards (NaCl, KCl & Ca(N03)2).

In Group 2, the linear regressions were done with data from spectra from five myocardial sites from freeze-dried sections of unperfused heart (cf. text).

The working equation 6 relates $(C_x)_{sp}$ to $(P/b)_x^{80}$ through all derived constants listed in Tables 5 and 6 : a, b, s_x and y_x. The C_x obtained is in mmole/ Kg dry weight. Later, some of these concentrations will be converted to mmole/Kg water by assuming a water content for cytoplasm (i.e. 80%) and a water content for the vascular (extracellular) space (i.e. 93%).

2.2.4. STATISTICAL ANALYSIS

The statistical analysis was done with the software Systat for Macintosh version 5.2. The General Linear Model was used to analyze the probability of statistically significant ($p < 0.05$) difference(s) between groups. The Post Hoc Tukey and Sheffé tests were done on defined independant variable(s) to identify the specific groups that were statistically different.

The analyses were done to answer three questions. First, is there a difference in elemental profiles for the three methods of transfer and freeze-drying? Second, is there heterogeneity for the elemental profiles between extracellular and intracellular spaces and between cellular components? Third, is there a difference in the elemental profiles between unperfused and Langendorff perfused hearts? The legends of Tables 11, 13 & 16 are defining the parameters (fixed factor(s); dependant variable; independant (categorical) variable(s)) used to answer the three questions.

3. RESULTS

3.1. GENERAL PREAMBLE

The elemental profiles from the unperfused (fast-frozen) hearts #1, #3, #4 & #5 were grouped together because they were similar, both qualitatively and quantitatively. Their data were used to compare the different methodologies (section 3.2.), to illustrate composition differences between the extracellular and intracellular spaces and between the cellular components (section 3.3.) and to calculate the concentration of elements in the cellular components and the extracellular space (section 3.4.). Based on the concentrations of the mobile elements (i.e. Na, Cl & K), we consider this group to represent the 'normal' physiological profiles of the myocyte.

The elemental profiles from the Langendorff perfused hearts (#6 & #7) and from the unperfused heart #2 were different, both qualitatively and quantitatively, from the physiological group. We believe these myocytes were in various states of deterioration.

The typical appearance of the freeze-dried, unfixed and unstained ultra-thin section of myocardium is shown in Figure 20. Notice that there is enough contrast to permit one to identify a sarcomere (S) with A- & I-bands and Z-lines; mitochondria (m); an intercalated disk (ID); a nucleus (N); extracellular reticular fibers (RF); a capillary (C) containing erythrocytes (E). Clearly, an electron beam of 200 nm of diameter could easily be positioned over and focused onto an A-band, a mitochondrion or a nucleus.

Figure 21 illustrates that almost every region of a unit sarcomere can be identified even although there is a lack of sharpness compared to a similar micrograph obtained conventionally (i.e. chemically fixed, dehydrated, plastinated and stained).

3.2. COMPARISON OF METHODS OF TRANSFER AND FREEZE-DRYING

The morphology associated with Method I-a (cryotransfer to the electron microscope, freeze-drying in the electron microscope at low temperature, x-rays collection at low temperature) is shown in Figures 22, 23 & 27. It is similar to the morphology obtained with Method 1-b (cryotransfer to the electron microscope, freeze-drying in the electron microscope at low temperature, x-rays collection after warming overnight to ambient temperature) as shown in Figures 24 & 28. On the other hand, the morphology obtained with Method II (cryotransfer to a vacuum chamber, freeze-drying in a vacuum chamber while warming to ambient temperature, transfer and x-rays collection at ambient temperature) is different. As shown in Figures 25 & 26, the myofilaments have a 'fused' or 'melted' look as if the sections had undergone denaturation during the freeze-drying process.

Table 11 is summarizing the statistical analysis of the elemental profiles of Methods I-a, I-b & II presented in Tables 7, 8, 9 & 10. Methods I-a & I-b do not reveal a single statistically significant difference ($p < 0.05$) except for S. Method II reveals also a lower S, but the Si is also found higher. The higher Si may be explained by the introduction of dust on the sections in the vacuum chamber. The lower S in Methods I-b & II might be related to temperature but the exact nature of the change cannot be explained. It is concluded that, except for S, the maintenance of a low temperature after freeze-drying is not found essential for x-rays collection. Also, except for S & Si, the elemental profiles obtained with two different methods of freeze-drying (Methods I-a & II) are found similar.

3.3. QUANTITATIVE PHYSIOLOGICAL ELEMENTAL PROFILES

The P/b's obtained with Method II (Tables 7-10) were converted to elemental concentrations (mmole/Kg dry weight and mmole/Kg water) using the equation 6, the constants listed in Tables 5 & 6 and the assumptions that the water content is 80% inside the myocyte and is 93% in the extracellular space. The calculated concentrations for each element in each cellular component and in the extracellular space are listed in Table 12.

3.4. HETEROGENEITY OF ELEMENTAL PROFILES

The elemental profiles in Tables 7-10 indicate differences between the A-band, the mitochondrion, the nucleus and the extracellular space. Table 13 summarizes the statistical analysis of the elemental P/b's of different sites probed (data from Method II). Statistically significant ($p < 0.05$) differences between the extracellular space and the intracellular compartments are seen for Na, Cl, P, K & Ca. Many statistically significant ($p < 0.05$) differences were also found between the cellular components. For example, P was found to be highest in the nucleus when compared to the mitochondrion and the A-band, and P was found higher in the mitochondrion when compared to the A-band. Also, more K was found in the nucleus when compared to the A-band and the mitochondrion. Interestingly, Na, Mg, Cl & Ca were found to be similar in all three cellular components and Mg was similar in the cellular components and the extracellular space. This, however might be a reflection of the size of the sampling. Nevertheless, Table 13 provides enough evidence to indicate that the extracellular space and each cellular components have their own unique elemental composition.

3.5. UNPERFUSED AND LANGENDORFF PERFUSED HEARTS

Table 14 lists the mean P/b values obtained from excised hearts, Langendorff perfused for 10 minutes before a tissue sample was removed and fast-frozen. Table 15 shows the conversion of P/b's for Langendorff perfused hearts to concentrations in mmole/Kg dry weight and mmole/Kg water. Table 16 summarizes a statistical analysis of data from unperfused hearts (Tables 7, 8, 9 & 10; Method II) and Langendorff perfused hearts (Table 14; Method II). With the exception of Ca in A-band and Ca & P in mitochondrion, notice that the Langendorff perfusion has changed ($p < 0.05$) the elemental composition in the A-band and the mitochondrion. Na & Cl had increased, whereas K, P (A-band only) & Mg had decreased. These changes are compatible with sarcolemmal leakiness.

Although not statistically significant, it appears that Ca had increased in the mitochondrion of the Langendorff perfused myocyte. An influx of Ca into mitochondrion could be responsible for the apparent retention of P by the mitochondrion.

A statistical analysis for the nucleus data would not have been meaningful because of the single result. Nevertheless, it appears that the changes in the one nucleus examined are in the same direction as those seen in the A-band.

When Figures 29 & 30 (Langendorff perfused hearts) are compared to Figures 25 & 26 (unperfused hearts), no appreciable differences in morphology are noted.

3.6. UNPERFUSED HEART #2

Table 17 lists the mean elemental profiles of four sites probed in the myocardium of the #2 rapidly excised unperfused heart. These data were not included in the mean data listed in Tables 7-10, because the Na & Cl levels were clearly elevated and the K level was reduced, indicating increased sarcolemmal permeability similar to Langendorff perfused hearts. There was a suspicion that the cube of heart tissue #2 was rotated 90 degrees before cryofixation. This rotation would allow sections damaged by the razor blade to be sectioned.

3.7. PATHOLOGICAL CHANGES IN MITOCHONDRIA

The mitochondria of some of the myocytes revealed varying amounts of dense dark bodies. The micrographs in Figure 31 is arranged to show the small dark bodies increasing in size and numbers. Table 18 lists the P/b's obtained from the circled areas. Notice how the Ca peak increases as the number and size of the dark bodies increase. It is also noteworthy that the P peak increases as the Ca peak increases.

Since the Na & Cl peaks are elevated, one can conclude that the sarcolemma of these myocytes was excessively permeable to the extracellular ions. No doubt, extracellular Ca also entered in excess and was selectively stored in the mitochondria.

3.8. MORPHOLOGY AND ELEMENTAL PROFILES

With the exception of the presence of small dark bodies in mitochondria (Figure 31), the morphology is not a good predictor of changes in the elemental profiles in this thesis. For examples, ice-crystals clefts (Figures 23 & 26) and the 'melted' appearance (Figures 25 & 26) are not associated with significant changes

in elemental profiles. Also, similar morphologies are associated with different elemental profiles as shown in Figures 25 & 26 compared to Figures 29 & 30 and in Figure 23 compared to Figure 28. These observations suggest that the elemental profile changes may preceed the morphological changes during the development of a pathological state.

FIGURE 20. Electron micrograph (TEM) of the myocardium of a mature rat. Tissue sample was excised in 3 minutes then fast-frozen (< -190°C). An hydrated section (200 nm) was obtained at -120°C. It was transferred(-140°C) to the electron microscope where it was freeze-dried (< -85°C) for 2 hours. No chemical fixative, stain or cryoprotectant was added. ID = intercalated disk; S = sarcomere; f = myofibrils; m = mitochondria; N = nucleus; C = capillary; E = erythrocytes; RF = reticular fibers; straight arrow = compression line; bar = 1.2 μm.

FIGURE 21. Electron micrograph (TEM) of a sarcomere in a myocyte from the myocardium of a mature rat. Tissue sample was excised in 3 minutes then fast-frozen (< -190°C). An hydrated section (200 nm) was obtained at -120°C. It was transferred (-140°C) to the electron microscope where it was freeze-dried (< -85°C) for 2 hours. No chemical fixative, stain or cryoprotectant was added. S = sarcomere; A = A-band; I = I-band; H = H-band; M = M-line; Z = Z-line; m = mitochondria; bar = 0.5 μm.

FIGURE 22. Electron micrograph (TEM) showing sarcomeres and mitochondria in a myocyte from the myocardium of a mature rat (Method I-a). Tissue sample was excised in 3 minutes then fast-frozen (< -190°C). An hydrated section (200 nm) was obtained at -120°C. It was transferred (-140°C) to the electron microscope where it was freeze-dried (< -85°C) for 2 hours. No chemical fixative, stain or cryoprotectant was added. S = sarcomere; A = A-band; I = I-band; Z = Z-line; m = mitochondria; t = t-tubule; straight arrow = compression line; bar = 0.5 μm. Letters f and m pinpoint where a 0.2 μm electron beam was focused (consecutively) for 200 Live sec to generate x-ray spectra from an A-band and from a mitochondrion from which P/b ratios were obtained:

	Na	Mg	Si	P	S	Cl	K	Ca
A-band :	.418	.389	.565	4.868	3.980	.463	7.086	.384
mitochondrion :	.606	.359	.922	3.958	3.364	2.619	17.291	.336

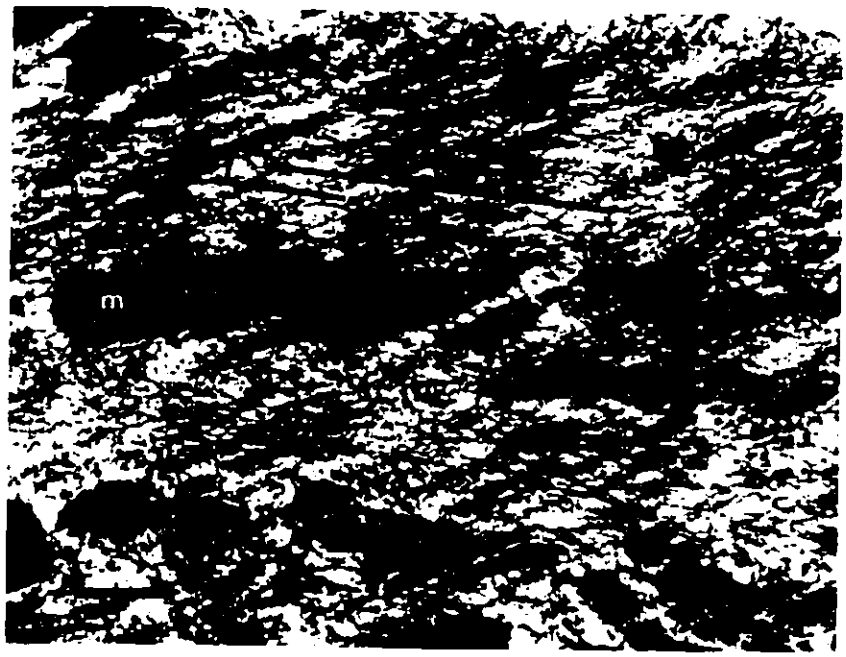

FIGURE 23. Electron micrograph (TEM) showing sarcomeres and mitochondria in a myocyte from the myocardium of a mature rat (Method I-a). Preparation of the freeze-dried cryosection was as outlined in legend to Figure 22. The letters and signs have the same significance as in Figure 22. The apparent vacuolization of the sarcomeres actually indicates the formation of ice crystals (the curved arrow points to a space occupied previously by an ice crystal). Letters f and m pinpoint where a 0.2 μm electron beam was focused (consecutively) for 200 Live sec to generate x-ray spectra from an A-band and from a mitochondria from which P/b ratios were obtained:

	Na	Mg	Si	P	S	Cl	K	Ca
A-band :	.438	.364	1.975	3.303	1.940	1.804	10.445	.254
mitochondrion :	.309	.265	1.164	5.820	3.167	1.063	7.334	.302

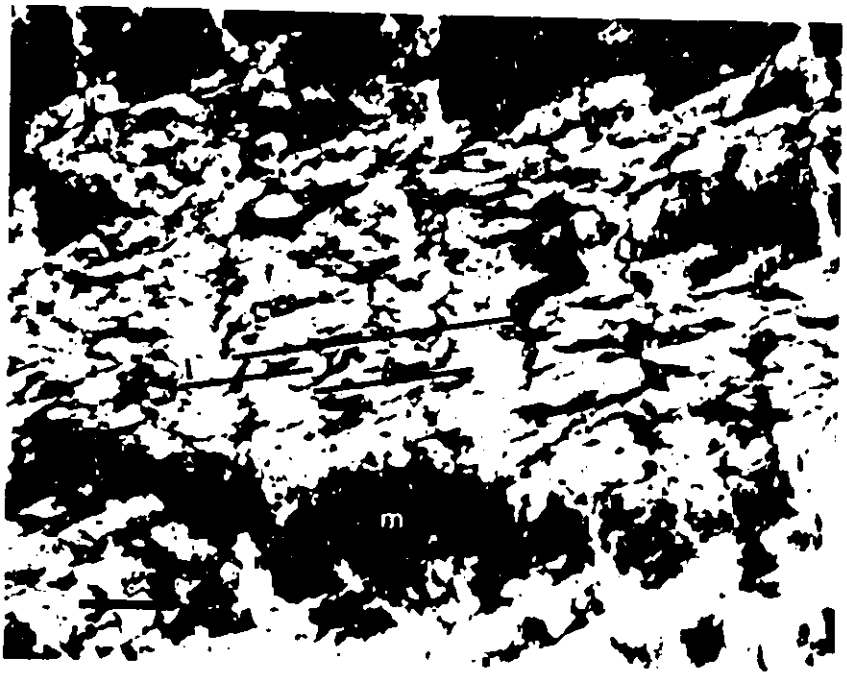

FIGURE 24. Electron micrograph (TEM) showing sarcomeres and mitochondria in a myocyte from the myocardium of a mature rat (Method I-b). Preparation of the freeze-dried cryosection was as outlined in legend to Figure 22. The only change in the protocol was that the freeze-dried section was permitted to warm-up at ambient temperature while in the electron microscope overnight. The letters and signs have the same significance as in Figures 22 & 23. Letters f and m pinpoint where a 0.2 μm electron beam was focused (consecutively) for 200 Live sec to generate x-ray spectra from an A-band and from a mitochondrion from which P/b ratios were obtained:

	Na	Mg	Si	P	S	Cl	K	Ca
A-band :	.721	.525	1.076	4.513	.717	2.401	20.264	.037
mitochondrion :	.603	1.407	2.345	11.104	1.789	1.244	12.742	.098

FIGURE 25. Electron micrograph (TEM) showing sarcomeres and mitochondria in a myocyte from the myocardium of a mature rat (Method II). Preparation of the cryosections was as outlined in Figure 22 except that the section was freeze-dried and warmed to ambient temperature in a vacuum chamber. Notice the apparent 'melting' of filaments and the loss of contrast (compare to Figure 22). Letters and signs have the same significance as in Figures 22 & 23. Letters f and m pinpoint where a 0.2 μm electron beam was focused (consecutively) for 200 Live sec to generate x-ray spectra from an A-band and from a mitochondrion from which P/b ratios were obtained:

	Na	Mg	Si	P	S	Cl	K	Ca
A-band :	.338	.474	3.873	3.605	3.171	.997	13.748	.225
mitochondrion :	.195	.404	2.219	6.243	3.497	.867	7.659	.149

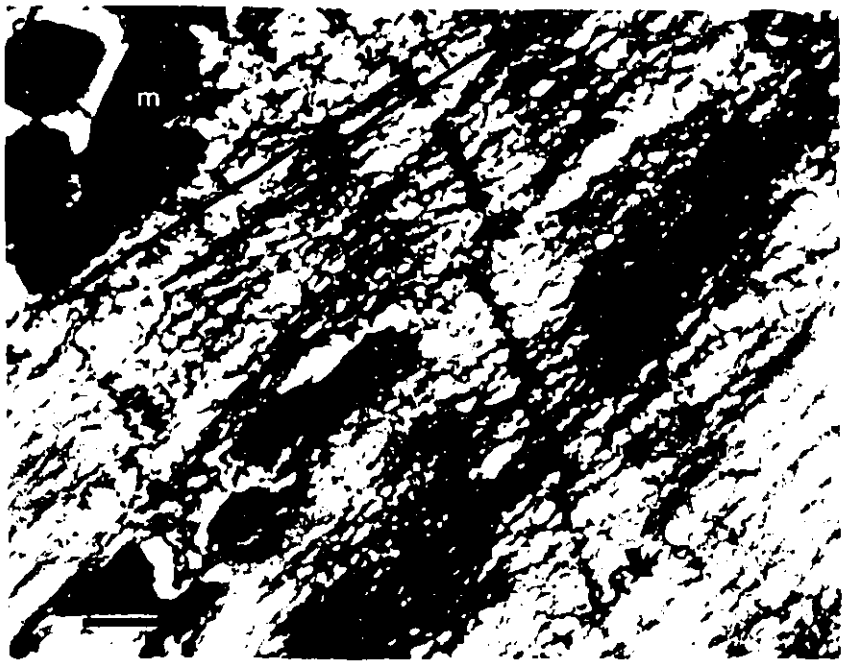

FIGURE 26. Electron micrograph (TEM) showing sarcomeres and mitochondria in a myocyte from the myocardium of a mature rat (Method II). Like Figure 25, this section was freeze-dried and warmed to ambient temperature in a vacuum chamber. Unlike Figure 25, considerable ice-crystals were present (curved arrow points to a defect produced by one ice crystal). The 'melting' appearance is less obvious. Letters and signs have the same significance as in Figures 22 & 23. Letters f and m pinpoint where a 0.2 μm electron beam was focused (consecutively) for 200 Live sec to generate x-ray spectra from an A-band and from a mitochondrion from which P/b ratio were obtained:

	Na	Mg	Si	P	S	Cl	K	Ca
A-band :	.443	.493	6.417	4.104	.817	1.073	12.802	.365
mitochondrion :	.339	.451	3.337	6.999	2.086	.770	9.984	.316

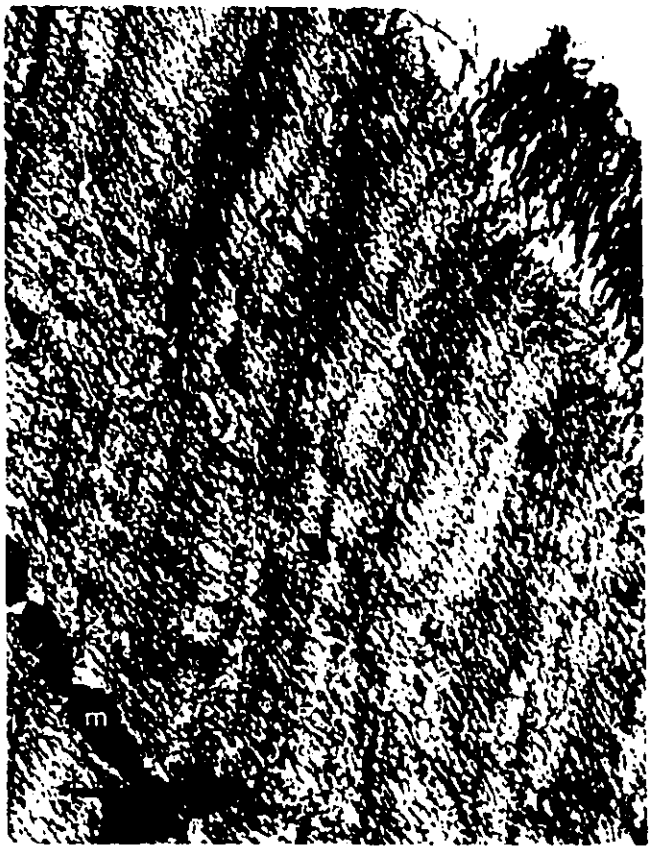

FIGURE 27. Electron micrograph (TEM) showing sarcomeres and mitochondria in a myocyte from the myocardium of a mature rat (Method I-a). Like Figure 22, this section was never permitted to warm-up and was freeze-dried in the electron microscope. The myofibrils reveal morphological disruption, but the filaments remain distinct. Unlike Figure 25 & 26, the melting phenomenon is absent. Letters and signs have the same significance as in Figures 22 & 23. RF = reticular fibers.

FIGURE 28. Electron micrograph (TEM) showing the section in Figure 27 after warming-up to ambient temperature in the electron microscope overnight (Method I-b). No appreciable change is seen. Letters f and m pinpoint where a 0.2 μm electron beam was focused (consecutively) for 200 Live sec to generate x-ray spectra from an A-band and from a mitochondrion from which P/b ratios were obtained :

	Na	Mg	Si	P	S	Cl	K	Ca
A-Band :	2.154	.108	1.797	3.194	2.003	7.008	8.580	.268
Mitochondrion :	1.395	.283	2.025	4.787	2.348	5.048	7.839	.339

FIGURE 29. Electron micrograph (TEM) showing sarcomeres and mitochondria in a myocyte from the myocardium of a Langendorff perfused heart. Like Figure 25, this cryosection was freeze-dried and warmed to ambient temperature in a vacuum chamber. Notice again the 'melting' of filaments and the loss of contrast. Letters and signs have the same significance as in Figures 22 & 23. Letters f and m pinpoint where a 0.2 μm electron beam was focused (consecutively) for 200 Live sec to generate x-ray spectra from an A-band and from a mitochondrion from which P/b ratios were obtained:

	Na	Mg	Si	P	S	Cl	K	Ca
A-band :	1.485	.206	2.522	3.182	3.300	7.069	11.060	.401
mitochondrion :	.833	.088	1.589	6.181	2.504	4.482	8.427	.329

FIGURE 30. Electron micrograph (TEM) showing sarcomeres and mitochondria in a myocyte from the myocardium of a Langendorff perfused heart. Like Figure 29, this cryosection was freeze-dried and warmed to ambient temperature in a vacuum chamber. Notice again the 'melting' of filaments and the loss of contrast. Letters and signs have the same significance as in Figures 22 & 23. Letters f and m pinpoint where a 0.2 μm electron beam was focused (consecutively) for 200 Live sec to generate x-ray spectra from an A-band and from a mitochondrion from which P/b ratios were obtained:

	Na	Mg	Si	P	S	Cl	K	Ca
A-band:	.932	.158	2.272	3.199	2.184	4.912	8.464	.401
mitochondrion:	1.076	.134	1.315	5.269	1.461	5.861	6.897	.444

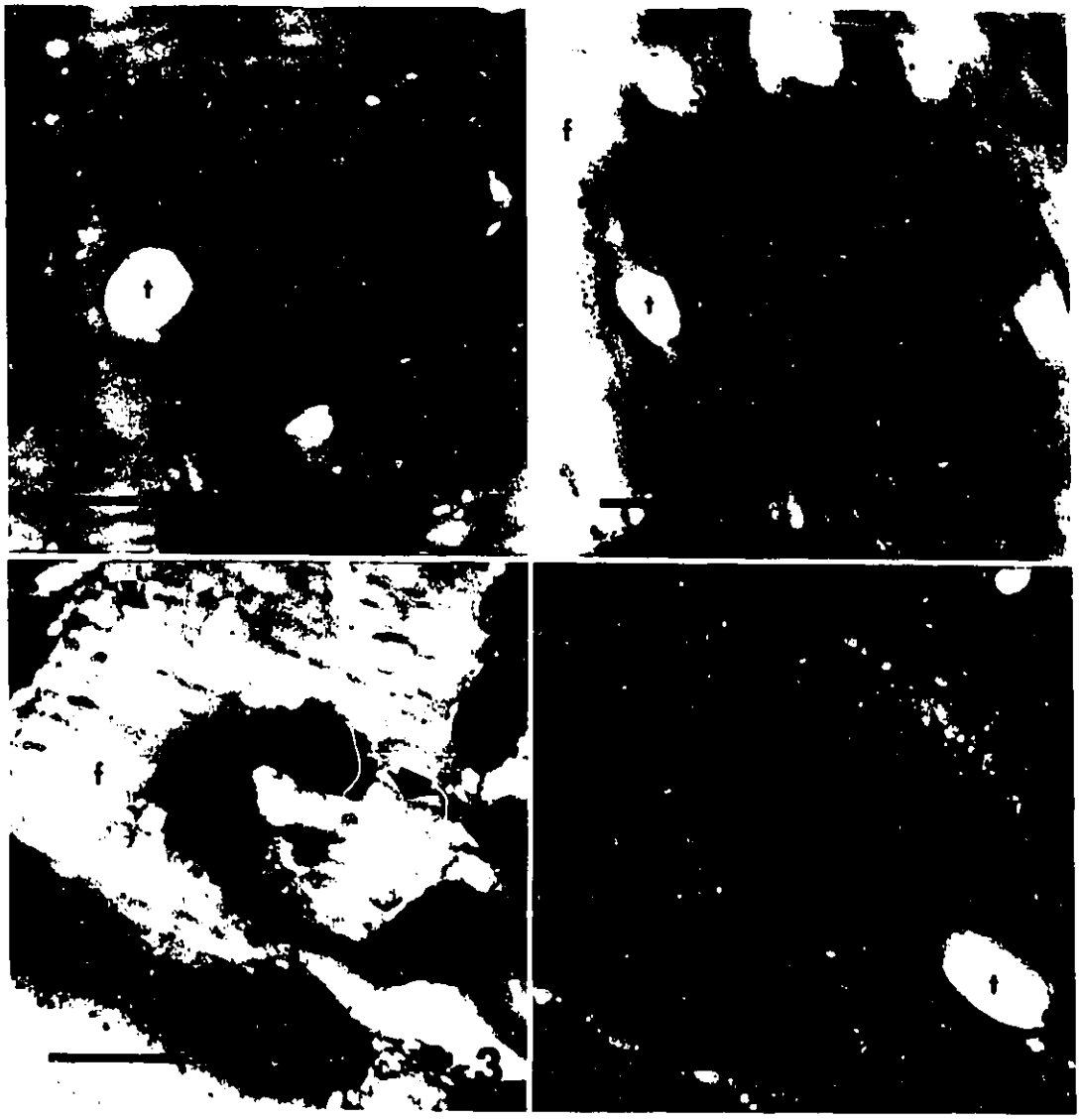

FIGURE 31 (31-1, 31-2, 31-3 & 31-4). Electron micrographs (TEM) of oblique sections of myofibrils (f) and mitochondria (dark areas) in myocytes from the myocardium of a mature rat. Figures 31-1, -2 & -4 are from Langendorff perfused hearts; Figure 31-3 is from an unperfused heart. All cryosections were freeze-dried and warmed to ambient temperature in a vacuum chamber. Notice the small dark bodies inside the mitochondria. They increase in size and number from 31-1 to 31-4. The letters and signs have the same significance as in Figures 22 & 23. The circle over each micrograph indicates the area over which the electron beam was focused for 200 Live sec to generate an x-ray spectrum from which P/b ratios were obtained (Table 18).

TABLE 7 : The elemental profile from the A-band of sarcomeres of myocytes (mean P/b from different methods of transfer and freeze-drying of cryosections)

		Element							
		Na	Mg	Si	P	S	Cl	K	Ca
	Method I-a (n=5)								
	Mean P/b	.757	.418	2.145	3.967	3.160	2.054	13.880	.459
M	s.d.	.230	.074	1.606	1.059	1.401	.227	3.215	.039
e	s.e.	.103	.033	.718	.474	.627	.102	1.438	.017
t	Method I-b (n=10)								
h	Mean P/b	.495	.378	1.425	4.850	2.415	3.419	16.538	.373
o	s.d.	.124	.086	.831	2.140	1.673	2.057	2.545	.132
d	s.e.	.039	.027	.263	.677	.529	.650	.805	.042
	Method II (n=11)								
	Mean P/b	.496	.454	5.042	4.250	1.500	1.385	14.566	.360
	s.d.	.194	.166	1.346	1.201	.886	.673	4.485	.123
	s.e.	.058	.050	.406	.362	.267	.203	1.292	.037

Legend

Method I-a = cryotransfer; freeze-drying in electron microscope at low temperature; x-rays collection at low temperature.
Method I-b = cryotransfer; freeze-drying in electron microscope at low temperature; x-rays collection after warming to ambient temperature.
Method II = freeze-drying in vacuum chamber while warming to ambient temperature; transfer and x-rays collection at ambient temperature.
The data were obtained from four unperfused hearts (#1, #3, #4 & #5).

TABLE 8 : The elemental profile from the mitochondrion of myocytes (mean P/b from different methods of transfer and freeze-drying of cryosections)

		Element							
		Na	Mg	Si	P	S	Cl	K	Ca
Method	Method I-a (n=3)								
	Mean P/b	.284	.365	1.062	5.867	4.259	.705	6.560	.378
	s.d.	.032	.136	.209	.617	.925	.300	.455	.080
	s.e.	.018	.079	.121	.356	.534	.173	.263	.046
	Method I-b (n=11)								
	Mean P/b	.319	.356	1.568	6.504	3.471	1.251	8.390	.314
	s.d.	.106	.121	1.056	.892	1.760	.392	1.544	.075
	s.e.	.032	.036	.318	.269	.531	.118	.466	.023
	Method II (n=9)								
	Mean P/b	.363	.386	3.292	6.549	1.964	1.031	9.941	.298
	s.d.	.191	.063	1.113	.965	.877	.498	3.505	.123
	s.e.	.064	.021	.371	.322	.292	.166	1.168	.041

Legend

Method I-a = cryotransfer; freeze-drying in electron microscope at low temperature; x-rays collection at low temperature.
Method I-b = cryotransfer; freeze-drying in electron microscope at low temperature; x-rays collection after warming to ambient temperature.
Method II = freeze-drying in vacuum chamber while warming to ambient temperature; transfer and x-rays collection at ambient temperature.
The data were obtained from four unperfused hearts (#1, #3, #4 & #5).

TABLE 9 : The elemental profile from the nucleus of myocytes (mean P/b from different methods of transfer and freeze-drying of cryosections)

		Element							
		Na	Mg	Si	P	S	Cl	K	Ca
Method	Method I-a (n=2)								
	Mean P/b	.374	.438	1.539	7.042	3.705	1.260	14.550	.537
	s.d.	.049	.203	.141	2.022	1.165	.090	1.537	.011
	s.e.	.035	.144	.100	1.430	.824	.064	1.087	.008
	Method I-b (n=7)								
	Mean P/b	.764	.338	2.967	8.175	1.777	2.234	18.461	.328
	s.d.	.488	.051	1.664	2.196	.802	1.182	4.672	.075
	s.e.	.184	.019	.629	.830	.303	.447	1.766	.028
	Method II (n=9)								
	Mean P/b	.270	.550	4.516	9.511	.753	1.116	21.552	.374
	s.d.	.094	.196	2.008	1.643	.578	.241	5.671	.128
	s.e.	.031	.065	.669	.548	.193	.080	1.890	.043

Legend

Method I-a = cryotransfer; freeze-drying in electron microscope at low temperature; x-rays collection at low temperature.
Method I-b = cryotransfer, freeze-drying in electron microscope at low temperature; x-rays collection after warming to ambient temperature.
Method II = freeze-drying in vacuum chamber while warming to ambient temperature; transfer and x-rays collection at ambient temperature.
The data were obtained from four unperfused hearts (#1, #3, #4 & #5).

TABLE 10 : The elemental profile from the extracellular space of myocardium (mean P/b from different methods of transfer and freeze-drying of cryosections)

		Element							
		Na	Mg	Si	P	S	Cl	K	Ca
Method	Method I-a (n=2)								
	Mean P/b	4.573	.273	1.706	1.355	2.626	11.964	5.912	.670
	s.d.	.953	.028	.344	.399	.768	4.859	1.762	.069
	s.e.	.674	.020	.243	.282	.543	3.436	1.246	.049
	Method I-b (n=4)								
	Mean P/b	4.021	.437	3.436	1.534	1.606	8.397	6.617	.703
	s.d.	1.247	.262	2.594	.189	.785	3.061	2.080	.128
	s.e.	.624	.131	1.297	.095	.393	1.531	1.040	.064
	Method II (n=4)								
	Mean P/b	5.160	.324	4.932	1.396	.968	12.301	8.048	.793
	s.d.	1.238	.025	.718	.489	.211	3.616	2.992	.174
	s.e.	.619	.013	.359	.245	.106	1.808	1.496	.087

Legend

Method I-a = cryotransfer; freeze-drying in electron microscope at low temperaure; x-rays collection at low temperature.
Method I-b = cryotransfer; freeze-drying in electron microscope at low temperature; x-rays collection after warming to ambient temperature.
Method II = freeze-drying in vacuum chamber while warming to ambient temperature; transfer and x-rays collection at ambient temperature.
The data were obtained from four unperfused hearts (#1, #3, #4 & #5).

TABLE 11 : Statistical analysis of P/b's obtained with different methods of transfer and freeze-drying of cryosections (Tables 7, 8, 9 & 10)

	Element							
	Na	Mg	Si	P	S	Cl	K	Ca
Statistical analysis								
General Linear Model (p)	NS	NS	<.0001	NS	<.0001	NS	NS	NS
Tukey tests (p)								
Methods I-a - I-b	NS	NS	NS	NS	<.04	NS	NS	NS
Methods I-a - II	NS	NS	<.0001	NS	<.0001	NS	NS	NS
Methods I-b - II	NS	NS	<.0001	NS	<.002	NS	NS	NS
Scheffé tests (p)								
Methods I-a - I-b	NS	NS	NS	NS	=.05	NS	NS	NS
Methods I-a - II	NS	NS	<.0001	NS	<.0001	NS	NS	NS
Methods I-b - II	NS	NS	<.0001	NS	<.002	NS	NS	NS

Legend

p = probability that the methods are similar; NS = non-significant ($p > 0.05$) difference.

The General Linear Model statistical analysis was done with the following parameters: data from unperfused hearts #1, #2, #3 & #5; independant variable #1 = Method (I-a, I-b & II); independant variable #2 = site probed (A-band, mitochondrion, nucleus, extracellular space); dependant variable = P/b reading (n = 77). The Post Hoc tests (Tukey and Scheffé) were done with the independant variable #1.

Three assumptions were made: the P/b's for a given element have a parametric distribution; the four hearts used have similar elemental profiles; the section obtained from a single heart have similar elemental profiles.

TABLE 12 : Elemental concentrations in the myocyte components and the extracellular space of the unperfused heart (from P/b's of Tables 7-10; Method II)

		Element						
		Na	Mg	P	S	Cl	K	Ca
Site Probed	**A-Band**							
	mmole/Kg dw*	54.5	47.8	383	99.1	93.4	574	3.13
	mmole/Kg w°	14	12	96	25	23	144	0.8
	Mitochondrion							
	mmole/Kg dw	25.4	27.3	672	140	51.7	372	0.06
	mmole/Kg w	6	7	168	35	13	93	0.014
	Nucleus							
	mmole/Kg dw	5.0	76.7	1045	33.7	61.7	879	3.83
	mmole/Kg w	1.2	19	261	8	15	220	1.0
	E.C.S.							
	mmole/Kg dw	1081	8.7	23.6	52.5	1378	289	24.6
	mmole/Kg w	81	0.7	1.8	4.0	104	22	1.8

Legend

dw = dry weight; w = water; E.C.S. = extracellular space.

* Obtained from equations 2, 3 & 6 using the constants listed in Tables 5 and 6.

° To convert to mmole/Kg water, the water content was assumed: 80% in the A-band, the mitochondrion and the nucleus; 93% in the extracellular space.

TABLE 13 : Statistical analysis of elemental P/b's obtained from four sites probed in the myocardium of unperfused heart (from P/b's of Tables 7-10; Method II)

	Element							
	Na	Mg	Si	P	S	Cl	K	Ca
Statistical analysis								
General Linear Model (p)	<.0001	NS	NS	<.0001	<.02	<.0001	<.0001	<.0001
Tukey tests (p)								
A-band-mitochondrion	NS	NS	NS	<.003	NS	NS	NS	NS
A-band-nucleus	NS	NS	NS	<.0001	NS	NS	<.01	NS
A-band-E.C.S.	<.0001	NS	NS	<.003	NS	<.0001	NS	<.0001
Mitochondrion-nucleus	NS	NS	NS	<.0001	<.02	NS	<.0001	NS
Mitochondrion-E.C.S.	<.0001	NS	NS	<.0001	NS	<.0001	NS	<.0001
Nucleus-E.C.S.	<.0001	NS	NS	<.0001	NS	<.0001	<.0001	<.0001
Scheffé tests (p)								
A-band-mitochondrion	NS	NS	NS	<.004	NS	NS	NS	NS
A-band-nucleus	NS	NS	NS	<.0001	NS	NS	<.02	NS
A-band-E.C.S.	<.0001	NS	NS	<.006	NS	<.0001	NS	<.0001
Mitochondrion-nucleus	NS	NS	NS	<.0001	<.03	NS	<.0001	NS
Mitochondrion-E.C.S.	<.0001	NS	NS	<.0001	NS	<.0001	NS	<.0001
Nucleus-E.C.S.	<.0001	NS	NS	<.0001	NS	<.0001	<.0001	<.0001

Legend

p = probability that the sites are similar; NS = non-significant ($p > 0.05$) difference; E.C.S. = extracellular space.
The General Linear Model statistical analysis was done with the following parameters: data of unperfused hearts #1, #2, #3 & #5 (Tables 7, 8, 9 & 10; data from Method II); independant variable #1 = site probed (A-band, mitochondrion, nucleus, extracellular space); dependant variable = P/b reading (n = 33). The Post Hoc tests (Tukey and Scheffé) were done with the independant variable #1.
Three assumptions were made: the P/b's for a given element have a parametric distribution; the four hearts used have similar elemental profiles; the sections obtained from a single heart have similar elemental profiles.

TABLE 14 : Mean elemental profiles from the myocyte components of the Langendorff perfused heart

Component		Element							
		Na	Mg	Si	P	S	Cl	K	Ca
Component	A-band (n=11)								
	Mean P/b	1.318	.174	2.633	2.784	2.192	5.972	8.006	.376
	s.d.	.303	.061	.514	1.036	.703	1.686	2.473	.111
	s.e.	.091	.018	.155	.312	.212	.508	.746	.033
	Mitochondrion (n=11)								
	Mean P/b	.981	.145	1.643	6.359	1.965	4.551	6.083	1.608
	s.d.	.399	.052	.254	1.225	.753	2.106	1.634	2.550
	s.e.	.120	.016	.080	.369	.227	.635	.493	.769
	Nucleus (n=1)								
	Mean P/b	1.654	.361	2.228	4.700	1.641	8.631	8.602	.340

Legend

The data were obtained from Langendorff perfused hearts (#6 & #7).

TABLE 15 : Elemental concentrations of the myocyte components of the Langendorff perfused heart (from the P/b's of Table 14)

		Element						
		Na	**Mg**	**P**	**S**	**Cl**	**K**	**Ca**
Component	**A-Band** mmole/Kg dw	235	-36	198	160	633	288	3.9
	Mitochondrion mmole/Kg dw	161	-45	648	140	466	204	65
	Nucleus mmole/Kg dw	308	20	440	111	946	314	2.1

Legend

dw = dry weight.

The elemental concentration in mmole/Kg dry weight was obtained as in Table 12.

TABLE 16 : Statistical analysis comparing unperfused (#1, #2, #3 & #4; Tables 7-8) and Langendorff perfused (#6 & #7; Table 13) hearts

	Element					
	Na	Mg	P	Cl	K	Ca
Statistical analysis						
General Linear Model (p)						
A-band + mitochondrion	<.0001	<.0001	<.03	<.0001	<.0001	NS
A-band	<.0001	<.0001	<.01	<.0001	<.0001	NS
Mitochondrion	<.0001	<.0001	NS	<.0001	<.005	NS
Tukey tests (p)						
A-band + mitochondrion	<.0001	<.0001	<.03	<.0001	<.0001	NS
A-band	<.0001	<.0001	<.01	<.0001	<.0001	NS
Mitochondrion	<.002	<.0001	NS	<.0001	<.01	NS
Scheffé tests (p)						
A-band + mitochondrion	<.0001	<.0001	<.03	<.0001	<.0001	NS
A-band	<.0001	<.0001	<.01	<.0001	<.0001	NS
Mitochondrion	<.0001	<.0001	NS	<.0001	<.005	NS

Legend

p = probability that unperfused and Langendorff perfused hearts are similar; NS = non-significant ($p > 0.05$) difference. The General Linear Model statistical analysis was done with the following parameters: data from Method II; independant variable #1 = heart preparation (unperfused hearts #1, #3, #4 & #5 - Tables 7-8 or Langendorff perfused hearts #6 & 7 - Table 13); independant variable #2 = site probed (A-band & mitochondrion); dependant variable = P b reading (n = 42). The Post Hoc tests (Tukey and Scheffé) were done on the independant variable #1. The analysis was also done with no independant variable #2 with data from A-band (n =22) and data from mitochondria (n=20). Three assumptions were made: the P/b's for a given element have a parametric distribution; the unperfused hearts have similar profiles and the Langendorff perfused hearts have similar profiles; the sections obtained from a single heart have similar profiles.

TABLE 17 : Mean elemental profiles from the myocardium of heart #2 (unperfused)

		Element							
		Na	Mg	Si	P	S	Cl	K	Ca
Site Probed	A-band (n=9)								
	Mean P/b	1.263	.164	9.288	2.839	1.125	4.160	7.289	.456
	s.d.	.191	.088	1.658	.472	.285	.580	3.364	.147
	s.e.	.064	.029	.553	.157	.095	.193	1.121	.049
	Mitochondrion (n=14)								
	Mean P/b	.815	.224	5.661	5.732	1.311	1.380	5.695	.482
	s.d.	.242	.122	1.078	1.019	.521	.661	1.248	.223
	s.e.	.064	.033	.288	.272	.139	.177	.334	.060
	Nucleus (n=5)								
	Mean P/b	1.026	.108	9.088	7.159	.729	2.472	8.970	.384
	s.d.	.329	.034	2.722	1.689	.124	.511	2.937	.136
	s.e.	.147	.015	1.217	.755	.055	.229	1.313	.061
	Extracellular space (n=1)								
	Mean P/b	4.383	.500	14.740	1.699	2.260	18.187	7.627	.762

TABLE 18: Calculated elemental P/b's from energy spectrum from mitochondria probed in Figure 31

		P/b			
		31-1	31-2	31-3	31-4
E	Na	.561	.900	.712	1.817
l	Mg	.136	.257	.156	.134
e	P	6.057	7.024	6.813	8.135
m	S	1.095	2.448	.782	1.039
e	Cl	1.868	3.751	1.819	6.210
n	K	4.282	4.611	3.322	4.697
t	Ca	.825	2.436	6.223	8.972

4. DISCUSSION

4.1. COMPARISON OF METHODS OF TRANSFER AND FREEZE-DRYING

Although some advocate a cryotransfer of the hydrated cryosection, followed by freeze-drying in the electron microscope column, followed by immediate electron-probe x-rays collection at low temperature (e.g. Zierold 1982; Hagler and Buja 1986; Walsh and Tormey 1988), others seem to advocate a cryotransfer to a liquid-nitrogen-cooled metal container, followed by freeze-drying in a vacuum chamber at ambient temperature (e.g. Dorge et al. 1978; Somlyo et al. 1977; Wendt-Gallitelli and Wolburg 1981; Sasaki et al. 1983; Tvedt et al. 1987; Jorgensen et al. 1988; Bond et al. 1989; Moravec and Bond 1991; Warley 1991; Ziegler et al. 1992) followed by a transfer to the electron microscope column where the freeze-dried section may or may not be recooled for x-rays collection. The second method is the more popular, probably because it is technically easier.

Our findings clearly show that there is no statistically significant difference between different methods of transfer and freeze-drying (**Method I-a: cryotransfer to the electron microscope, freeze-drying in the column of the electron microscope at low temperature, x-rays collection at low temperature; Method I-b: cryotransfer to the electron microscope, freeze-drying in the column of the electron microscope at low temperature, x-rays collection after warming at ambient temperature; Method II: cryotransfer to a vacuum chamber; freeze-drying in a vacuum chamber while warming at ambient temperature, transfer and x-rays collection at ambient temperature**) for the profiles of Na, Mg, P, Cl, K & Ca. More Si is found with Method II but this can be explained by the introduction of dust in the vacuum chamber. Less S

is found with Method I-b & II. This change seems related to ambient temperature but its exact nature cannot be explained. Our changes in Si and S correlate well with the data reported by von Zglinicki and Uhrik (1988).

Views differ on the question of whether a freeze-dried section must be cooled in the electron microscope column during the collection of x-rays (Hagler and Buja 1986; von Zglinicki and Uhrik 1988). Our findings indicate that, except for S, the elemental profiles obtained from the freeze-dried section at ambient temperature are statistically comparable to the profiles obtained from the freeze-dried section at -85°C. Like von Zglinicki and Uhrik (1988), we do not see a need for maintaining a freeze-dried section at a low temperature during the collection of x-rays from an electron-activation zone. In our experience, when freeze-drying is complete, the section is stable and resistant to heat from electron bombardment.

One striking difference between the Methods I & II is the morphology. Method II produces a 'fused' or 'melted' appearance to the filaments. This 'melted' appearance is suggestive of a partial dissolving of the filaments and of an increased retention of bound water even though freeze-drying has occurred.

The 'melted' appearance (e.g. Frederik and Busing 1981; Barnard 1982; Zierold 1984; Hagler and Buja 1986) was thought to be a result of rehydration following exposure with ambient atmosphere (e.g. Frederik and Busing 1981; Zierold 1984; Hagler and Buja 1986), even after only two minutes of exposure (von Zglinicki and Zierold 1989). Carbon coating was suggested as a way of preventing the 'melted' appearance' (e.g. von Zglinicki and Uhrik 1988). Hagler and Buja (1986) associated increased Na and Cl with the 'melted' look whereas von Zglinicki and Zierold (1989) found a decrease in S and a slight decrease in K.

Our sections were never carbon coated before exposure to ambient atmosphere, and the exposure was always minimal. With the exception of S, the 'melted' appearance was not detrimental to the elemental profiles in our sections.

We think that the hypothesis of rehydration after exposure to ambient atmosphere is doubtful for many reasons. If rehydration is a fact, one would expect instability of the sections under the electron beam. Also, one would expect dehydration of the rehydrated sections under the vacuum of the column of the electron microscope. Our freeze-dried sections obtained with Method II were always stable under the electron beam and no reversal of the 'melted' appearance was ever observed while the sections were subjected to the electron microscope vacuum. We often did the following experiments with sections prepared by Methods I-b: x-rays profiles were collected on day 1; the sections were stored in a covered petri-dish at ambient atmosphere for up to seven days; additional x-rays profiles were obtained. One would have expected a 'melted' appearance in these sections after storage, but this was never observed even after 7 days of storage. These facts speak against rehydration as the causal factor. The 'melted' appearance might be more a failure to extract tightly bound water from the section. Perhaps, the vacuum should be less than 10^{-5} torr. One also wonders whether this melting could be eliminated by a slower warming, or by the use of a larger brass transfer unit.

Based on our results, we can recommend Method II as being satisfactory in preserving the elemental contents of Na, Mg, P, Cl, K & Ca. We also recommend that no re-cooling is necessary during x-rays collection as long as the section is in a stable freeze-dried state. Without doubt, Method II should be the first one attempted by a novice because it is the easiest to master. However, if S is important, Method II cannot be recommended and Method I-a is the method of choice.

4.2. QUANTITATIVE PHYSIOLOGICAL ELEMENTAL PROFILES AND COMPARABLE DATA IN THE LITERATURE

4.2.1. Cellular components

Elemental profiles for the myofibril, the mitochondrion and the nucleus of the unsegregated myocyte of the mature rat cardiac muscle have been published. They are summarized in Tables 19, 20 & 21. The following selection criteria was used: mean data were excluded if in histogram format; mean data were excluded if they represented data from more than one animal species (i.e. cat and rat, as in Wendt-Gallitelli et al. 1979); myofibrils, myofilaments, cytoplasm and A-bands data were included in the myofibrils group (Table 19); data were excluded if they were clearly a repeat from a previous paper (e.g. mitochondria von Zglinicki et al. 1986; von Zglinicki and Bimmler 1987); in case of uncertainty (e.g. myofibrils von Zglinicki et al. 1986; von Zglinicki and Bimmler 1987), the two groups were included; when they were two groups of data representing different conditions (e.g. Hagler and Buja 1986; Warley 1989), the group with the lowest Na, the lowest Cl and the higher K was included; when they were two groups representing similar conditions (e.g. Wendt-Gallitelli and Wolburg 1981), the group with the largest n was selected.

In all cases, the specimen was cryofixed and cryosectioned. Notice that the elemental concentrations are in mmole/Kg dry weight, reflecting the fact that the probed section was freeze-dried. X-rays were generated most often using a 80 KV except for Warley (1989, 1991) who used 100 KV. Notice at the bottom of Tables 19 & 20 that we have calculated 'global means' for the myofibrils and for the mitochondria (the contributions being weighted by their n value). Our mmole/Kg dry weight data in Table 12 should be compared with the data in Tables 19, 20 & 21. Our data for S should not be used for comparison because of the differences found between Methods I-a & II.

TABLE 19 : Literature review of mean elemental profiles of myofibrils in ultrathin freeze-dried cryosections of rat cardiac muscle

			Element (mmole/Kg dry weight)						
		n	Na	Mg	P	S	Cl	K	Ca
LITERATURE	Wendt-Gallitelli and Wolburg 1981 mean (s.e.)	34	116(49)	63(28)	144(47)	124(43)	131(37)	390(90)	9(6)
	Hagler and Buja 1986 mean (s.e.)	56	12(116)	105(60)	485(121)	-	102(42)	692(176)	-
	Cantino et al. 1986 mean (s.e.)	-	-	-	-	-	-	-	3(4)
	von Zglinicki et al. 1986 mean (s.e.)	40	65(14)	55(11)	233(26)	150(15)	61(6)	407(41)	-
	von Zglinicki and Bimmler 1987 mean (s.e.)	22	34(33)	60(48)	242(28)	122(16)	79(7)	396(32)	-
	Jorgensen et al. 1988 mean (s.e.)	68	56(2)	52(1)	259(5)	337(6)	167(4)	617(4)	0.5(.2)
	Warley 1989 mean (s.e.)	79	73(6)	61(4)	353(10)	121(5)	100(4)	473(10)	-
	Warley 1991 mean (s.e)	4	71(7)	61(4)	349(14)	126(19)	98(16)	478(18)	1.0(2)
Global Mean = sum (mean * n) / sum of n		303	59	66	309	186	112	522	3.2
A-band data from Table 12		11	54.5	47.8	383	99.1	93.4	574	3.13

TABLE 20 : Literature review of mean elemental profiles of mitochondria in ultrathin freeze-dried cryosections of rat cardiac muscle

			Element (mmole/Kg dry weight)						
		n	Na	Mg	P	S	Cl	K	Ca
LITERATURE	Wendt-Gallitelli and Wolburg 1981 mean (s.e.)	34	88(40)	54(22)	293(34)	216(107)	117(43)	450(58)	9(6)
	Cantino et al. 1986 mean (s.e.)	-	-	-	-	-	-	-	3(4)
	von Zglinicki et al. 1986 mean (s.e.)	24	51(63)	19(11)	410(57)	215(32)	30(6)	246(31)	-
	Jorgensen et al. 1988 mean (s.e.)	50	26(2)	25(1)	475(10)	325(4)	61(3)	293(9)	0.2(.2)
	Warley 1989 mean (s.e.)	60	42(4)	37(3)	438(7)	107(4)	47(3)	270(6)	-
	Warley 1991 mean (s.e.)	4	39(4)	36(2)	443(8)	125(18)	40(9)	269(5)	2(2)
Global Mean = sum (mean * n) / sum of n		172	48	34	416	207	62	309	3.7
Mitochondrion data from Table 12		9	25.4	27.3	672	140	51.7	372	0.06

TABLE 21 : Literature review of mean elemental profiles of nucleus in ultrathin freeze-dried cryosections of rat cardiac muscle

	n	Element (mmole/Kg dry weight) Na	Mg	P	S	Cl	K	Ca
LITERATURE Wendt-Gallitelli and Wolburg 1981 mean (s.e.)	6	308(162)	293(34)	108(49)	117(43)	174(71)	283(80)	7(7)
Nucleus data from Table 12	9	5.0	76.7	1045	33.7	61.7	879	3.83

In the case of our A-band profile, Na and Cl tend to be lower, K tends to be higher and Ca is similar. In the case of the mitochondrion, the same pattern is observed except that our Ca is much lower than the global mean (Table 20). Taken together, the data indicate that our myocytes were in a better physiological state than some of the myocytes examined by others. The diffusible elements (Na, Cl, K & Ca) are still the best measure of normality and good health (i.e. a low Na, Cl & Ca and a high K) for a myocyte because their content depends on an intact sarcolemma with normal ionic exchanges.

The one profile shown in Table 21 for the nucleus (Wendt-Gallitelli and Wolburg 1981) is radically different from our mean profile (Table 12). The high Na, Cl & Ca values and low K value indicate that the myocytes were at least leaky, if not physically damaged. By way of contrast, our elemental profile for the nucleus reveals a low Na, Cl & Ca and a high K.

Our estimates of Mg (in all cellular components) are consistently lower than those reported by others. These differences may be explained by an algebric artefact. As shown in Table 6, the R^2 value in linear regression for Mg was only 0.53. The negative values obtained for Mg in the Langendorff perfused heart (Table 15) are further support for an algebric artefact.

Our estimates of P (in all cellular components) are consistently higher than those reported by others. Once again, these differences may result from an algebric artefact. As shown in Table 6, the R^2 value in linear regression for P was only 0.56. However, a real difference is also possible. According to Randle and Tubbs (1979), the perfused beating rat heart muscle contains the following mobile phosphates (in mmole/Kg dry weight whole muscle): creatine phosphate, 39.4; ATP, 25.0; ADP, 4.0; AMP, 0.5; phosphate, 8.5. These add up to 77.4 mmole/Kg dry weight whole tissue, or about 100 mmole/Kg dry weight myocyte (assuming a 25% extracellular space). But, our A-band, with the lowest P content, contains about 2.5 times more elemental P than the estimation for mobile phosphates. Clearly large quantities of P are associated with other molecules,

most of which are probably incorporated into complex structures (i.e. DNA, RNA, polysomes, matrix proteins, macromolecules, polymers, etc.). Having high elemental P concentrations may be an indication of viability, both because of retention of mobile phosphates and of integrity of the P containing macromolecules. High P concentrations in the cellular components may well be a sign of a healthy myocyte.

Table 22 lists some estimates of whole myocyte concentrations (mmole/Kg water) obtained either from flame spectroscopic analyses of whole tissue (corrected for extracellular space contaminations through a two compartments model) or from analyses of isotope efflux curves. These whole myocyte concentrations resemble best our concentration estimates for the A-band. This seems reasonable when one considers that the myofibrils occupy about 61% of the myocyte volume (Barth et al. 1992).

4.2.2. Extracellular space

We were unable to find from among those working on the rat heart measured profile for the extracellular space (E.C.S.) of the heart muscle. However, several are available for the rabbit heart (Wendt-Gallitelli 1982; Wheeler-Clark and Tormey 1987; Walsh and Tormey 1988). Of these, the E.C.S. profile reported by Walsh and Tormey (1988) is the only one which can be translated into mmole/Kg water concentrations and which reflects the advertised content of the perfusate used.

Since our E.C.S. results are from unperfused hearts, they must be compared with the elemental content of serum (Table 23) or lymph, and not to a perfusate. Notice that our mean E.C.S. profile demonstrate a Na concentration (81 mmole/Kg water) which is too low and a K concentration (22 mmole/Kg water) which is too high. The concentrations for Mg & Ca are lower than expected. The concentrations of Cl & P are about as they should be.

TABLE 22 : Total cellular elemental concentrations (mmole/Kg water) of the myocyte in the ventricle of the rodent*

Species	Element Na	Mg	Cl	K	Ca	Reference
rat	16	17	13	144	0.9	Poliemi 1974
rabbit	33			135		Lee & Fozzard 1975
rabbit	36			142		Nguyen-Thi et al. 1981
rabbit			39			Caillé et al. 1981
hamster		10			1.9	Crawford et al. 1987
rabbit					1.9	Langer 1990

Legend

* Intracellular concentrations were determined either from flame spectroscopic analyses (corrected for extracellular space) or from analyses of isotope efflux curves.

TABLE 23 : Elemental profile of serum electrolytes in rat

Element	Concentration (mmole/l)	Reference
Na	141-150	a
Mg	1.07-1.28	b
P	1.99-3.77	b
Cl	99-114	a
K	5.2-7.8	a
Ca	2.67-3.43	b

Legend

a Baseline haematology and clinical chemistry values for Charles River Wistar rats as a function of age and sex. Charles River Techn. Bull., Vol. 1, no 2, 1982.

b The Clinical Chemistry of Laboratory Animals. Ed. by W.F. Loeb and F.W. Quimby. Pergamon Press, New York, 1989, pp. 417-476.

The underestimation of Mg may be an algebric artefact as explained above. In the case of K, the over-estimation may be also an algebric artefact, arising from the fact that y_x for K has a negative value (see Table 5). According to equation 2, a negative y_x value (compared to a positive y_x value) leads to a larger K concentration. This type of artefact would be more noticeable at lower P/b values such as are found in the E.C.S..

It is, of course, quite possible that the E.C.S. of the static unperfused ventricular muscle does in fact loses Na and Ca and accumulates K, indicating an exchange with the cellular components. Since most of our E.C.S. profiles were obtained in capillary lumens, the cells which are most likely involved in the exchange of intracellular K for extracellular Na and the influx of Ca would have to be the erythrocyte and the endothelium. We have probed both these cells and have indeed found evidence of relatively high Na and low K. Unfortunately, our data were only preliminary, hence did not warrant the analysis required to prove the point.

4.3. HETEROGENEITY OF ELEMENTAL PROFILES

It is well known that the normal extracellular content is different from the intracellular content. For example, the concentrations of Na, Cl & Ca are higher in the extracellular space and the concentrations of K, P & Mg are higher in the intracellular space (Guyton 1991). All these facts are partially confirmed by the differences found between extracellular space and intracellular space as shown in Table 13. The new evidence presented here is that composition varies from component to component. As shown in Table 13, the P content differs in the nucleus, the mitochondrion and the A-band. Also, more K is found in the nucleus than in the A-band and the mitochondrion. By increasing the limit of detection of Mg & Ca by more refined equipments of detection and by increasing the number of readings, further statistically significant differences might be

found. No doubt these differences reflect differences in macromolecules composition and unfixed charges.

Heterogeneity within a cellular component is also possible (von Zglinicki and Bimmler 1988), but it was not looked for in this thesis.

4.4. UNPERFUSED AND LANGENDORFF PERFUSED HEARTS

4.4.1. Comparison of data obtained

Table 14 lists the P/b values of the cellular components of the ventricular myocyte following a 10 minutes Langendorff perfusion of oxygenated HCO_3^-/CO_2 buffered modified Krebs-Henseleit balanced salts solution at 37°C. Compare with the data from unperfused hearts (Tables 7 & 8; statististical analysis in Table 15) and notice the large increases in Na & Cl, and the decreases in K in all three cellular components. Clearly, the ionic permeabilities of the sarcolemma have been seriously altered to permit transmembrane diffusion of Na, Cl & K down their respective transmembrane gradients. Notice also that these sarcolemmal ionic exchanges initiate similar trans-mitochondrial and trans-nuclear exchanges, at least for Na, Cl & K.

Notice next the large sequestration of Ca in the mitochondrion from 0.298 to 1.608 (not statistically significant because of the small n). This type of sequestration is associated with the appearance of dark dense bodies inside the mitochondrion (e.g. Figure 31-4). Because of the magnitude of the Ca, one can be certain that most of it had to come from the perfusate (i.e. extracellular space) rather than from the sarcoplasmic reticuium.

Notice also the lower P content both in the A-band and in the nucleus, but not in the mitochondrion. Also, the perfusion have lowered the Mg in the A-band, the mitochondrion and the nucleus.

In order to gain a better understanding of the changes in the myocyte

following perfusion, we carried out simple estimates of the apparent osmolarity and of the apparent fixed (immobile) charge inside each cellular component both for the unperfused and Langendorff perfused myocytes. These estimates are listed in Table 24. Also included are ratios of Cl/Na to provide an easy reference to the entry of negative Cl relative to the entry of positive Na.

Notice that the apparent osmolarity increases in all cellular components following perfusion. Since the osmotic term is in mmole/Kg dry weight, we can speculate that these increases may be a result of: a) loss of dry mass; b) swelling; c) or a combination of a) & b).

Notice also that the apparent fixed charge in all three cellular components in the unperfused myocyte is negative and that the apparent fixed charge in all three cellular components in the Langendorff perfused myocyte is positive. This suggests that the macromolecules have been radically altered either by depolymerization or denaturation. The ion most responsible for this charge reversal is Cl (see the Cl levels in Table 15 and the increases in Cl/Na in Table 24).

4.4.2. Comparison with literature

In a recent study, Walters III et al. (1992) compared the functional status of blood-perfused and modified Krebs-Henseleit Langendorff perfused hearts during and after global ischemia. There were significant differences in systolic recovery, in coronary resistance, in mean water content, in ATP and in the energy charge. These findings illustrate that one should be careful when transposing data obtained on crystalloid-Langendorff perfused heart to blood-perfused heart system. Our Langendorff perfused hearts might have been damaged by the perfusion process.

The only studies reporting elemental profiles in cellular components of ventricular myocyte following in vitro perfusion of coronary arteries have been

TABLE 24 : Changes in the apparent osmolarity and in the apparent fixed charge in the myocyte components following Langendorff perfusion

	Heart preparation					
	Unperfused			**Langendorff Perfused**		
	Apparent Osmolarity (mOs)	Cl/Na	Apparent Fixed Charge (mEq)	Apparent Osmolarity (mOs)	Cl/Na	Apparent Fixed Charge (mEq)
Component						
A-Band	723	1.7	-638	1156	2.7	174
Mitochondrion	449	2.0	-399	831	2.9	61
Nucleus	946	12.3	-984	1568	3.1	280

Legend

All data are from Tables 12 & 15.

Apparent Osmolarity = [(Na) + (Cl) + (K)].

These elements should account for most of the osmotic activity of each component. The divalent cations are excluded because most (> 90%) are known to be bound out of solution. Some of the P could have been included as mobile ATP, ADP, AMP, or CrP.

mOs = mmole/Kg dry weight.

Apparent Fixed Charge = -[(Na) + 2 (Mg) - (Cl) + (K) + 2 (Ca)].

It is assumed that all these elements function as either a counter-ion or a co-ion to charged macromolecules making up the ultrastructure in each component. It is also assumed that all the P and S are incorporated into the macromolecules.

mEq = meq/Kg dry weight.

done on the rabbit (Buja et al. 1983; Walsh and Tormey 1988). Buja et al. (1983) perfused the interventricular septum through the septal artery, a branch of the left coronary artery. Three groups were tested: control, unperfused; control, perfused; hypoxic, perfused. The controls were similar but very different from our control unperfused hearts. They show higher Na, Cl & Ca and a lower K. Clearly, both the perfused and unperfused hearts were damaged. The hypoxic perfused hearts show signs of damage similar to our Langendorff perfused hearts through higher Na, Cl & Ca and lower K, P & Mg.

Walsh and Tormey (1988) perfused the right ventricular wall of the rabbit through a cannulation of the right coronary artery. From their data, we have calculated apparent osmolarities and apparent fixed charge (Table 25) as in Table 24. Notice how their 'control' data listed compare well with our data for the unperfused A-band (Table 12). These authors subjected the heart to a period of ischemia (second row data) followed by reperfusion (third row data) without obtaining serious alterations in the Na, Cl & K content and in the apparent fixed charge in the myofibrils. These good results may be related to the fact that their perfusate contained 5% Dextran (in addition to a balanced salts composition) and 10 I.U./l of insulin. Presumably, the Dextran has inhibited the transfer of water from the extracellular space to the intracellular space and the insulin prevented the breakdown of glycogen (as well as lipid and protein) and the loss of K. Finally, notice the severely injured group (fourth row data) reported by Walsh and Tormey. Like our Langendorff perfused hearts data (Table 15 & 24), this group shows higher Na, Cl, Ca & osmolarity; lower K, P & Mg and loss of fixed negative charge.

The denses particles in the mitochondria of myocyte (Figure 31) have been recognized before in ultrathin frozen dry sections (Buja et al. 1976; Hagler et al. 1977; Hagler et al 1979; Hagler et al. 1981; Buja et al 1983; Buja et al. 1988). In these studies, the particles were produced in the dog heart after temporary or permanent ligation of a coronary artery. Two types of particles

TABLE 25 : Changes in the apparent osmolarity and in the apparent fixed charge in the myofibrils of the rabbit ventricular myocyte following perfusion, ischemia and reperfusion (Walsh and Tormey 1988*)

	Element (mmole/Kg dry weight)			Apparent Osmolarity		Apparent Fixed
	Na	K	Cl	(mOs)	Cl/Na	Charge (mEq)
Group						
1 Control	78	484	130	692	1.7	-529
2 Ischemia	69	540	105	712	1.5	-600
3 Reperfused I	177	509	180	866	1.0	-610
4 Reperfused II	794	33	562	1389	0.7	-310
Unperfused A-band data from Table 12	54.5	574	93.4	732	1.7	-638
Langendorff perfused A-band data from Table 15	235	288	633	1156	2.7	174

Legend

* The perfusate used by Walsh and Tormey (1988) contained 5% Dextran (mean molecular weight, 86,000) and 10 I.U./l insulin in a bicarbonate buffered balanced salts solution.

Apparent Osmolarity = [(Na) + (Cl) + (K)].

mOs = mmole/Kg dry weight.

Apparent Fixed Charge = -[(Na) + 2 (Mg) - (Cl) + (K) + 2 (Ca)].

mEq = meq/Kg dry weight.

have been described: large particles which do not contain calcium or phosphorus and smaller ones which did. Both types were related to ischemia and hypoxia. Our mitochondrial findings of particles were found to be rich in calcium and phosphorus and were found mainly in Langendorff perfused hearts.

Our reduction in Mg (Table 15) may be related to the breakdown and loss of adenosine phosphate compounds, which normaly bind Mg (Opie 1991). It is well known that free Mg increases 10 folds during ischemia (Opie 1991).

It is well known that energy phosphates (e.g. creatine phosphate and ATP) break down during ischemia to increase the concentration of inorganic phosphates (Opie 1991). High energy phosphates and inorganic phosphates are mobile phosphates. Since most of the P seems to be in the fixed organic form as shown in section 4.2.1., one wonders if the more complex structures containing P may also be breaking down during hypoxia or ischemia. Margination of the chromatin at the periphery of the nucleus is a morphological sign associated with ischemia (Jennings et al. 1978, 1985; Schaper et al. 1979). This indicates that the DNA (with P in its nucleic acids) may be affected by ischemia. Lower elemental concentrations of P detected in our Langendorff perfused myocytes may be secondary to the efflux of mobile phosphates, but also to the breakdown of more complex molecules containing P. The unchanged P in the mitochondria of our Langendorff perfused myocytes may be explained by postulating that the mitochondrial P prefers to bind to the influxing Ca.

Increases in both the intracellular ionic strength and osmolarity may be observed following ischemia or hypoxia (Cotran et al. 1989). Increased osmolarity can result from the production of new osmolytes (e.g. lactic acid) or by the breakdown of large osmotically inactive molecules to smaller osmotically active molecules (e.g. glycogen to glucose; proteins to amino acids; etc.).

The apparent reversal of the fixed charge (from net negative to net positive) calculated for the interior of our Langendorff perfused myocytes (Table 24) is indicative of either denaturation or depolymerization (or both) of the

structural macromolecules which are responsible for the fixed charge in the cellular components. Charge reversal does not arise from a change in pH because the latter was carefully maintained throughout the perfusion. Depolymerization leads to an increases in monomers which may have charges with different pKa's. Denaturation may lead simply to a change in the pKa of existing charges. Depolymerization usually leads to smaller units with increased solubility (hence increased osmolarity) whereas denaturation usually leads to decreased solubilization of existing molecules. Whatever the explanations might be, there can be no doubt that profound changes (beyond the membrane) occurred in the myocytes of our Langendorff perfused hearts.

One must conclude that the myocyte components (A-band & mitochondrion) in the Langendorff perfused heart only with a balanced salts solution is vulnerable to serious deterioration (increased Na, Cl & apparent osmolarity; decreased K, Mg & P (A-band only); sequestration of Ca in mitochondrion; shift of fixed charge). Hypoxia and/or ischemia might be responsible for the change, but accepted cellular parameters (e.g. ADP & ATP levels) of hypoxia would have to be measured. Furthermore, controlled experiments inducing hypoxia and/or ischemia would have to be done.

4.5. CONSIDERATIONS ON SOME TECHNICAL POINTS

4.5.1. Handling of specimen before cryofixation

The unperfused heart #2 revealed some changes in its elemental profiles and distribution which were qualitatively similar to those of the Langendorff perfused hearts (Table 14). However, there were no mitochondrial dense particles. Perhaps the myocytes in heart #2 were in an early stage of damage. One possibility is that the dissected cube of tissue may have been rotated 90 degrees before being put on the aluminium pin and cryofixed. In this case, we

would have collected profiles from myocytes damaged with the razor blade. The changes seen are consistent with this type of damage (Warley 1989; Zierold 1989). Of course, the changes could be due to hypoxic damage rather than physical damage.

Our findings on Langendorff perfused heart and heart #2 illustrates how careful one must be in all excision, perfusion, sampling and cryofixing procedures.

4.5.2. Cryofixation

In our hands, the 'impact freezing' method worked well to produce a 12 μm layer free of large crystals (e.g. > 0.2 μm). Of course, high pressure cryofixation (Riehle 1968; Riehle and Hoechli 1973; Moor et al. 1980; Moor 1987; Zierold 1991) can produce thicker zones devoided of large crystals. However, once the cryosectioning skills are achieved, enough 200 nm sections can be obtained in the first 10-12 μm layer.

4.5.3. Cryosectioning

The mechanics of cutting with the glass knife have been addressed (e.g. Thornburg and Mengers 1956; Saubermann 1977; Saubermann et al. 1980; Frederik et al. 1982; Lickfeld 1985). The possible melting of the sections during sectioning has been refuted (Frederik and Busing 1981; Karp et al. 1982). Nevertheless, one should probably cut at low speeds in order to minimize the risk. It would be interesting to compare the elemental profiles from sections obtained at high and low speeds. This has never been done to our knowledge.

Static electricity is a major problem during cryosectioning (Zierold 1986). It varies with the condition of ultramicrotome and with the humidity in the air. Static electricity interferes with the sectioning as well as with the transfer

of the grid. It also contributes to the formation of compression lines (e.g. Figure 22), which cannot be eliminated by xylene or chloroform as in conventional microtomy. We managed to control the problem but we never eliminated it. Better control might have been achieved with an ionizer (e.g. Maloney and Wheeler-Clark 1991).

To avoid elemental changes, the cryosection cannot be floated on liquid (Barnard and Sevéus 1978; Sevéus 1978). We found that a glass capillary was more effective than the eye lash (Barnard and Sevéus 1978; Sévéus 1978) in picking up cryosections. Some advantages of the capillary are as follows: they can be made straight; the point is smaller; the stock of glass is larger than the stock of eye lashes.

4.5.5. Cryotransfer

The Philips cryotransfer equipment proved to be difficult to master. To our knowledge, few investigators seem to make use of it today. To achieve successful transfers, we had to make significant modifications. The original equipment has a number of poor design features: the interacting between stations (ultramicrotome, workstation and goniometer); cumbersome plumbing and Dewars; an unreliable injection mechanism for fixing the grid; an unreliable opening mechanism of the sleeve over the grid.

The Gatan Model 626 Cryotransfer system for TEM is now the most popular system in North America (e.g. Hagler and Buja 1986; Wheeler-Clark and Tormey 1987; LeFurgey et al. 1988; Walsh and Tormey 1988; Jorgensen et al. 1988; Bond et al. 1989; Moravec and Bond 1991; Ziegler et al. 1992). This system also transports the grid on three stations (ultramicrotome, workstation and goniometer), but the transfer and clamping of the grid on the holder are done manually, the temperature control is achieved without cumbersome plumbing and Dewars and the shutter (sleeve) is controlled by the operator. Although we did

manage after modifications to operate the Philips transfer system, we suspect that the Gatan System may have a better design.

An even better design would be one which requires only two stations: i.e. one which permits receiving and clamping of the grid in the ultramicrotome chamber instead of in a workstation. Such a system seems to exist in Europe (von Zglinicki and Uhrik 1988).

4.5.6. Morphology

In this study, we were able to associate 'normal' morphology with 'normal' and 'abnormal' elemental profiles; also 'abnormal' morphology with 'normal' and 'abnormal' elemental profiles. Except for the small dark particles in mitochondria, the quality of morphology could not be used to predict the elemental profiles. The ultrastructure need only be of a quality which permits identification of morphology, so that the electron beam can be directed to and focused on the site of choice.

4.5.7. Electron probe x-ray microanalysis

The available detecting system did not permit us to probe small compartments such as sarcoplasmic reticulum and the t-tubules. Furthermore, the Mg & Ca concentrations in most locations were at the limit of detection of our system. To detect changes in Ca during excitation-contraction, for example, one would require better detectors or real time imaging in the STEM mode (Somlyo 1984; Saubermann 1988; Le Furgey et al. 1992).

4.5.8. Quantitative analysis

Ideally, the standard and the specimen should have similar compositions

and be probed under similar conditions (HT; spot; Live sec; cps; constant geometry of detector). Had we been meticulously consistant about these rules, we could have minimized the mathematical manipulations in our analyses (see Materials and Methods).

The background generated by the pioloform membrane was not subtracted from the spectra because it was assumed by inexperience to be biologically insignificant in all cases. The possible importance of this subtraction was realized at the end of this project when it was too late to carry out the necessary x-rays collections. The background generated by pioloform could have been easily measured in a spot free of specimen on the same grid supporting the specimen section (Hall 1973). Despite this shortcoming, the results are still comparable with those in the literature (Tables 12, 19 & 20).

The thickness of our standards was assumed to be similar to our sections. Thickness of standard and specimen can be measured by diffraction using the electron microscope. Also, the thickness can be evaluated indirectly by measuring the area of the continuum (white radiation) which is proportional to the amount of biological material present in the probed area. We avoided both of these 'matching' requirements by making use of mean calibration lines constructed from many standards differing in thickness.

When converting to mmole/Kg water, most investigators continue to assume a water content for a given site before freeze-drying. They also assume as we have done that all the water is driven off in the final freeze-dried state when the x-rays collection is done. To avoid these assumptions, a number of techniques have been proposed (e.g. Dorge et al. 1978; Zierold 1986; Warner 1986; von Zglinicki et al. 1987; Roomans 1990; von Zglinicki 1991; Hall 1991). Unfortunately, all of them introduce new assumptions which tend to weaken their value and justification. There is however one approach which has minimal assumptions (Hinke, personal communication) and should be tried. It involves the equilibration of living tissue (before cryofixing) with dimethylsulfoxide (DMSO).

This small molecule is known to penetrate all water compartments and water states to the same specific activity as the bathing solution, and without altering ionic strength or osmolarity at concentration of less than 1%. Since DMSO contains S and since S is not supposed to be altered during freeze-drying using Method I-a, one has a way of calculating the water content in each cellular component and in the extracellular space simply by calculating the S content increase (before and after DMSO treatment) from P/b data.

5. CONCLUSIONS

1) The main objective of this thesis was to master the electron probe x-ray microanalysis technique to permit one to obtain physiologically meaningful elemental profiles for the components of a given cell. The methods and techniques which had to be mastered were: preparation of adult mammalian (rat) cardiac muscle; 'rapid' cryofixation, cryosectioning, transfer and freeze-drying, electron probe x-rays collection and analyses. To master the methodology, new tools were adopted and major modifications of existing equipment became necessary.

2) Different methods of transfer and freeze-drying were compared. **Method I-a:** cryotransfer to the electron microscope, freeze-drying in the column of the electron microscope, x-rays collection at low temperature; **Method I-b:** cryotransfer to the electron microscope, freeze-drying in the column of electron microscope, x-rays collection at ambient temperature; **Method II:** cryotransfer to a vacuum chamber, freeze-drying in a vacuum chamber while warming at ambient temperature, transfer and x-rays collection at ambient temperature Only the elemental content of Si & S were statistically different. The higher Si in Method II is probably related to dust contamination. The lower S found with Methods I-b & II seems to be related to a change in temperature but the exact nature of the change cannot be explained. A morphological 'melting' of the filamentous ultrastructure was consistently observed with Method II. It may indicate incomplete extraction of tightly bound water to macromolecules, perhaps because of insufficient vacuum. The easier Method II is recommended for the quantitative analysis of Na, Cl, K, P, Mg & Ca. Recooling of the sections after freeze-drying with Method II was not found essential to x-rays collection. However, if S is important, Method II cannot be recommended and Method I-a is the method of choice.

3) Quantitative (mmole/Kg water) physiological elemental profiles were established for the A-band, the mitochondrion and the nucleus of the myocyte in the fast frozen quickly excised cardiac muscle. They compared favorably with comparable data in the literature. Differences between intracellular and extracellular spaces as well as differences among cellular components were observed.

4) Elemental profiles for the myocyte components were also obtained from Langendorff perfused hearts. Compared to the data obtained from quickly excised unperfused hearts, the elemental profiles from all cellular components were radically altered. The cellular components had higher Na & Cl and lower K & Mg. The Ca was sequestrated in the mitochondria. The P was lower in all cellular components except in mitochondria. Simple stoichiometric arguments revealed significant changes in the apparent osmolarity and in the apparent fixed charge of cellular components. These changes indicate that serious deterioration of structural macromolecules might also have occurred. The author advises caution when a Langendorff perfused mammalian heart preparation is being contemplated as a model of 'normal' physiology.

6. BIBLIOGRAPHY

Adrian, M. et al. (1984). Cryo-electron microscopy of viruses. Nature, 308:32-36.

Allison, D.P., Daw, C.S. and M.C. Rorvik (1987). The construction and operation of a simple inexpensive slam freezing device for electron microscopy. Journal of Microscopy, 147:103-108.

Aldoroty, R.A., Garty, N.B. and E.W. April (1987). Donnan potentials from striated muscle liquid crystals. Biophysical Journal, 51:371-381.

Altmann, R. (1890). Die Elementarorganismen und ihre Beziehungen zur den Zellen. Veit, Leipzig.

Appleton, T.C.. Ultra-thin Frozen Sections for Electron Microscopy. LKB Report, LKB Instruments Inc., 12221 Parklawn Drive, Rockville, Maryland 20852, U.S.A..

Bald, W.B. (1983). Optimizing the cooling block for the quick freeze method. Journal of Microscopy, 131:11-23.

Bald, W.B. (1986). On crystal size and cooling rate. Journal of Microscopy, 143:89-102.

Barnard, T. and L. Sevéus (1978). Preparation of biological material for X-ray microanalysis of diffusible elements II. Comparison of different methods of drying ultrathin cryosections cut without a trough liquid. Journal of Microscopy, 112:281-291.

Barnard, T. (1980). Ultrastructural effects of the high molecular weight cryoprotectants Dextran and polyvinyl pyrrolidone on liver and brown adipose tissue in vitro. Journal of Microscopy, 120:93-104.

Barnard, T. (1982). Thin frozen-dried cryosections and biological X-ray microanalysis. Journal of Microscopy, 126:317-332.

Barth, E. et al. (1992). Ultrastructural Quantitation of Mitochondria and Myofilaments in Cardiac Muscle From 10 Different Animal Species Including Man. Journal of Molecular and Cell Cardiology, 24:669-681.

Bearer E.L. and L. Orci (1986). A Simple Method for Quick Freezing. Journal of Electron Microscopy Technique, 3:233-241.

Bernhard, W. and M.-T. Nancy (1964). Coupes à congélation ultrafines de tissu inclus dans la gélatine. Journal de Microscopie, 3:579-588.

Bernhard, W. and E.H. Leduc (1967). Ultrathin frozen sections I. Methods and Ultrastructural preservation. The Journal of Cell Biology, 34:757-771.

Bond, M. et al. (1989). Subcellular Calcium Content in Cardiomyopathic Hamster Hearts In Vivo: An Electron Probe Study. Circulation Research, 64:1001-1012.

Boyne, A.F. (1979). A gentle, bounce free assembly for quick freezing tissues for electron microscopy: application to isolated torpedine ray electrocyte stacks. Journal of Neuroscience Methods, 1:353-364.

Bruggeller, P. and E. Mayer (1980). Complete vitrification in pure liquid water and dilute aqueous solutions. Nature, 288:569-571.

Buja, L.M. et al. (1976). Analytical electron microscopic study of mitochondrial inclusions in canine myocardial infarcts. The Journal of Histochemistry and Cytochemistry, 24 (3):508-516.

Buja, L.M. et al. (1983). Subcellular localization and significance of pathological calcium accumulation in myocardium. In Pathobiology of cell membranes, Vol. III, Academic Press Inc., New York, pp. 87-115.

Buja, L.M. et al. (1983). Quantitative x-ray microanalysis of the elemental composition of individual myocytes in hypoxic rabbit myocardium. Circulation, 68 (4):872-882.

Buja, L.M., Hagler, H.K. and J.T. Willerson (1988). Altered calcium homeostasis in the pathogenesis of myocardial ischemic and hypoxic injury. Cell Calcium, 9:205-217.

Caillé, J.-P., Ruiz-Ceretti, E. and O.F. Schanne (1981). Intracellular chloride activity in rabbit papillary muscle: effect of ouabain. The American Journal of Physiology, 240:C183-C188.

Cameron, D.A. (1956). A note on breaking glass knives. The Journal of Biophysical and Biochemical Cytology, 2 (4) suppl.: 57-59.

Cantino, M.E. et al. (1986). X-ray microanalysis of rat papillary muscle. In Microbeam Analysis (Ed. by A.D. Romig Jr. and W.F. Chambers), San Francisco Press Inc., San Francisco, p. 226.

Chandler, J.A. (1977). X-ray Microanalysis in the Electron Microscope. In Practical Methods in Electron Microscopy (Ed. by A.M. Glauert), North-Holland Publishing Company, Amsterdam-New York-Oxford, 547 p..

Chandler, J.A. (1985). X-ray microanalysis of biological tissues - an examination of comparative specimen preparation techniques using prostatic tissue as a model. Scanning Electron Microscopy, II:731-744.

Chiesi, M. et al. (1981). Primary Role of Sarcoplasmic Reticulum in Phasic Contractile Activation of Cardiac Myocytes with Shunted Myolemna. Journal of Cell Biology, 91:728-742.

Christensen, A.K. (1971). Frozen thin sections of fresh tissue for electron microscopy, with a description of pancreas and liver. Journal of Cell Biology, 51:772-804.

Cotran, R.S., Kumar, V. and S.L. Robbins (1989). Robbins Pathologic Basis of Disease. Fourth edition, W.B. Saunders Company, Philadelphia.

Crawford, A.J. and S.K. Bhattacharya (1987). Excessive Intracellular Zinc Accumulation in Cardiac and Skeletal Muscles of Dystrophic Hamsters. Experimental Neurology, 95:265-276.

Dalen, H. et al. (1983). An ultrastructural study of cryofractured myocardial cells with special attention to the relationship between mitochondria and sarcoplasmic reticulum. Journal of Microscopy, 131:35-46.

Dalen, H. and P. Scheie (1991). A correlative study of the freezing patterns in rat myocardium using scanning and transmission electron microscopes. Acta Physiol. Scand., S599:47-60.

Dempsey, G.P. and S. Bullivant (1976). A copper block method for freezing non-cryoprotected tissue to produce ice-crystal-free regions for electron microscopy I. Evaluation using freeze-substitution. Journal of Microscopy, 106:251-260.

Dorge, A. et al. (1978). Preparation of Freeze-Dried Cryosections for Quantitative X-Ray Microanalysis of Electrolytes in Biological Soft Tissues. Pflugers Archiv, 373:85-97.

Dow, J.W., Harding, N.G.L. and T. Powell (1981). Isolated cardiac myocytes I Preparation of adult myocytes and their homology with the intact tissue. Cardiovascular Research, 15:483-514.

Dow, J.W., Harding, N.G.L. and T. Powell (1981). Isolated cardiac myocytes II Functional aspects of mature cells. Cardiovascular Research, 15:549-579.

Dubochet, J. and A.W. McDowall (1981). Vitrification of pure water for electron microscopy. Journal of Microscopy, 124:RP3-RP4.

Dubochet, J. et al. (1982). Electron microscopy of frozen water and aqueous solutions. Journal of Microscopy, 128:219-237.

Dubochet, J. and A.W. McDowall (1984). Frozen hydrated sections. In The Science of Biological Specimen Preparation for Microscopy and Microanalysis (Ed. by J.P. Revel et al.), Scanning Electron Microscopy Inc., AMF O'Hare, Chicago, pp. 147-152.

Dubochet, J. et al. (1987). Cryoelectron Microscopy of Vitrified Specimens. In Cryotechniques in Biological Electron Microscopy (Ed. by R.A. Steinbrecht and K. Zierold), Springer-Verlag, Berlin and Heidelberg, pp. 114-131.

Edelman, L. (1986). Freeze-dried embedded specimens for biological microanalysis. Scanning Electron Microscopy, IV:1337-1356.

Edelman, L. (1991). Freeze-substitution and the preservation of diffusible ions. Journal of Microscopy, 161:217-228.

Elliott, G.F. and E.M. Rome (1969). Liquid-Crystalline Aspects of Muscle Fibers. Molecular Crystals and Liquid Crystals, 8:215-218.

Eranko, O. (1954). Quenching of tissues for freeze-drying. Acta anatomica, 22:331-336.

Escaig, J. (1982). New instruments which facilitate rapid freezing at 83 K and 6 K. Journal of Microscopy, 126:221-229.

Farrant, J. et al. (1977). Structural and functional aspects of biological freezing techniques. Journal of Microscopy, 111:17-34.

Fernandez-Moran, H. (1952). Application of the ultrathin freezing-sectioning technique to the study of cell structures with the electron microscope. Arkiv For Fysik, 4 (31):471-483.

Franks, F. (1977). Biological freezing and cryofixation. Journal of Microscopy, 111:3-16.

Frederik, P.M. and W.M. Busing (1981). Ice crystal damage in frozen thin sections: freezing effects and their restoration. Journal of Microscopy, 121:191-199.

Frederik, P.M. and W.M. Busing (1981). Strong evidence against section thawing whilst cutting on the cryo-ultratome. Journal of Microscopy, 122:217-220.

Frederik, P.M., Busing, W.M. and A. Persson (1982). Concerning the nature of the cryosectioning process. Journal of Microscopy, 125:167-175.

Frederik, P.M. (1982). Cryoultramicrotomy - recognition of artifacts. Scanning Electron Microscopy, II:709-721.

Frederik, P.M., Busing, W.M. and A. Persson (1984). Surface defects on thin cryosections. Scanning Electron Microscopy, I:433-443.

Gersh, I. (1932). The Altmann technique for fixation by drying while freezing. The Anatomical Record, 53 (3):309-337.

Gilkey, J.C. and L.A. Staehelin (1986). Advances in Ultrarapid Freezing for the Preservation of Cellular Ultrastructure. Journal of Electron Microscopy Technique, 3:177-210.

Glaeser, R.M. and K.A. Taylor (1978). Radiation damage relative to transmission electron microscopy of biological specimens at low temperature: a review. Journal of Microscopy, 112:127-138.

Griffith, G. (1984). Selective contrast for electron microscopy using thawed frozen sections and immunocytochemistry. In The Science of Biological Specimen Preparation for Microscopy and Microanalysis (Ed. by J.P. Revel et al.), Scanning Electron Microscopy Inc., AMF O'Hare, Chicago, pp. 153-159.

Gupta, B.L. et al. (1976). Distribution of ions in a fluid-transporting epithelium determined by electron-probe X-ray microanalysis. Nature, 264:284-287.

Gupta, B.L. and T.A. Hall (1981). The x-ray microanalysis of frozen hydrated sections in scanning electron microscopy: an evaluation. Tissue & Cell, 13 (4):623-643.

Gupta, B.L. (1991). Ted Hall and the Science of Biological Microprobe X-Ray Analysis: a Historical Perspective of Methodology and Biological Dividends. Scanning Microscopy, 5 (2):379-426.

Guyton, A.C. (1991). Textbook of medical physiology. Eighth Ed., W.B. Saunders Company, Philadelphia.

Hagler, H.K. et al. (1977). Energy dispersive x-ray spectroscopic (EDS) analysis of small particulate inclusions in hypoxic and ischemic myocardium. Scanning Electron Microscopy, II:145-152.

Hagler, H.K., Sherwin, L. and L.M. Buja (1979). Effect of Different Methods of Tissue Preparation on Mitochondrial Inclusions of Ischemic and Infarcted Canine Myocardium. Laboratory Investigation, 40 (5):529-544.

Hagler, H., Burton, K. and L. Buja (1981). Electron probe x-ray microanalysis of normal and injured myocardium: methods and results. In Microprobe analysis of biological systems (Ed. by T.E. Hutchinson and A.P. Somlyo), Academic Press Inc., New York, pp. 127-155.

Hagler, H.K. and L.M. Buja (1984). New techniques for the preparation of thin freeze dried cryosections for x-ray microanalysis. In The Science of Biological Specimen Preparation for Microscopy and Microanalysis (Ed. by J.P. Revel et al.), Scanning Electron Microscopy Inc., AMF O'hare, Chicago, pp. 161-166.

Hagler, H.K. (1986). Cryoultramicrotomy. In Microbeam analysis (Ed. by A.D. Romig Jr. and W.F. Chambers), San Francisco Press Inc., San Francisco, pp. 231-232.

Hagler, H.K. and L.M. Buja (1986). Effect of specimen preparation and section transfer techniques on the preservation of ultrastructure, lipids and elements in cryosections. Journal of Microscopy, 141:311-317.

Hall, T.A., Clarke Anderson, H. and T. Appleton (1973). The use of thin specimens for X-ray microanalysis in biology. Journal of Microscopy, 99:177-182.

Hall, T.A. (1986). The history and the current status of biological electron-probe x-ray microanalysis. Micron and Microscopica Acta, 17 (2):91-100.

Hall, T.A. (1989). The History of Electron Probe Microanalysis in Biology. In Cryotechniques in electron microscopy (Ed. by R.A. Steinbrecht and K. Zierold), Springer-Verlag, Berlin and Heidelberg, pp. 11-15.

Hall, T.A. (1989). Quantitative electron probe x-ray microanalysis in biology. Scanning Microscopy, 3 (2):461-466.

Hall, T.A. (1991). Suggestions for the quantitative X-ray microanalysis of thin sections of frozen-dried and embedded biological tissues. Journal of Microscopy, 164:67-79.

Harvey, D.M.R. (1980). The preparation of botanical samples for ion localization studies at the subcellular level. Scanning Electron Microscopy, II:409-420.

Harvey, D.M.R. (1982). Freeze-substitution. Journal of Microscopy, 127:209-221.

Heath, I.B. (1984). A simple and inexpensive liquid helium cooled 'slam freezing' device. Journal of Microscopy, 135:75-82.

Heide, H.G. and S. Grund (1974). Eine Tielkuhlkette zum Uberfuhren von wasserhaltigen biologischen Objekten ins Elektronenmikroskop. Ultrastructure Research, 48:259-268.

Heide, H.-G. (1984). Observations on ice layers. Ultramicroscopy, 14:271-278.

Heuser, J.E. et al. (1979). Synaptic vesicle exocytosis captured by quick freezing and correlated with quantal transmitter release. The Journal of Cell Biology, 81:275-300.

Iglesias, J.R., Bernier, R. and R. Simard (1971). Ultracryotomy: A Routine Procedure. Journal of Ultrastructure Research, 36:271-289.

Ingram, F.D. and M.J. Ingram (1980). Freeze-dried, plastic embedded tissue preparation: a review. Scanning Electron Microscopy, IV:147-160.

Ingram, F.D. and M.J. Ingram (1984). Influences of freeze-drying and plastic embedding on electrolyte distributions. In The Science of Biological Specimen Preparation for Microscopy and Microanalysis (Ed. by J.P. Revel et al.), Scanning Electron Microscopy Inc., AMF O'Hare, Chicago, pp. 167-174.

Jennings, R.B. et al. (1978). Relation Between High Energy Phosphate and Lethal Injury in Myocardial Ischemia in the Dog. American Journal of Pathology, 92:187-214.

Jennings, R.B. et al. (1985). Effect of Reperfusion Late in the Phase of Reversible Ischemic Injury. Changes in Cell Volume, Electrolytes, Metabolites, and Ultrastructure. Circulation Research, 56:262-278.

Jones, G.J. (1984). On estimating freezing times during tissue rapid freezing. Journal of Microscopy, 136:349-360.

Jorgensen, A.O. et al. (1988). Two Structurally Distinct Calcium Storage Sites in Rat Cardiac Sarcoplasmic Reticulum: An Electron Microprobe Analysis Study. Circulation Research, 63:1060-1069.

Karp, R.D., Silcox, J.C. and A.V. Somlyo (1982). Cryoultramicrotomy: evidence against melting and the use of a low temperature cement for specimen orientation. Journal of Microscopy, 125:157-165.

Kendall, M.D., Warley, A. and I.W. Morris (1985). Differences in apparent elemental composition of tissues and cells using a fully quantitative X-ray microanalysis system. Journal of Microscopy, 138:35-42.

Kopstad, G. and A. Elgsaeter (1982). Theoretical analysis of the ice crystal size distribution in frozen aqueous specimens. Biophysical Journal, 40:155-161.

Kopstad, G. and A. Elgsaeter (1982). Theoretical analysis of specimen cooling rate during impact freezing and liquid-jet freezing freeze-etch specimens. Biophysical Journal, 40:163-170.

Krebs, H.A. and K. Henseleit (1932). Untersuchungen uber die Harnstoffbildung im Tierkorper. Hoppe-Seyler's Zeitschrift f. physiol. Chemie, pp. 33-66.

Kulenkampff, H. (1955). Zur Technik der Gefriertrocknung histologischer Praparate I. Mitteilung: Die Frage der Strukturerhaltung. Z. wiss. Mikrosk., 62:427-438.

Langendorff, O. (1895). Untersuchungen am uberlebenden Saugethierherzen. In Archiv fur die gesammte physiologie des menschen und der thiere (Ed. by E.F.W. Pfluger), Verlag Von Emil Strauss, Bonn, pp. 291-332.

Langer, G.A. (1990). Calcium Exchange and Contractile Control. In Calcium and the Heart (Ed. by G.A. Langer), Raven Press, New York, pp. 355-378.

Latta, H. and J.F. Hartmann (1950). Use of a Glass Edge in Thin Sectioning for Electron Microscopy. Proc. Soc. Exp. Biol. and Med., 74:436-439.

Leaf, A. (1959). Maintenance of concentration gradients and regulation of cell volume. Annals New York Academy of Sciences, 72:396-404.

Leaf, A. (1970). Regulation of Intracellular Fluid Volume and Disease. American Journal of Medicine, 49 (3):291-295.

Lee, C.O. and H.A. Fozzard (1975). Activities of Potassium and Sodium Ions in Rabbit Heart Muscle. The Journal of General Physiology, 65:695-708.

LeFurgey, A., Ingram, P. and M. Lieberman (1988). Quantitative microchemical imaging of calcium in Na-K pump inhibited heart cells. Cell Calcium, 9:219-235.

LeFurgey, A. and P. Ingram (1990). Calcium Measurements with Electron Probe X-Ray and Electron Energy Loss Analysis. Environmental Health Perpectives, 84:57-73.

LeFurgey, A. et al. (1992). Real-time quantitative elemental analysis and mapping: microchemical imaging in cell physiology. Journal of Microscopy, 165:191-223.

Lepault, J., Booy, F.P. and J. Dubochet (1983). Electron microscopy of frozen biological suspensions. Journal of Microscopy, 129:89-102.

Lickfeld, K.G. (1985). Ein Beitrag zur Frage welche Krafte und Faktoren Dunnstschneiden bewirken. Journal of Ultrastructure Research, 93:101-115.

Linner, J.G. et al. (1984). Cryopreparation of tissue for electron microscopy. In The Science of Biological Specimen Preparation for Microscopy and Microanalysis (Ed. by J.P. Revel et al.), Scanning Electron Microscopy Inc., AMF O'Hare, Chicago, pp. 165-174.

Linner, J.G. et al. (1986). A New Technique for Removal of Amorphous Phase Tissue Water Without Ice Crystal Damage: A Preparative Method for Ultrastructural Analysis and Immunoelectron Microscopy. The Journal of Histochemistry and Cytochemistry, 34 (9):1123-1135.

Livesey, S.A. et al. (1991). Cryofixation and ultra-low-temperature freeze-drying as a preparative technique for TEM. Journal of Microscopy, 161:205-215.

Lupton, J.B. and A.J. Saubermann (1986). A new and simple method for preparation of thin aminoplastic standards for x-ray microanalysis. Journal of Microscopy, RP3-RP4.

Luyet, B.J. (1937). The vitrification of organic colloids and of protoplasm. Biodynamica, 29:1-14.

Majno, G., La Gattuta, M. and T.E. Thompson (1960). Cellular Death and Necrosis: Chemical, Physical and Morphological Changes in Rat Liver. Virchows Arch. path. Anat., 333:421-465.

Maloney, J.A. and E.S. Wheeler-Clark (1991). Visualization of ultrastructure in freeze-dried sections of coronary muscle. In Microbeam Analysis (Ed. by D.G. Howitt), San Francisco Press Inc., San Francisco, pp. 9-10.

Marshall, A.T. (1980). Freeze-substitution as a preparation technique for biological x-ray microanalysis. Scanning Electron Microscopy, II:395-408.

McDowall, A.W. et al. (1983). Electron microscopy of frozen hydrated sections of vitreous ice and vitrified biological samples. Journal of Microscopy, 131:1-9.

McDowall, A.W. et al. (1984). Cryo-electron Microscopy of Vitrified Insect Flight Muscle. Journal of Molecular Biology, 178:105-111.

Meryman, H.T. (1971). Cryoprotective agents. Cryobiology, 8:173-183.

Michalske, T.A. and B.C. Bunker (1987). The Fracturing of Glass. Scientific American, December:122-129.

Moor, H. et al. (1980). The Influence of High Pressure Freezing on Mammalian Nerve Tissue. Cell and Tissue Research, 209:201-216.

Moor, H. (1987). Theory and Practice of High Pressure Freezing. In Cryotechniques in Biological Electron Microscopy (Ed. by R.A. Steinbrecht and K. Zierold), Springer-Verlag, Berlin and Heidelberg, pp. 175-191.

Moravec, C.S. and M. Bond (1991). Calcium is released from the junctional sarcoplasmic reticulum during cardiac muscle contraction. American Journal of Physiology, 260:H989-H997.

Moravec, C.S. and M. Bond (1992). Effect of Inotropic Stimulation on Mitochondrial Calcium in Cardiac Muscle. Journal of Biological Chemistry, 267:5310-5316.

Morgan, A.J., Davies, T.W. and D.A. Erasmus (1978). Specimen preparation. In Electron-Probe x-ray Microanalysis in Biology (Ed. by D.A. Erasmus), Chapman and Hall, London, pp. 94-147.

Morgan, A.J. (1985). X-ray microanalysis in electron microscopy for biologists. Royal Microscopic Society-Oxford University Press, Oxford, 79 p..

Nguyen-Thi, A., Ruiz-Ceretti, E. and O.F. Schanne (1980). Electrophysiologic effects and electrolyte changes in total myocardial ischemia. Can. J. Physiol. Pharmacol., 59:876-883.

Opie, L. (1991). The Heart Physiology and Metabolism. Second Ed., Raven Press, New York, 513 p..

Philips, T.E. and A. F. Boyne (1984). Liquid Nitrogen-based Quick Freezing: Experiences with Bounce-free Delivery of Cholinergic Nerve Terminals to a Metal Surface. Journal of Electron Microscopy Technique, 1:9-29.

Pinto da Silva, P. and B. Kachar (1980). Quick freezing vs. chemical fixation: capture and identification of membrane fusion intermediates. Cell Biology International Reports, 4:625-640.

Plattner, H. and L. Bachmann (1982). Cryofixation: a Tool in Biological Ultrastructural Research. International Review of Cytology, 79:237-304.

Polinemi, P.I. (1974). Extracellular space and ionic distribution in rat ventricle. American Journal of Physiology, 227 (3):676-683.

Powell, T. (1985). Isolated adult heart cells. The development of a new experimental model. Basic Research in Cardiology, 80 (Suppl. 1):9-12.

Randle, P.J. and P.K. Tubbs (1979). In Handbook of Physiology. Section 2: The Cardiovascular System (Ed. by R.M. Berne, N. Sperelakis and S.R. Geiger), American Physiological Society, Bethesda, Maryland, U.S.A., pp. 805-844.

Rash, J.E. (1983). The rapid-freeze technique in neurobiology. T.I.N.S., June:208-212.

Reimer, K.A. and R.E. Ideker (1987). Myocardial Ischemia and Infarction: Anatomic and Biochemical Substrates for Ischemic Cell Death and Ventricular Arrythmias. Human Pathology, 18 (5):462-475.

Riehle, U. (1968). Schnellgefrieren organischer Praparate fur die Elektronen-Mikroskopie. Chemie-Ing.-Techn., 40:213-218.

Riehle, U. and M. Hoechli (1973). The theory and technique of high pressure freezing. In Freeze-etching techniques and applications (Ed. by E.L. Benedetti and P. Favard), Société Française de Microscopie Electronique, Paris, pp. 31-61.

Robards, A.W. and U.B. Sleytr (1985). Low Temperature Methods in Biological Electron Microscopy. In Practical Methods in Electron Microscopy (Ed. by A. M. Glauert), Vol. 10, Elvesier, Amsterdam-New York-Oxford, 531 p..

Roomans, G.M. and L.A. Sevéus (1976). Subcellular localization of diffusible ions in the yeast saccharomyces cerevisiae: quantitative microprobe analysis of thin freeze-dried sections. J. Cell Sci., 21:119-127.

Roomans, G.M. (1979). Standards for x-ray microanalysis of biological specimens. Scanning Electron Microscopy, II:649-657.

Roomans, G.M. (1988). Introduction to X-Ray Microanalysis in Biology. Journal of Electron Microscopy Technique, 9:3-17.

Roomans, G.M. (1990). The Hall equation in the quantitative x-ray microanalysis of biological specimens: a review. Scanning Microscopy, 4 (4):1055-1063.

Roos, N. and T. Barnard (1984). Aminoplastic standards for quantitative x-ray microanalysis of thin sections of plastic-embedded biological material. Ultramicroscopy, 15:277-286.

Roos, N. and T. Barnard (1985). A comparison of subcellular element concentrations in frozen-dried, plastic embedded, dry-cut sections and frozen-dried cryosections. Ultramicroscopy, 17:335-344.

Roos, N. and T. Barnard (1986). Preparation methods for quantitative electron probe x-ray microanalysis of rat exocrine pancreas: a review. Scanning Electron Microscopy, II:703-711.

Russ, J.C. (1980). Standardization techniques for quantitative biological microanalysis. Scanning Electron Microscopy, IV:139-146.

Sasaki, S. et al. (1983). Intracellular Calcium Store and Transport of Elements in Acinar Cells of the Salivary Gland Determined by Electron Probe X-Ray Microanalysis. Japanese Journal of Physiology, 33:69-83.

Saubermann, A.J., Riley, W.D. and R. Beeuwkes (1977). Cutting work in thick cryomicrotomy. Journal of Microscopy, 111:39-49.

Saubermann, A.J. et al. (1981). Application of Scanning Electron Microscopy to X-ray Analysis of Frozen-hydrated Sections I. Specimen Handling Techniques. The Journal of Cell Biology, 88:257-267.

Sauberman, A.J. (1988). X-Ray Mapping of Frozen Hydrated and Frozen Dried Cryosections Using Electron Microprobe Analysis. Scanning, 10:239-244.

Schaper, J. et al. (1979). Ultrastructural, Functional, and Biochemical Criteria for Estimation of Reversibility of Ischemic Injury: A Study on the Effects of Global Ischemia on the Isolated Dog Heart. Journal of Molecular and Cellular Cardiology, 11:521-541.

Sevéus, L. and L. Kindel (1974). Dry cryo-sectioning of human and animal tissue at a very low temperature (-140°C). In Eight International congress on electron microscopy, Canberra, p. 52.

Sevéus, L. (1978). Preparation of biological material for X-ray microanalysis of diffusible elements I. Rapid freezing of biological tissue in nitrogen slush and preparation of ultrathin frozen sections in the absence of trough liquid. Journal of Microscopy, 112:269-279.

Sevéus, L. and C. Tarras-Wahlberg (1984). The glass knife in ultramicrotomy. In The Science of Biological Specimen Preparation for Microscopy and Microanalysis (Ed. by J.P. Revel et al.), Scanning Electron Microscopy Inc., AMF O'Hare, Chicago, pp. 129-134.

Shuman, H., Somlyo, A.V. and A.P. Somlyo (1976). Quantitative electron probe microanalysis of biological thin sections: methods and validity. Ultramicroscopy, 1:317-339.

Simpson, W.L. (1940). An experimental analysis of the Altmann technic of freezing-drying. Anatomical Record, 80:173-189.

Sitte, H. et al. (1977). Fast freezing device. Journal of Microscopy, 111:35-38.

Sitte, H. (1979). Cryofixation of Biological Material without Pretreatment - A Review. Mikroscopie, 35:14-20.

Sitte, H., Neumann, K. and L. Edelmann (1985). Cryofixation and cryosubstitution for routine work in transmission electron microscopy. In Science of Biological Preparation (Ed. by M. Muller et al.), AMF O'Hare, Chicago, pp. 103-118.

Sitte, H., Edelmann, L. and K. Neumann (1987). Cryofixation Without Pretreatment at Ambient Pressure. In Cryotechniques in Biological Microscopy (Ed. by R.A. Steinbrecht and K. Zierold), Springer-Verlag, Berlin and Heidelberg, pp. 87-113.

Skaer, H. (1982). Chemical cryoprotection for structural studies. Journal of Microscopy, 125:137-147.

Slabe, T.J., Rasmussen, S.T. and B. Tandler (1990). A simple method for improving glass knives. Journal of Electron Microscopy Technique, 15:316-317.

Somlyo, A.V., Shuman, H. and A.P. Somlyo (1977). Elemental distribution in striated muscle and the effects of hypertonicity. The Journal of Cell Biology, 74:828-857.

Somlyo, A.P. and H. Shuman (1982). Electron probe and electron energy loss analysis in biology. Ultramicroscopy, 8:219-234.

Somlyo, A.P. (1984). Compositional Mapping in Biology: X Rays and Electrons. Journal of Ultrastructure Research, 88:135-142.

Somlyo, A.P. (1985). Cell calcium measurement with electron probe and electron energy loss analysis. Cell calcium, 6:197-212.

Stephenson, J.L. (1956). Ice crystal growth during rapid freezing of tissues. The Journal of Biophysical and Biochemical Cytology, 2 (4):45-52.

Talmon, Y. et al. (1979). Mass loss and etching of frozen hydrated specimens. Journal of Microscopy, 117:321-332.

Talmon, Y. (1982). Thermal and radiation damage to frozen hydrated specimens. Journal of Microscopy, 125:227-237.

Talmon, Y. (1987). Electron Beam Radiation Damage to Organic and Biological Cryospecimens. In Cryotechniques in Biological Electron Microscopy for Microscopy and Microanalysis (Ed. by R.A. Steinbrecht and K. Zierold), Springer-Verlag, Berlin and Heidelberg, pp. 64-84.

Thornburg, W. and P.E. Mengers (1956). An analysis of frozen section techniques: I. sectioning of fresh-frozen tissue. The Journal of Histochemistry and Cytochemistry, 5:47-52.

Tranum-Jensen, J. et al. (1981). Tissue Osmolality, Cell Swelling, and Reperfusion in Acute Regional Myocardial Ischemia in the Isolated Porcine Heart. Circulation Research, 49:364-381.

Tokuyasu, K. and S. Okamura (1959). A New Method for Making Glass Knives for Thin Sectioning. The Journal of Biophysical and Biochemical Cytology, 6: 305-309.

Tvedt, K.E. et al. (1987). Subcellular Concentrations of Calcium, Zinc, and Magnesium in Benign Nodular Hyperplasia of the Human Prostate: X-Ray Microanalysis of Freeze-Dried Cryosections. Cancer Research, 47:323-328.

Van Harreveld, A. and J. Crowell (1964). Electron Microscopy after Rapid Freezing on a Metal Surface and Substitution Fixation. Anatomical Record, 149:381-386.

Van Harreveld, A., Trubatch, J. and J. Steiner (1974). Rapid freezing and electron microscopy for the arrest of physiological processes. Journal of Microscopy, 100:189-198.

Van Venrooij, G.E.P.M. et al. (1975). Freeze-Etching: Freezing Velocity and Crystal Size at Different Locations in Samples. Cryobiology, 12:46-61.

Van Zyl, Q.G. et al. (1976). Freeze-substitution of plant and animal tissue for the localization of water-soluble compounds by electron probe x-ray microanalysis. Micron, 7:213-224.

Verna, A. (1983). A Simple Quick-Freezing Device for Ultrastructure Preservation: Evaluation by Freeze-Substitution. Biology of the Cell, 49:95-98.

von Zglinicki, T., Rimmler, M., and H.-J. Purz (1986). Fast cryofixation technique for X-ray microanalysis. Journal of Microscopy, 141:79-90.

von Zglinicki, T., Bimmler M. and W.Krause (1987). Estimation of organelle water fractions from frozen-dried cryosections. Journal of Microscopy, 146:67-75.

von Zglinicki, T. and M. Bimmler (1987). The intracellular distribution of ions and water in rat liver and heart muscle. Journal of Microscopy, 146:77-85.

von Zglinicki, T. and B. Uhrik (1988). X-ray microanalysis with continuous specimen cooling: is it necessary ?. Journal of Microscopy, 151:43-47.

von Zglinicki, T. and K. Zierold (1989). Elemental concentrations in air-exposed and vacuum-stored cryosections of rat liver cells. Journal of Microscopy, 154:227-235.

von Zglinicki, T. (1991). The measurement of water distribution in frozen specimens. Journal of Microscopy, 161:149-158.

Walsh, L.G. and J. McD. Tormey (1988). Subcellular electrolyte shifts during in vitro myocardial ischemia and reperfusion. American Journal of Physiology, 255:H917-H928.

Walters III, H.L. et al. (1992). The Response to Ischemia in Blood Perfused vs. Crystalloid Perfused Isolated Rat Heart Preparations. Journal of Molecular and Cellular Cardiology, 24:1063-1077.

Warley, A. (1987). X-ray microanalysis of cells in suspension and the application of this technique to the study of the thymus gland. Scanning Microscopy, 1 (4):1759-1770.

Warley, A. (1989). Cryofixation of heart tissue for x-ray microanalysis. Scanning Microscopy, 3 (4):1247-1252.

Warley, A. (1989). X-ray Microanalysis of Freshly Isolated Cells in Suspension. In Electron Probe Microanalysis: Applications in Biology and Medicine (Ed. by Zierold, K. and H.K. Hagler), Springer-Verlag, Berlin and Heidelberg, pp. 169-179.

Warley, A. (1990). Standards for the application of X-ray microanalysis to biological specimens. Journal of Microscopy, 157:135-147.

Warley, A. (1991). Changes in sodium concentration in cardiac myocytes from diabetic rats. Scanning Microscopy, 5 (1):239-245.

Warner, R.R. (1986). Water content from analysis of freeze-dried thin sections. Journal of Microscopy, 142:363-369.

Wendt-Gallitelli, M.F., Wolburg, H. and W. Schlote (1979). Problems in the quantitation of diffusible ions in unstained heart muscle cryosections by X-ray microanalysis. Arzneim.-Forsch/Drug Res., 29 (II):1814-1815.

Wendt-Gallitelli, M.F. and H. Wolburg (1981). Electron probe microanalysis of frozen dried sections of heart muscle prepared using low temperature techniques. Scanning Electron Microscopy, II:455-462.

Wendt-Gallitelli, M.F. and R. Jacob (1982). Rhythm-dependent Role of Different Calcium Stores in Cardiac Muscle: X-ray Microanalysis. Journal of Molecular and Cellular Cardiology, 14:487-492.

Wendt-Gallitelli, M.F. and G. Isenberg (1985). X-ray microanalysis of single cardiac myocytes frozen under voltage-clamp conditions. American Journal of Physiology, 256:H574-H583.

Wheeler-Clark, E.S. and J. McD. Tormey (1987). Electron Probe X-Ray Microanalysis of Sarcolemma and Junctional Sarcoplasmic Reticulum in Rabbit Papillary Muscles: Low Sodium-Induced Calcium Alterations. Circulation Research, 60:246-250.

Wollenberger, A., Ristau, O. and G. Schoffa (1960). Eine einfache Technik der extrem schnellen Abkuhlung groberer Gewebestucke. Pfulgers Archiv, 270:399-412.

Wroblewski, R. and J. Wroblewski (1984). Freeze-drying and freeze substitution combined with low temperature-embedding. Preparation techniques for microprobe analysis of biological tissues. Histochemistry, 81:469-475.

Wroblewski, R. et al. (1990). A low temperature vacuum embedding procedure for x-ray microanalysis of biological specimens at subcellular level. Scanning Microscopy, 4 (3):787-793.

Ziegler, A., Somlyo A.V. and A.P. Somlyo (1992). Beta-adrenergic effects on cellular Na, Mg, Ca, K and Cl in vascular smooth muscle: Electron probe analysis of rabbit pulmonary artery. Cell Calcium, 13:593-602.

Zierold, K. (1982). Cryopreparation of mammalian tissue for X-ray microanalysis in STEM. Journal of Microscopy, 125:149-156.

Zierold, K. (1984). Quantitative x-ray microanalysis of biological cryosections depends on ice crystal damage. Journal de Physique, C2-447-C2-450.

Zierold, K. (1984). The morphology of ultrathin cryosections. Ultramicroscopy, 14:201-210.

Zierold, K. (1985). Contrast of biological cryosections in scanning transmission electron microscopy. Journal of Microscopy, 140:65-71.

Zierold , K. (1986). The determination of wet weight concentrations of elements in freeze-dried cryosections from biological cells. Scanning Electron Microscopy, II:713-724.

Zierold, K. (1987). Cryoultramicrotomy. In Cryotechniques in Biological Electron Microscopy (Ed. by R.A. Steinbrecht and K. Zierold), Springer-Verlag, Berlin and Heidelberg, pp. 132-148.

Zierold, K. (1988). X-Ray Microanalysis of Freeze-Dried and Frozen-Hydrated Cryosections. Journal of Electron Microscopy Technique, 9:65-82.

Zierold, K. and D. Schafer (1988). Preparation of cultured and isolated cells for x-ray-microanalysis. Scanning Microscopy, 2 (3):1775-1790.

Zierold, K. (1989). Cryotechniques for biological microanalysis. In Microbeam analysis (Ed. by P.E. Russell), San Francisco Press Inc., San Francisco, pp. 109-111.

Zierold, K., Tobler M. and M. Muller (1991). X-ray microanalysis of high-pressure and impact frozen erythrocytes. Journal of Microscopy, 161:RP1-RP2.

Zierold, K. (1992). Comparison of cryopreparation techniques for electron probe microanalysis of cells as examplified by human erythrocytes. Scanning Microscopy, 6 (4):1137-1145.